

AN EXPERIMENTAL INVESTIGATION OF  
SHIP MANOEUVRABILITY IN PACK ICE

CENTRE FOR NEWFOUNDLAND STUDIES

---

**TOTAL OF 10 PAGES ONLY  
MAY BE XEROXED**

(Without Author's Permission)

ROBERT C. BROWN







# **AN EXPERIMENTAL INVESTIGATION OF SHIP MANOEUVRABILITY IN PACK ICE**

By

©Robert C. Brown, B.Eng.

A thesis submitted to the School of Graduate  
Studies in partial fulfillment of the  
Requirements for the degree of  
Master of Engineering

Faculty of Engineering and Applied Science  
Memorial University of Newfoundland

August 2002

St. John's

Newfoundland

Canada

*This thesis is dedicated*

*To the loving memory of my Mother, Belle*

# Abstract

A 1:40 scale model of the R-Class icebreaking hullform and a 1:80 scale model of the MV. Arctic bulk carrier were tested in the Faculty of Engineering and Applied Science towing tank at Memorial University of Newfoundland. The models were tested first in open water and then in modelled pack ice covered water at approximately 8.3 tenths concentration. The pack ice model consisted of various sizes of hexagonally shaped paraffin wax with a mean thickness of about 13mm.

Two main types of tests were conducted for both models in each water surface condition – constant velocity and constant acceleration. The former involved towing at constant velocities of 0.5 and 1.0m/s to determine sway velocity damping coefficients while the latter was a new technique proposed for determining acceleration manoeuvring coefficients and for quickly determining the sway velocity damping coefficients compared with conventional constant velocity test methods. The accelerations used for testing were 0.02 and 0.04  $m/s^2$ .

The test series consisted of simple straight-line towing for each model with constant heading angles 0°, 2°, 4°, 6°, 8° and 10° and rudder angles 10° port and starboard, 5° port and starboard and rudder amidships. A total of 480 tests were conducted in all.

It was shown that crosstalk in a three-component dynamometer could be mathematically removed by developing a 3x3 calibration matrix whose off-diagonal terms represented the crosstalk coefficients. Removing crosstalk measurements provided a more accurate measurement of the actual load applied to the individual load cells.

The manoeuvring coefficients for sway velocity damping and rudder were calculated using results from the constant velocity segment of the test series. Only coefficients for the sway and yaw equations were calculated for this study. The coefficient values found during the open water portion of the test series were compared with those found from

semi-empirical methods given in the literature. The coefficients compared closely. As well, the sign of the coefficients for sway force were correct according to the literature and the sign of yaw moment implied that both models were bow-dominant.

Comparison of the constant velocity pack ice test results with those in open water showed in general that the loads were higher, regression fits were more nonlinear, the spread in the data points increased with increasing sway velocity, the bow remained dominant for both models and differences forces for varied rudder angles were less distinct. Sway velocity damping coefficients were calculated in pack ice using the same methods as for open water.

It was shown that by employing a constant tow carriage acceleration, manoeuvring coefficients for sway acceleration could be determined for open water, but that using the same methodology for pack ice resulted in poor regression fits to the data.

Finally, it has been shown that through the use of constant tow carriage acceleration, the sway velocity damping coefficients can be calculated in a fraction of the time required by using conventional constant velocity testing methods.

# Acknowledgement

I would like to thank my thesis supervisor Dr. M.R. Haddara for his patient, continuous support and thoughtful discussion throughout my studies; your (often) much needed guidance and persistence will never be forgotten.

The technical support of Andrew Kuczora and Darryl Sparkes, formerly of Memorial's Division of Technical Services, was invaluable to the success of the experiments conducted. Thank-you Andrew for keeping me sane during the long hours of testing. Also, thanks are given to Bruce Parsons, John Bell, and the electronics shop guys at the National Research Council's Institute for Marine Dynamics (NRC-IMD); these people were instrumental (no pun intended) in preparing the dynamometer for calibration and testing. Also thanks to Mary Williams at NRC-IMD for suggestions and guidance for the experiments conducted.

For the many thoughtful discussions, and sincere interest in the experimental work completed, I extend warmest thanks and respect to Luksa Luznik, my good friend and office mate during the full-time portion of study.

I would also like to thank the Atlantic Accord Career Development Awards Program and the Society of Naval Architects and Marine Engineers for financial assistance throughout the first two years of this project. Thanks also goes to my colleagues at C-CORE for moral and financial support for the part-time portion of my study period.

Finally, thanks to my wife Michelle for her support during the entire process of presenting this work. Without your persistence this probably would not be finished.

# Table of Contents

Abstract .....	i
Acknowledgement .....	iii
Table of Contents .....	iv
List of Tables .....	vii
List of Figures .....	ix
Nomenclature .....	xiv
<b>CHAPTER 1 : INTRODUCTION .....</b>	<b>1</b>
1.1 BACKGROUND.....	1
1.2 STUDY OBJECTIVES .....	1
1.3 APPROACH .....	2
1.4 THESIS LAYOUT.....	3
<b>CHAPTER 2 : LITERATURE REVIEW .....</b>	<b>4</b>
2.1 BACKGROUND.....	4
2.2 ICE CONSIDERATIONS .....	5
2.2.1 General.....	5
2.2.2 Formation, Properties and Classification of Sea Ice.....	7
2.2.3 Ice Models.....	10
2.2.3.1 General.....	10
2.2.3.2 Refrigerated Ice Models.....	12
2.2.3.3 Synthetic Ice Models.....	13
2.2.3.4 Hybrid Ice Models .....	14
2.3 SHIP MANOEUVRABILITY.....	14
2.3.1 Manoeuvrability Theory .....	14
2.3.2 Semi-Empirical Methods for Coefficient Determination .....	16
2.3.3 Scaled Model Testing for Coefficient Determination.....	18

2.4	SHIP MANOEUVRABILITY IN ICE .....	18
2.4.1	General.....	18
2.4.2	Ship Manoeuvrability in Level Ice .....	19
2.4.3	Ship Manoeuvrability in Pack Ice.....	19
2.5	M.V. ARCTIC AND R-CLASS – SPECIFIC STUDIES .....	21
<b>CHAPTER 3 : EXPERIMENT DESIGN.....</b>		<b>22</b>
3.1	GENERAL .....	22
3.2	DETERMINATION OF VARIABLES.....	22
3.2.1	General Assumptions and Simplifications.....	22
3.2.2	Equations of Motion for a Ship Manoeuvring in the Horizontal Plane ....	24
3.3	DIMENSIONAL ANALYSIS AND SIMILARITY.....	27
3.4	METHODS FOR DETERMINING COEFFICIENTS .....	34
3.5	TEST MATRIX AND FULL-SCALE IMPLICATIONS .....	36
<b>CHAPTER 4 : DESCRIPTION AND PREPARATION OF APPARATUS.....</b>		<b>38</b>
4.1	SHIP MODELS.....	38
4.2	FORCE MEASUREMENT .....	42
4.2.1	Dynamometer Description.....	42
4.2.2	Sizing the Load Cells .....	44
4.2.3	Flex-Link Design .....	47
4.3	TOWING TANK .....	52
4.4	MODEL ICE .....	55
<b>CHAPTER 5 : EXPERIMENTAL METHOD .....</b>		<b>60</b>
5.1	GENERAL .....	60
5.2	DYNAMOMETER CALIBRATION .....	60
5.3	PRE-TEST PROCEDURE FOR SHIP MODELS .....	65
5.4	TOWING TANK TESTS .....	65
5.4.1	Open Water.....	67
5.4.2	Pack Ice.....	68
5.4.3	Concluding the Testing Process.....	69

<b>CHAPTER 6</b>	<b>: RESULTS AND DISCUSSION</b>	<b>71</b>
6.1	GENERAL	71
6.2	CALIBRATION EXPERIMENT RESULTS	71
6.3	CONSTANT VELOCITY TEST RESULTS	74
6.3.1	Method of Analysis	74
6.3.2	Open Water Tests	76
6.3.3	Pack Ice Tests	80
6.4	CONSTANT ACCELERATION TEST RESULTS	85
6.4.1	Method of Analysis	85
6.4.2	Open Water Tests	88
6.4.3	Pack Ice Cover	92
6.5	DAMPING COEFFICIENT TEST EFFICIENCY	95
<b>CHAPTER 7</b>	<b>: CONCLUSIONS</b>	<b>99</b>
<b>CHAPTER 8</b>	<b>: RECOMMENDATIONS</b>	<b>102</b>
<b>CHAPTER 9</b>	<b>: REFERENCES</b>	<b>105</b>
<b>APPENDIX A</b>	<b>: SHIP MODEL DETAILS</b>	<b>115</b>
<b>APPENDIX B</b>	<b>: LOAD CELL AND FLEX-LINK DETAILS</b>	<b>126</b>
B.1	LOAD CELLS	127
B.2	FLEX-LINKS	130
<b>APPENDIX C</b>	<b>: IMAGE ANALYSIS OF WAX CONCENTRATION</b>	<b>131</b>
<b>APPENDIX D</b>	<b>: CALIBRATION PLOTS</b>	<b>135</b>
<b>APPENDIX E</b>	<b>: CONSTANT VELOCITY TEST RESULTS</b>	<b>139</b>
<b>APPENDIX F</b>	<b>: CONSTANT ACCELERATION TEST RESULTS</b>	<b>144</b>

# List of Tables

Table 3.1	Variable dimensions, assuming the [M][L][T] system.....	28
Table 3.2	Experimental methods available for determining hydrodynamic coefficients (Gill, 1980 & Crane et al., 1989).....	34
Table 3.3	Experiment test matrix.....	36
Table 3.4	Full scale values for velocities tested and wax sizes.....	37
Table 4.1	Ship model particulars.....	39
Table 4.2	Coefficients, geometric ratios, and appendages for the models tested and the mariner hullform.....	45
Table 4.3	Input and output parameters for flex-link design.....	50
Table 4.4	A/F Ratio rating criteria.....	51
Table 4.5	Typical hull forces associated with ice coverage (Personal Conversation, Mary Williams, 1996).....	56
Table 4.6	Weights of individual containers of paraffin wax.....	57
Table 4.7	Mean and standard deviation of sampled wax geometry.....	57
Table 6.1	Open water sway and yaw manoeuvring coefficients computed for the M.V. Arctic model (-- means the coefficient could not be predicted using this method).....	79
Table 6.2	Open water sway and yaw manoeuvring coefficients computed for the R-Class hullform model (-- means the coefficient could not be predicted using this method).....	80
Table 6.3	Sway and yaw manoeuvring coefficients computed for the M.V. Arctic model in 8.3 tenths pack ice (showing the open water and ice components of the overall coefficient).....	84
Table 6.4	Sway and yaw manoeuvring coefficients computed for the R-Class hullform model in 8.3 tenths pack ice (showing the open water and ice components of the overall coefficient).....	85
Table 6.5	Open water sway and yaw acceleration manoeuvring coefficients computed for the M.V. Arctic model.....	89

Table 6.6	Open water sway and yaw acceleration manoeuvring coefficients computed for the R-Class hullform model.....	89
Table 6.7	Pack ice sway and yaw acceleration manoeuvring coefficients computed for the M.V. Arctic model.....	95
Table 6.8	Pack ice sway and yaw acceleration manoeuvring coefficients computed for the R-Class hullform model.....	95
Table 7.1	Summary of all manoeuvring coefficients determined from this study for the M.V. Arctic and R-Class models in open water and pack ice.....	100
Table 7.2	Hullform ratios and coefficients for the M.V. Arctic and R-Class models.....	101

# List of Figures

Figure 2.1	Breakdown of ice topics considered in this chapter.....	6
Figure 2.2	Example schematic of the commonly used sea ice concentration classifications (Canadian Coast Guard, 1977). ....	9
Figure 2.3	Typical Egg-Code chart showing pack ice conditions off the coast of Newfoundland for the week of March 3, 1997 (NIC, 1997). ....	10
Figure 2.4	Ship's hull showing six degrees of freedom (three translational, three rotational).....	15
Figure 3.1	Sign conventions (all positive directions shown) used for development of manoeuvring equations of motion. ....	25
Figure 4.1	Bow view of M.V. Arctic model, showing turbulence stimulators. ....	40
Figure 4.2	Stern view of M.V. Arctic model showing the nozzle, rudder, and rudder angle set device.....	40
Figure 4.3	Bow view of the R-Class model, with turbulence stimulators removed for pack ice testing. ....	41
Figure 4.4	Stern view of R-Class model showing the rudder, and rudder angle set device.....	41
Figure 4.5	Schematic showing dynamometer connection to ship model.....	43
Figure 4.6	Dynamometer schematic and internal components. ....	43
Figure 4.7	Photograph of dynamometer and internal components. ....	44
Figure 4.8	Photograph of three different flex-link sizes used. ....	48
Figure 4.9	Schematic of flex-link indicating directions of desirable flexibility and stiffness. ....	48
Figure 4.10	Sample of the flex-link design spreadsheet. ....	49
Figure 4.11	Conversion of tow post horizontal force to vertical flex-link force through moment equation. ....	52
Figure 4.12	Towing tank schematic. ....	53
Figure 4.13	Carriage acceleration wiring schematic.....	54
Figure 4.14	Carriage acceleration test plot showing velocity as a function of time.....	55

Figure 4.15	Three different wax sizes used during the tests .....	56
Figure 4.16	Elevation and plan view schematics of ice barrier, ship model and wax pieces.....	58
Figure 4.17	Photograph of typical wax-covered area of tank. ....	59
Figure 5.1	Calibration bracket showing weights on weight pan during a step in the calibration process.....	63
Figure 5.2	In-line load cell calibration setup.....	63
Figure 5.3	Close-up of in-line load cell during calibration of the aft sway load cell.....	64
Figure 5.4	Computer setup used for calibration experiment, along with A/D converter and signal conditioner. ....	64
Figure 5.5	M.V. Arctic being ballasted to its design waterline in the ballasting tank. Here, an inclinometer is used to check that the model is not heeled to a significant amount. ....	66
Figure 5.6	M.V. Arctic being ballasted to its design waterline in the ballasting tank. Here, an inclinometer is used to check that the model is on an even keel. ....	66
Figure 5.7	R-Class model being towed at 6° heading angle down the towing tank in open water. ....	68
Figure 5.8	Towing tank before a test in pack ice. Note the high surface concentration.....	69
Figure 5.9	Stern view of the M.V. Arctic ship model showing the channel in pack ice as it passes through. ....	70
Figure 6.1	Calibration plot of applied load (N) vs. voltage measured in the in-line load cell (negative applied load implies tension).....	72
Figure 6.2	Forward load cell calibration plot of applied load (N, as measured by the in-line load cell) vs. voltage measured in the forward load cell (negative applied load implies tension, positive applied load implies compression). ....	72
Figure 6.3	Aft load cell calibration plot of applied load (N, as measured by the in-line load cell) vs. voltage measured in the aft load cell (negative	

	applied load implies tension, positive applied load implies compression).....	73
Figure 6.4	Surge load cell calibration plot of applied load (N, as measured by the in-line load cell) vs. voltage measured in the surge load cell (negative applied load implies tension, positive applied load implies compression).....	73
Figure 6.5	Sample plot of all four calibrated channels measured during a constant velocity open water test of the R-Class model set at 10° heading angle, 5° rudder angle to starboard. Note that zeros have not been removed from these plots. ....	76
Figure 6.6	Nondimensional sway force vs. nondimensional sway velocity for the M.V. Arctic ship model constant velocity test series in open water.....	77
Figure 6.7	Nondimensional sway force vs. nondimensional sway velocity for the R-Class hullform model constant velocity test series in open water.....	77
Figure 6.8	Nondimensional yaw moment vs. nondimensional sway velocity for the M.V. Arctic ship model constant velocity test series in open water.....	78
Figure 6.9	Nondimensional yaw moment vs. nondimensional sway velocity for the R-Class hullform model constant velocity test series in open water.....	78
Figure 6.10	Nondimensional sway force vs. nondimensional sway velocity for the M.V. Arctic ship model constant velocity test series in 8.3 tenths ice cover. ....	81
Figure 6.11	Nondimensional sway force vs. nondimensional sway velocity for the R-Class hullform model constant velocity test series in 8.3 tenths ice cover. ....	82
Figure 6.12	Nondimensional yaw moment vs. nondimensional sway velocity for the M.V. Arctic ship model constant velocity test series in 8.3 tenths pack ice. ....	82

Figure 6.13	Nondimensional yaw moment vs. nondimensional sway velocity for the R-Class hullform model constant velocity test series in 8.3 tenths pack ice. ....	83
Figure 6.14	Sample plot of all four calibrated channels measured during a constant acceleration open water test of the M.V. Arctic model set at 10° heading angle, 10° rudder angle to port. Note that zeros have not been removed from these plots. ....	87
Figure 6.15	Sample plot of total sway force as a function of sway velocity, along with the least squares regression fit to the data.....	88
Figure 6.16	Sway force as a function of sway acceleration for the M.V. Arctic model in open water for a family of rudder angles.....	90
Figure 6.17	Sway force as a function of sway acceleration for the R-Class hullform model in open water for a family of rudder angles.....	90
Figure 6.18	Yaw moment as a function of sway acceleration for the M.V. Arctic model in open water for a family of rudder angles.....	91
Figure 6.19	Yaw moment as a function of sway acceleration for the R-Class hullform model in open water for a family of rudder angles.....	91
Figure 6.20	Sway force as a function of sway acceleration for the M.V. Arctic model in 8.3 tenths pack ice for a family of rudder angles.....	93
Figure 6.21	Sway force as a function of sway acceleration for the R-Class hullform model in 8.3 tenths pack ice for a family of rudder angles.....	93
Figure 6.22	Yaw moment as a function of sway acceleration for the M.V. Arctic model in 8.3 tenths pack ice for a family of rudder angles.....	94
Figure 6.23	Yaw moment as a function of sway acceleration for the R-Class hullform model in 8.3 tenths pack ice for a family of rudder angles.....	94
Figure 6.24	Comparison of constant acceleration test results (light lines with dark line regression fit) for the M.V. Arctic model in pack ice, rudder amidships with constant velocity data analysis results for same conditions (circles).....	96
Figure 6.25	Comparison of constant acceleration test results (light lines with dark line regression fit) for the M.V. Arctic model in open water, rudder	

	amidships with constant velocity data analysis results for same conditions (circles).....	97
Figure 6.26	Comparison of constant acceleration test results (light lines with dark line regression fit) for the R-Class model in open water, rudder amidships with constant velocity data analysis results for same conditions (circles).....	97
Figure 6.27	Comparison of constant acceleration test results (light lines with dark line regression fit) for the R-Class model in pack ice, rudder amidships with constant velocity data analysis results for same conditions (circles).....	98

# Nomenclature

$X_o, Y_o$	Ship hull forces in the global $x_o$ and $y_o$ directions (N)
$N$	Yaw moment of the ship (N-m)
$\Delta_s$	Mass displacement of the ship (kg)
$\ddot{x}_{oG}, \ddot{y}_{oG}$	Ship accelerations in the global $x_o$ and $y_o$ directions ( $m\cdot s^{-2}$ )
$I_z$	Mass moment of inertia of the ship about the vertical $z_o$ -axis ( $kg\cdot m^2$ )
$X, Y$	Ship hull forces relative to the ship's own axis system (N)
$u, \dot{u}$	Ship surge velocity and acceleration ( $m\cdot s^{-1}$ & $m\cdot s^{-2}$ )
$v, \dot{v}$	Ship sway velocity and acceleration ( $m\cdot s^{-1}$ & $m\cdot s^{-2}$ )
$r, \dot{r}$	Ship yaw velocity and acceleration ( $radians\cdot s^{-1}$ & $radians\cdot s^{-2}$ )
$u_I$	Surge velocity in the initial condition ( $u_I = V_{ini}$ ) ( $m\cdot s^{-1}$ )
$\Delta u$	Change in surge velocity ( $u - u_I$ ) ( $m\cdot s^{-1}$ )
$X^\circ, Y^\circ$ & $N^\circ$	Forces on the hull at the equilibrium condition ( $u_I = V$ ) (N)
$V$	Ship velocity with respect to the global frame of reference ( $m\cdot s^{-1}$ )
$g$	Acceleration due to gravity ( $m\cdot s^{-2}$ )
$\rho_w, \rho_i$	Water and ice densities, respectively ( $kg\cdot m^{-3}$ )
$\mu$	Dynamic viscosity ( $kg\cdot m^{-1}\cdot s^{-1}$ )
$\psi$	Yaw angle (radians)
$\dot{\psi}$	Yaw velocity (rate of turn) ( $radians\cdot s^{-1}$ )
$\ddot{\psi}$	Yaw acceleration ( $radians\cdot s^{-2}$ )
$\dot{V}$	Ship acceleration ( $m\cdot s^{-2}$ )
$L, B, T$	Ship's length, breadth, and draught, respectively (m)
$\Delta_o, \Delta_i$	Mass displacement of ship and ice pieces, respectively (kg)
$C$	Concentration of ice cover
$f$	Friction coefficient between ice and ship hull
$t$	Ice thickness (mm)
$\sigma_o, \sigma_f$	Compressive and flexural strength of ice, respectively ( $kg\cdot m^{-1}\cdot s^{-2}$ )

$E$	Young's modulus of ice ( $\text{kg}\cdot\text{m}^{-1}\cdot\text{s}^{-2}$ )
$\delta_R$	Ship's rudder angle (radians)
$X^{App}$	Load applied to the surge load cell during dynamometer calibration (N)
$X^{Meas}$	Load measured in the surge load cell during dynamometer calibration (N)
$Y_F^{App}, Y_A^{App}$	Loads applied to the forward and aft sway load cells (respectively) during dynamometer calibration (N)
$Y_F^{Meas}, Y_A^{Meas}$	Loads measured in the forward and aft sway load cells (respectively) during calibration (N)
$a_i$	Surge force calibration coefficients ( $i=1..3$ )
$b_i$	Forward sway force calibration coefficients ( $i=1..3$ )
$c_i$	Aft sway force calibration coefficients ( $i=1..3$ )
$l_i$	Inverted surge force calibration coefficients ( $i=1..3$ )
$J_i$	Inverted forward sway force calibration coefficients ( $i=1..3$ )
$K_i$	Inverted aft sway force calibration coefficients ( $i=1..3$ )
$\beta$	Drift angle (radians)
$X_{oG}, Y_{oG}$	Location of model centre of gravity in the global coordinate system
$\nu$	Kinematic viscosity ( $\text{m}^2 \text{s}^{-2}$ )
$\lambda$	Model scale factor
$C_B$	Block coefficient
$C_P$	Prismatic coefficient
$A/F$	Axial to flexural stiffness ratio used in flexible link design
$M_{wax}$	Mass of wax (kg)
$\rho_{wax}$	Wax density ( $\text{kg}\cdot\text{m}^{-3}$ )
$V_{wax}$	Wax volume ( $\text{m}^3$ )
$A_{wax}$	Surface area for total wax coverage ( $\text{m}^2$ )
$r$	Correlation coefficient
$A_{water}$	Total area of water in image analysis of surface cover ( $\text{mm}^2$ )
$A_{image}$	Total area of image ( $\text{mm}^2$ )
$A_{ship}$	Total area of ship's bow in image ( $\text{mm}^2$ )

$M$	Expected maximum moment on dynamometer (N-m)
$F_h$	Expected maximum horizontal force on tow post (N)
$F_v$	Expected maximum vertical force on vertical flex links (N)
$s$	Span between vertical flex links in the longitudinal direction (cm)
$h$	Length of tow post (cm)
$CG$	Centre of gravity of the ship
$\mathcal{C}$	Centreline of the ship
$WL$	Waterline of the ship
$\mathcal{M}$	Midships

Manoeuvring coefficients for the forces  $X$ ,  $Y$  and moment  $N$  are given as the specific force label with a subscript to show which parameter the partial derivative is taken with respect to. All possible subscripts for the analysis presented in this thesis are  $u$ ,  $\dot{u}$ ,  $v$ ,  $\dot{v}$ ,  $r$ ,  $\dot{r}$ , and  $\delta$  and combinations of these subscripts up to the third order. The meaning of the subscripts is defined above.

For example:

$X_u$	First partial derivative of surge force with respect to surge velocity
$Y_{vv}$	Second partial derivative of sway force with respect to sway velocity
$N_{vr\delta}$	Third partial derivative of yaw moment with respect to sway and yaw velocities and rudder angle

' (prime) Denotes a variable that has been nondimensionalised (applicable nondimensionalising factors are given in the text as required)

# Chapter 1: Introduction

## 1.1 BACKGROUND

The annual presence of pack ice off the coast of Newfoundland and Labrador provides both mariners and ship designers with a challenging environment. Various questions must be considered by naval architects for ship operations in this condition, such as:

- Will a ship operating in pack ice have enough power to overcome the floe resistance?
- Will the hull be strong enough to withstand pack ice floe impacts without jeopardizing the safety of crew and the environment?
- Will steering gear and appendages be able to withstand ice impact forces?

Another important question relates to the ship's ability to manoeuvre effectively in pack ice. Studies of ship manoeuvrability have been used for decades to determine how a vessel would be expected to react to changes in rudder angle while in both open and restricted waterways. With the onset of offshore oil developments on the Grand Banks in recent years and the development of mines at Voisey's Bay in Labrador, the need is apparent for a greater understanding of ship manoeuvrability in the pack ice environment.

Little direct research has been conducted into the field of ship manoeuvrability in pack ice. The work described in this thesis was carried out in an effort to provide a better understanding of this problem.

## 1.2 STUDY OBJECTIVES

The objectives of this study were:

- to determine the velocity dependant (damping) straight-line manoeuvring coefficients for two ship models in open water and modelled pack ice, using conventional towing tank techniques,
- to compare the results of these experiments/calculations to analytically define the overall effect of the presence of pack ice on ship manoeuvring motion,
- to determine the straight-line sway acceleration manoeuvring coefficients for two ship models in open water and modelled pack ice using an innovative new method involving carriage acceleration, and
- to determine the velocity dependant (damping) straight-line manoeuvring coefficients for two ship models in open water and modelled pack ice using an innovative new method involving tow carriage acceleration which would dramatically reduce the overall number of tank tests required for coefficient determination.

The results from this study will be limited in the sense that a full set of manoeuvring coefficients required to simulate a ship manoeuvre will not be available from the experiments conducted alone.

An attempt will be made to verify the experimentally obtained open water coefficients with published semi-empirical coefficient prediction equations that use standard ship geometric parameters.

### **1.3 APPROACH**

Determination of a ship's manoeuvring ability at the design stage can be made using numerical simulation tools available. Such tools are based on the general application of the equations of motion, laid out by Newton's Second Law. In order to predict the manoeuvrability of a particular ship, a set of ship-specific hydrodynamic coefficients must be known. The best way to determine these coefficients is through scaled model testing of the hullform in question. Thus, the approach used in this work is primarily experimental in nature.

In order to gain an understanding of the effect of pack ice on a ship's manoeuvrability, two different ship models were first tested in open water and then in pack ice covered water. The purpose of the former was to obtain an experimental control for comparison with results from the latter.

## **1.4 THESIS LAYOUT**

This thesis is divided into nine chapters. Chapter 1 provides background information about the general problem of ships manoeuvring in pack ice and the need to better understand this problem. It also presents the objectives of the study along with the method of approach. Chapter 2 gives a discussion of literature that deals with the various aspects of ship manoeuvrability, ice modelling and ship manoeuvrability studies in ice. Chapter 3 deals with the design of the experiments from a similitude/dimensional analysis perspective and develops the equations of motion for ships manoeuvring in a broken ice environment. Chapter 3 also presents the standard methods for experimentally determining a ship's manoeuvring characteristics. Chapter 4 describes the apparatus utilised in the experimental program and provides a discussion of the apparatus preparation, including the ship models, dynamometer, towing tank and the model ice. Chapter 5 explains the experimental method followed for dynamometer calibration and presents the calibration results, as well as a description of the towing tank test procedure. Experimental results and analysis are reported in Chapter 6 along with a discussion of the meaning of these data. Conclusions of the study are presented in Chapter 7 and recommendations for future research and experimental practice are given in Chapter 8. Chapter 9 provides a list of references used.

# Chapter 2: Literature Review

## 2.1 BACKGROUND

Individually, the subjects of *ship manoeuvrability* and *ice* constitute a tremendous amount of research work, where the latter has been studied rigorously at times since at least the 1950s and the prior since the early 1900s (Gill, 1980). Combining these two fields of study to get *ship manoeuvrability in ice* makes a slightly smaller volume of literature, however, not one that is insignificant. The review presented in this chapter attempts to provide the reader with some of the more important works that can be found in the literature and to give a reasonable overview of those consulted for this thesis. It is, by no means, a complete review of the literature available as this could provide enough work for a major study in itself.

According to Riska & Varsta (1977), three important aspects must be accounted for when designing ships to operate in ice environments: ice resistance for sizing machinery, ice loads for structural design and propeller/propeller shaft loads. These aspects of ship operations in ice environments have been extensively studied since Riska & Varsta proposed these criteria in 1977 (for example, see Edwards et al. (1981), Kendrick et al. (1984) & Kostilainen (1986)). More recently, ship performance in ice, in terms of manoeuvrability has become an issue.

Studies of ship manoeuvrability in level ice and broken ice have been conducted at full and model scale. These studies have become quite useful in understanding ship behaviour in specific environments. The development of numerical tools for prediction and simulation of ship manoeuvres provides useful aids the to evaluation of ship design, selection of navigation routes and operations planning (Williams & Waclawek, 1998).

The experimental portion of work described in this thesis was conducted during the summer of 1996. Available literature was reviewed at that time and used to help design the experiments (Chapter 3) and develop the experimental procedure (Chapter 5). For

completeness, the author has found it necessary to more recently conduct another survey of literature in hopes that any further developments in the field of ships manoeuvring in pack ice might be included.

The remainder of this chapter is laid-out in four main sections. First, a discussion of ice considerations is given, including general ice types, properties and ice modelling materials. Next is a discussion of ship manoeuvrability theory in general, followed by an overview of ship manoeuvrability in ice and finally a mention of other studies of the M.V. Arctic and R-Class hullform.

## **2.2 ICE CONSIDERATIONS**

### **2.2.1 General**

Ice found in offshore environments can be grouped into three main types: *glacial*, *level* and *pack* (Figure 2.1). These ice types are found in many different regions of the world, and have differing properties, depending on their location and type. In-depth discussions of the global presence of ice are given in Sanderson (1988) and Cammaert & Muggerridge (1988). Some general information is presented below.

Icebergs and ice islands floating in the ocean are remnants of *glacial ice* that have calved from glaciers and ice shelves in the Arctic and Antarctic regions (Cammaert & Muggerridge, 1988). *Glacial ice* is comparatively more dense and stronger than sea ice and tends to have random crystal size and orientation. These properties are a result of the way in which the ice formed - primarily through net snow accumulation over long periods of time. Icebergs are generally classified according to size and shape. Ships operating in bergy water always try to avoid contact with *glacial ice*, regardless of its size or shape, since even small iceberg pieces could do serious local damage to a ship's hull.

*Level ice* forms when ice crystals grow vertically downward from the water surface (for both salt and fresh water). Stable ice sheets are found primarily in areas that are more sheltered and outside the reach of rough open sea conditions. For this reason, the term landfast ice is often used to describe the ice sheets that form over bays and inlets and are frozen to the shoreline. *Level ice* sheets formed in more open regions are usually agitated by sea conditions which tend to break the sheets into individual ice pieces of varying size. Fields of these individual floes are commonly referred to as *pack ice*. The ice environment work presented in this thesis deals exclusively with ships operating in *pack ice*. A more detailed discussion of *pack ice* is given in the following sections. The flowchart in Figure 2.1 outlines the ice topics covered in this chapter.

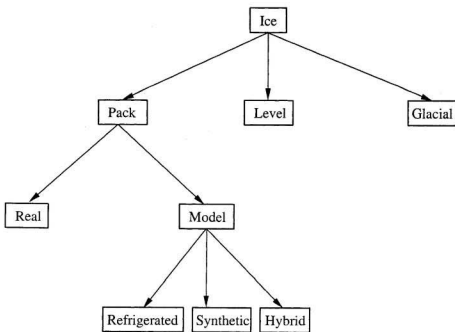


Figure 2.1 Breakdown of ice topics considered in this chapter.

## 2.2.2 Formation, Properties and Classification of Sea Ice

The freezing point for sea water is variable, depending on the amount of salinity, but is about  $-1.9^{\circ}\text{C}$  for standard sea water with a salinity of about 35 parts per thousand (Sanderson, 1988). Sanderson explains that as an ice cover develops on the sea surface, it goes through various stages of formation, beginning with small crystals of *frazil ice* (up to a few cm across) that are often nucleated at the water surface by snowflakes and cold air temperatures. The next stage of development involves the growth of *grease ice* that gives the sea surface a smooth viscous appearance. Depending on the amount of wave action, an *ice rind* then forms of solid surface ice up to 5 cm thick. Under wave action, this ice breaks into thin plates of fragile ice that abrade each other and form irregular rounded discs called *pancake ice*. The pancake ice then merges into a stable, solid surface layer of ice from 5 to 30 cm thick and is referred to as *young ice*. Sanderson (1988) goes on to explain that ice crystals at this stage of development are essentially pure ice, since much of the salt in the water is expelled during the freezing process. However, brine and different gases become trapped within the solid ice crystal matrix, causing the ice structure to contain brine and gas pockets.

The structure of first-year ice depends greatly on where it forms; first-year landfast ice structure is not necessarily representative of first-year ice that grows further out to sea (Sanderson, 1988). The mechanical action to which this ice is subjected determines greatly the form it takes.

Ice ridges are formed when two ice sheets come in contact with each other. Sanderson (1988) states that, depending on the type of interaction, three different types of first-year ridges can form: compression, shear, and rafted. Ridges typically have sail heights of up to 4 m and keel depths to 10 m, however ridge keels have been known to reach 30m depths and scour the seabed. The size of a ridge is dependant on the thickness of the ice from which it forms and the amount of ice failure that occurred during its formation (which implicitly gives an indication of the forces driving the ice together).

Ice that has survived for more than one summer season is normally defined as second year and multi-year ice. These types are formed as the ice is subjected to the thaw and freeze cycles that occur during summer months and then refrozen during the winter season. It is virtually impossible to distinguish between second year ice and ice that is older (Sanderson, 1988). Second and multi-year ice tends to be thicker and stronger than first year ice, since most of the brine has been expelled during the summer months and reconsolidation has occurred. For further reading on the subject of ice ridge formation and growth, the reader is referred to the excellent work of Sanderson (1988), Michel (1978) and Cammaert and Muggeridge (1988).

The presence of pack ice off the coast of Newfoundland and Labrador is the result of the break-up of landfast ice sheets formed locally around the shoreline and the drift of Arctic ice each spring from the north. The maximum extent of sea ice in this region usually occurs in March and has generally retreated by mid June. According to Tang (1990), the mean floe size on the northern Grand Banks is different depending on where in the field a measurement is made; generally, it is 5.4m with a standard deviation of 3.4m at the ice edge and 10.9m with a standard deviation of 7.3m, 5km into the pack. Sanderson (1988) states that the overall thickness of pack ice in the region of Newfoundland and Labrador is 1.18m. Typically, multi-year ice does not drift south of 64°N (Sanderson, 1988).

Pack ice is classified depending on its age, concentration, thickness and size. Figure 2.2 presents the commonly used sea ice concentration classifications. Figure 2.3 is an example egg-code chart for the Grand Banks. Egg-code charts like this one are the standard means by which sea ice conditions are logged and presented by ice data collection agencies around the world.

The work described in this thesis assumes floes are freely floating, unridged, unconsolidated discrete ice pancakes with no pressure on the ice cover. The various means available for modelling this material type are given in the following section.

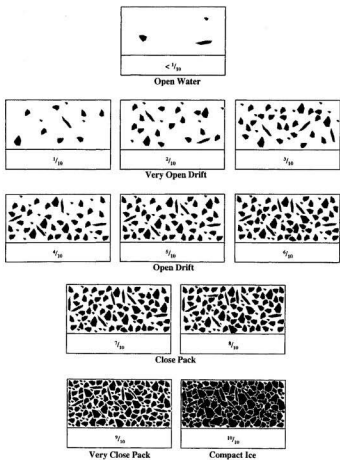


Figure 2.2 Example schematic of the commonly used sea ice concentration classifications (Canadian Coast Guard, 1977).

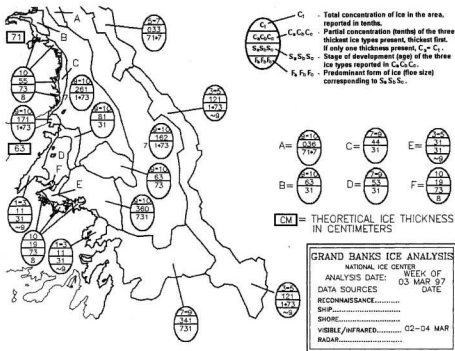


Figure 2.3 Typical Egg-Code chart showing pack ice conditions off the coast of Newfoundland for the week of March 3, 1997 (NIC, 1997).

## 2.2.3 Ice Models

### 2.2.3.1 General

Correctly scaling the frictional coefficients of model ice is important when testing ships in ice, since these coefficients can have a significant effect on test results. If care is taken to match the finish of the model to that of the prototype, static and dynamic ice-ice and ice-structure frictional coefficients should be properly simulated and scaled reasonably well for all scale factors (Timco, 1983a).

For more in-depth study of important properties for consideration when modelling ice, refer also to Weeks & Assur (1967), Peyton (1966), Barnes et al. (1971), Koyama et al. (1988), Tatinclaux & Hirayama (1982), Timco (1979, 1980, 1981a, 1981b, 1983a, 1983b, 1984 & 1985) and Sanderson (1988).

Researchers have attempted to model ice in laboratories in various different ways, not all of which were successful. The history of model testing in ice is fairly short - beginnings were in the 1950s in Russia and by the 1970s it became standard practice to conduct ice model tests; first with ships and then with offshore structures (Wilkman et al., 1991). When modelling ice, ideally, all full-scale mechanical properties of the material are correctly scaled during the test. Since such complete modelling is not possible (Cammaert & Muggeridge, 1988), compromises must be made so that the more important mechanical properties are modelled closely and the less important ones are either ignored or corrections applied (IAHR, 1992). Material limitations may allow for dynamic similarity but not geometric similarity. From similitude relationships developed in Cammaert & Muggeridge (1988), it is evident that natural ice cannot be used as-is for scaled model testing, since even though friction and Poisson's ratio would remain the same, strength properties would have to be scaled in proportion to the geometric scaling factor.

Main test scenarios for ship manoeuvrability in model ice include investigations in both pack ice and level ice. Tests in *level ice* require modelling strength properties of the ice sheet, since icebreaking from flexural failure are involved. Therefore, careful attention should be paid to the material property scaling. Studies of ship interaction with *pack ice* generally do not involve ice breaking but rather deal more with rigid body interactions and some crushing at the ice edge. Hence, ice strength properties are not an important issue, as long as floe size is small compared with the ship so that flexural failure is minimal.

Types of ice models developed for testing of ice-structure interaction can be divided into three main groups – synthetic ice models, refrigerated ice models and hybrid ice models (Figure 2.1). A short overview of the most important of these models is presented below.

### 2.2.3.2 Refrigerated Ice Models

The first model ice was developed in Russia by freezing a high saline solution (~2% sodium chloride). This saline ice was scaled to represent the flexural strength of sea ice by controlling the temperature of the ice and thus the size of brine pockets in the sheet (IAHR, 1992). Significant progress was made in understanding the properties of this ice by Lavrov (1969) and Enkvist (1972).

In the early days of testing in refrigerated ice, most models involved the use of a refrigerated basin of fresh water doped with certain chemicals to reduce the strength properties of grown ice to a more realistic level for the model scale (Timco, 1981). One of the early doped ice types was carbamide (urea) ice, developed by Timco (1979). It possessed the near ideal characteristics of high rigidity and low flexural strength, among other favourable properties from a practical testing standpoint.

Timco (1986) developed a superior model to the urea model – known as *EG/AD/S* ice. This model was grown from an aqueous solution of ethylene glycol (EG), aliphatic detergent (AD) and sugar (S). This model was shown to be far superior to any model ice developed at that time in all respects and was widely utilised in ice modelling basins around the world.

Narita et al. (1988) introduced a granular-structured ice similar to the fine-grain (fg) ice developed in Finland as described by Enkvist (1983) and Enkvist and Makinen (1984). Little information has been published about mechanical properties of this slightly more recent granular ice, however. In 1990, researchers in Finland continued work on their fg-ice model as detailed in Enkvist (1990) and Nortala-Hoikkanen (1990).

In 1990, Spencer and Timco presented a system for controlling the overall density of an ice sheet. Termed CD (controllable density) ice, it involved incorporating fine air bubbles into the ice as it grew and was used in conjunction with a doped tank solution. In general, the authors found that adding air improved scaling of the ice density as well as other mechanical properties of the sheet.

### ***2.2.3.3 Synthetic Ice Models***

Synthetic ice models include those produced by a means other than freezing water or a solution thereof. Though testing of ships in ice is best done using refrigerated ice models, solid synthetic materials can be used when only density, roughness and ice edge shape are important. Materials used previously in this category include polyethylene, polypropylene, wood and paraffin. Care should be taken when using these materials to ensure that friction effects are correctly scaled (Cammaert & Mugeridge, 1988).

Breakable synthetic materials can be used when internal ice strength properties need to be modelled and refrigerated ice model testing is not an option. Level ice sheets have been modelled in the past by spraying a wax mixture over the water in a towing tank. Such efforts have produced model ice with a high flexural strength and high coefficient of friction compared with real ice sheets. Michel (1978) developed a type of wax with various components added to adjust the strength and flexural characteristics. This material was heated and then poured over the water surface for testing in level ice sheets in non-refrigerated basins. Another material was developed by Tryde (1975), consisting of plaster of Paris that had been weakened by adding various constituents. The material was poured into separate forms and lowered onto the water surface. After testing, it was not reusable. Herfjord (1982) produced a synthetic model ice composed of a mixture of organic fat compounds. Grande et al. (1983) experimented with mixtures of polyethylene pellets, paraffin wax and oil. The pellets were spread over the water surface and a warm mixture of paraffin and oil was sprayed over the top to bind the pellets together, repeating the process until the desired thickness was achieved. A similar model was utilised by Cammaert et al. (1983) to assess the manoeuvrability of a model LNG carrier in level ice.

Aboulazm (1989) conducted a study of ship resistance in pack ice by using individual paraffin wax cakes spread across the surface of a towing tank to simulate the ice pack. In this type of test, the ice strength characteristics have a relatively minor effect since discrete floes are more likely to be pushed from the path of an advancing ship than they would be to

fracture. This is especially true when the floes are of small to moderate size (Aboulazm, 1989). Aboulazm considered the modelling to be totally hydrodynamic and thus followed Froude scaling laws. No attempt was made to model the ice structure properties or the ship structure flexibility.

#### ***2.2.3.4 Hybrid Ice Models***

The first hybrid ice was developed in Russia and is described by Belyakov (1984). This model was created by freezing a layer of plastic beads floating on the surface of fresh water. Little is reported about the properties of this ice.

IAHR (1992) reports that a hybrid ice model was developed by Fleet Technology Ltd. whereby plastic beads were frozen into the surface of an EG/AD/S solution. The resultant model ice sheet was produced in significantly shorter time than was previously possible with refrigerated ice and allowed for greater control over the ice density and floe size. The main difficulty with using this ice type, however, lay in the handling of it – producing ice sheets in large testing basins required sophisticated equipment to apply a uniform layer of beads before freezing.

For an excellent discussion of the history of model ice up to 1992, the reader is referred to the details presented in IAHR (1992).

## **2.3 SHIP MANOEUVRABILITY**

### ***2.3.1 Manoeuvrability Theory***

The full rigid body motion of a ship can be defined by the six degrees of freedom pitch, roll, heave, surge, sway and yaw (shown in Figure 2.4). A ship's seakeeping ability is defined by the first three degrees of freedom, while manoeuvrability is generally limited to definition of the latter three, which define the motions in the horizontal plane alone.

The method for mathematically defining a ship's manoeuvrability can be derived from Newton's second law. It is not deemed instructive to completely derive these equations here from first principles. A more in-depth discussion is given in Section 3.2.2, along with a dimensional analysis of the problem. For more detail, the reader is referred to Norrbin (1971), Gill (1980), Kijima et al. (1981 & 1988) and especially Crane et al. (1989).

The manoeuvring equations of motion have been developed in such a way that a given hullform's manoeuvring characteristics can be defined by a set of coefficients termed *hydrodynamic derivatives*, or *hydrodynamic coefficients*. Used in conjunction with a ship simulator, coefficients for a given hullform can be employed to predict a vessel's manoeuvring characteristics at the design stage. The main difficulty in predicting a ship's manoeuvrability lies in accurately determining these coefficients. Various methods for determining manoeuvring coefficients are given in Crane et al. (1989), including slender body strip theory, systems identification, semi-empirical methods with regression analysis, three dimensional potential flow analyses and model testing. It is worth noting that since the equations of motion in open water were developed using linear small perturbation theory, there may be problems using these equations in ice.

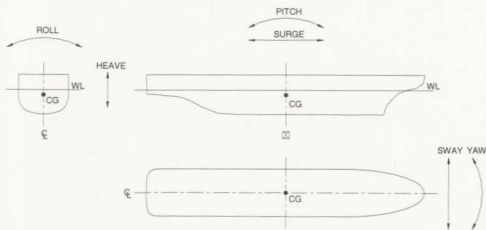


Figure 2.4 Ship's hull showing six degrees of freedom (three translational, three rotational)

### 2.3.2 *Semi-Empirical Methods for Coefficient Determination*

Semi-empirical equations for calculating sway velocity damping derivatives were developed by Wagner Smitt (1971), Norrbin (1971) and Innoe et al. (1981). These formulations were derived as a function of ship particulars and were based on data from rotating arm and planar motion mechanism tests. The resulting equations for sway and yaw velocity derivatives from Wagner Smitt (1971), Norrbin (1971) and Innoe et al. (1981) are written respectively as:

$$\begin{aligned} Y'_v &= -5.0 \left( \frac{T}{L} \right)^2 \\ N'_v &= -1.94 \left( \frac{T}{L} \right)^2 \end{aligned} \quad (1)$$

$$\begin{aligned} Y'_v &= -\pi \left( \frac{T}{L} \right)^2 \left[ 1.69 + 0.08 \frac{C_B \cdot B}{\pi \cdot T} \right] \\ N'_v &= -\pi \left( \frac{T}{L} \right)^2 \left[ 0.64 + 0.04 \frac{C_B \cdot B}{\pi \cdot T} \right] \end{aligned} \quad (2)$$

$$\begin{aligned} Y'_v &= -\pi \left( \frac{T}{L} \right)^2 \left[ 1.0 + \frac{1.4C_B \cdot B}{\pi \cdot T} \right] \\ N'_v &= -\pi \left( \frac{T}{L} \right)^2 \left[ \frac{2.0}{\pi} \right] \end{aligned} \quad (3)$$

Clarke (1982) compared these formulae against velocity derivatives available in the literature and used multiple regression analysis to further develop semi-empirical formulae for both sway velocity and acceleration derivatives. These equations take a similar form as presented in Equations (1), (2) & (3) which are based on ship particulars and are written as:

$$\begin{aligned}
Y'_v &= -\pi \left(\frac{T}{L}\right)^2 \left[ 1.0 + 0.4C_B \cdot \frac{B}{T} \right] \\
N'_v &= -\pi \left(\frac{T}{L}\right)^2 \left[ 0.5 + 2.4 \frac{T}{L} \right] \\
Y'_\phi &= -\pi \left(\frac{T}{L}\right)^2 \left[ 1.0 + 0.16C_B \frac{B}{T} - 5.1 \left(\frac{B}{L}\right)^2 \right] \\
N'_\phi &= -\pi \left(\frac{T}{L}\right)^2 \left[ 1.1 \frac{B}{L} - 0.041 \frac{B}{T} \right]
\end{aligned} \tag{4}$$

Results of these semi-empirical methods are statistically significant, but no methods have produced simulation results as accurate as those from experimental methods (Crane et al., 1989).

Kijima et al. (1993) compared the results of a zigzag manoeuvre for free-running model tests and simulated manoeuvres using the coefficients predicted by equations in Innoe et al. (1981). The results of this comparison showed good agreement between the model test results and the simulation results. This indicates that the method proposed by Kijima et al. (1993) would be useful for predicting ship manoeuvrability at the design stage. However, the authors indicate that there are still problems with predicting the manoeuvring performance of a full-scale ship.

Biancardi (1997) proposed an alternative means by which manoeuvring coefficients could be computed at the design stage. His method accounted for the ship form in geometric relationships, free surface effects and the effects of interaction between the propeller, hull and rudder. The results of his study were verified and correlated by comparison with model test data of surface ships.

### **2.3.3 Scaled Model Testing for Coefficient Determination**

The most popular and reliable means of accurately predicting hydrodynamic coefficients is through experimental methods. The different experimental techniques include straight line towing (typically for determining velocity dependant damping coefficients only), rotating arm towing (rotational coefficients only) and planar motion mechanism (PMM) towing (rotational damping and acceleration coefficients). Of these methods, PMM tests provide the ability to determine the largest number of manoeuvring coefficients (Gill, 1980). A more detailed description of these methods and the coefficients that can be determined is given in Section 3.4.

Barr (1993) noted a concern, related to scale effects, for simulation models based on results from small-scale model tests. Barr presented the results of tests performed by the Society of Naval Architects of Japan (SNAJ) on three different scale models of the ship *ESSO Osaka*. Results from turning circle and zigzag manoeuvres showed significant differences between the models. For further reading on the importance of scale effects in model manoeuvring tests, refer also to Oltmann et al. (1980) and Nikolaev & Lebedeva (1980).

## **2.4 SHIP MANOEUVRABILITY IN ICE**

### **2.4.1 General**

Model testing of ships in ice dates to 1955 in the USSR when the world's first ice tank was built (Keinonan, 1983). Since that time, many improvements have been made in this field of research both from the development of ice modelling materials and facilities allowing researchers to investigate the various parameters of interest. Model testing of ships in ice has been concentrated mainly on propeller-ice interaction, and ship resistance studies. To a lesser degree and only more recently, studies of ship manoeuvrability in ice have been conducted in both level and pack ice (Keinonan, 1983).

### **2.4.2 Ship Manoeuvrability in Level Ice**

As previously discussed, the mechanics of ships manoeuvring is very different in level ice than in pack ice. Floes larger than a specified cut-off level can be considered infinite and thus constitute level ice (Riska & Varsta, 1977). This distinction is important for the work described in this thesis because the interaction processes for each of the two ice sizes are different: finite floes generally suffer only from crushing on impact with a ship and then are cleared, while infinite fields crush first and then fail by bending (Riska & Varsta, 1977). For a discussion of ship manoeuvrability in level ice, the reader is referred to Tue-Fee & Keinonan (1986), Edwards et al. (1976), Edwards et al. (1981), Kendrick et al. (1984), Jones (1989), Peirce & Hart (1990) and Williams et al. (1992)

### **2.4.3 Ship Manoeuvrability in Pack Ice**

Modelling a ship's manoeuvring characteristics in pack ice is a little known area of research. Numerous papers make mention of ship manoeuvrability in pack ice but do not go into significant detail about the processes involved or the findings of study on this subject. Aboulazm (1993) analytically defined the forces involved in steady ship turning in pack ice. His work represents a starting point for the analytic solution of the manoeuvring equations of motion for ships in pack ice. Since no further work by Aboulazm has been found in this field, it is difficult to know if his analytic model properly predicts the forces involved in steady ship turning in pack ice. Thomas and Schultz (1990) presented model test results of a naval vessel operating in model pack ice that was neither real nor urea-doped, hence allowing for testing in a non-refrigerated facility. However, results from this study were not deemed to be useful for the work presented herein, since the tests were primarily conducted to determine safe operating speeds for these vessels in the marginal ice zone. These speeds were defined in terms of ice interaction with various hull appendages.

Williams & Waclawek (1998) state that the manoeuvring equations of motion in ice are different than those for open water. No further detailed information is given on this

comment. Kostilainin (1986) also notes that certain manoeuvring coefficients related to cross-coupling of ship motions are ignored in open water formulations of manoeuvring. However, this cannot always be done when modelling ships operating in heavy ice, due to the significant heaving, pitching and rolling inherent in the process. Since the testing done for this thesis used a fully constrained model, the concerns of Kostilainin should not play a role in accurately determining the damping and inertial coefficients for sway and yaw.

To accurately conduct experiments and analysis of ships manoeuvring in pack ice, it was deemed useful by the author to consider various ways in which the process of ship-ice interaction could occur. Through consultation with several researchers in the fields of ship manoeuvrability and ice mechanics, and review of the limited works in this area, two possible situations were considered:

1. The ice acts on the ship's hull as an external force. Each piece of ice perturbs the movement of the vessel by a small amount as it impinges onto the hull, depending on the size of the piece and the location of impact. The difficulty with this scenario is that a broken ice field is not an ordered phenomenon - the location, and number of impacts is something that will occur in a random fashion. Similar to this approach, Aboulazm (1993) briefly looks at the interaction process analytically as a loss of energy from the hull as it impacts many ice pieces. Aboulazm's formulation assumes the forces and moments on the ship hull are dependant on ship size, geometry, and speed, as well as rudder geometry and ice floe size, shape, and concentration.
2. The ice is part of the environment. The difference between hydrodynamic coefficients determined in open-water, and pack ice is purely the result of the ice presence. The analysis for this type of situation would allow for the use of statistical modelling of data to provide the overall effect of ice for different ice cover concentrations, different ship models, and for different vessel speeds. If the results are deemed accurate (through some validation method) then a more rigorous analysis of the situation on a smaller scale (as suggested by point 1. above) could be conducted. A mathematical model could then be validated at a later date.

For analysis of manoeuvring coefficients in pack ice, this study uses the assumption presented in Kendrick et al. (1984); that the hydrodynamic derivatives in ice have open water and in-ice values such that:

$$Y = Y_{open\ water} + Y_{pack\ ice}$$

where the nondimensional linear sway damping manoeuvring coefficient can be written as:

$$Y'_v = Y'_{v\ open\ water} + Y'_{v\ pack\ ice}$$

Kendrick et al. (1984) goes on to state that the ice components of these coefficients will be average figures since the process of transiting through an ice field is discontinuous. Ice coefficients would also be expected to vary with the characteristics and thickness of the ice. Since each test in the pack ice experiments conducted for this thesis deal with the same field of ice, it is assumed that this condition will remain constant throughout the test series and not play a role in varying the ice coefficients.

## **2.5 M.V. ARCTIC AND R-CLASS – SPECIFIC STUDIES**

Numerous other studies have been performed in both model and prototype scale for the M.V. Arctic and R-Class hullform. Much of this work dealt with sizing of machinery, strengthening of hulls, determination of resistance in ice, icebreaking performance in level ice, vessel manoeuvrability in level ice, new developments in icebreaking performance and, to a much lesser degree, manoeuvrability in pack ice (the reader is referred to Edwards et al. (1981), Kendrick et al. (1984), Browne (1990) and Menon et al. (1986) for examples of these works).

The work of Williams & Waclawek (1998) utilised a 1:20 scale R-Class hullform model for manoeuvrability tests in both level and pack ice. The results of this analysis were not made public in this paper.

# Chapter 3: Experiment Design

## 3.1 GENERAL

The research objective of this chapter is to develop a method for assessing the effect of a pack ice field on the manoeuvrability of a ship transiting it. The overall objective has been divided into more manageable parts that should be carefully considered in the model scale:

1. Modelling the ship's manoeuvring characteristics and
2. Modelling the ice environment.

Both these problems can be overcome separately using methods of experimentation and analysis based on past research, and will be outlined in the sections that follow. A partial analysis is presented in which the problem has been simplified based on physical constraints of the modelling environment while still maintaining an accurate description of the full scale.

Past researchers have developed ways to accurately define the manoeuvring characteristics of ships operating in various conditions. Through the valid assumptions and simplifications described in greater detail in the sections that follow, the test methods, facility limitations, and coefficients are explained.

## 3.2 DETERMINATION OF VARIABLES

### 3.2.1 *General Assumptions and Simplifications*

The purpose of scaled model research is to provide information about some complex problem for which a solution is not easily attainable through some other method, be it analytic, numeric, or full-scale study. If it is not possible to model every aspect of the

full-scale, the problem must be reduced to something that is manageable and yet representative enough of the full-scale to allow for conclusions to be drawn or theories/mathematical models to be derived which would explain the full-scale. Thus, various assumptions and simplifications must be made which make the problem less complicated while still accurately representing the full-scale.

The problem described herein is no exception to this practice, as it would not be possible to model every aspect of a ship manoeuvring in a broken ice field. The reasons being that various experimental controls must be maintained for purposes of comparison and, more importantly, the behaviour of the full-scale situation is such that it does not allow for complete modelling in a controlled laboratory environment. In formulating this problem, several assumptions and simplifications were made before any partial analysis was conducted. Assumptions for the full-scale can be classed into three main groups which are related to the main components of the process: ship, ice, and ship-ice interaction. Many of these assumptions are commonly made by other researchers in this field of study, and in particular, reference is made to Aboulazm (1989):

### *Ice*

- ice pieces are considered to be homogeneous, isotropic, and continuous,
- size of the ice pieces are considered small compared to the ship size,
- ice pieces are considered to act as freely floating rigid bodies thus requiring no modelling of their mechanical properties,
- no external pressure exists on the ice cover and thus individual pieces are free to move when struck by the ship, and
- the drift velocity of an ice floe is small compared with the ship's velocity.

### *Ship*

- the vessel is assumed to behave as a rigid body,
- the ship is symmetric about its vertical centreline plane, and
- the centre of gravity is located amidships.

### *Ship-ice interaction*

- ship speed is assumed to remain constant during the interaction process,
- change in the ship's trim due to impact with ice pieces is negligible,
- interaction between the hull and ice is considered to be an impact or collision process where ice pieces are forced from the ship's path, and
- ice does not enter the propeller at any stage in the interaction process.

It is also important to note that in conducting the partial analysis, other simplifying assumptions were made which are not only justifiable, but necessary to conduct the experiments. These will be explained as the need arises.

### **3.2.2 Equations of Motion for a Ship Manoeuvring in the Horizontal Plane**

To understand the method of experimentation required, it is necessary to give some explanation of the mathematical representation of ships manoeuvring in open water.

A ship manoeuvring in water experiences motions in six degrees of freedom - three rotational: pitch, roll, and yaw, and three translational: surge, sway, heave (see Figure 2.4). Since the objective of this research is to define the manoeuvring motion of a ship (i.e. motion in the horizontal plane), the equations and analysis have been limited to the three motions of surge, sway, and yaw ( $X, Y, N$  respectively) which are the most influential for manoeuvring.

If we consider the conventions shown in Figure 3.1 and use Newton's Second Law, the equations of motion for a ship can be written as forces on the hull (Crane et al., 1989) in global co-ordinates as

$$\begin{aligned} X_o &= \Delta_s \ddot{x}_{oG} \\ Y_o &= \Delta_s \ddot{y}_{oG} \\ N &= I_z \ddot{r} \end{aligned} \tag{5}$$

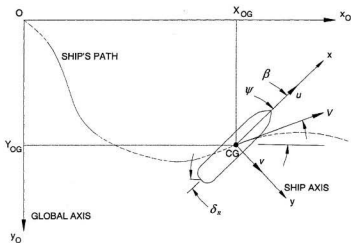


Figure 3.1 Sign conventions (all positive directions shown) used for development of manoeuvring equations of motion.

From this global representation, we can transform the equations into a more useful form - relative to the ship's own axes such that

$$\begin{aligned}
 X &= \Delta_x (\dot{u} - vr) \\
 Y &= \Delta_y (\dot{v} + ur) \\
 N &= I_z \dot{r}
 \end{aligned}
 \tag{6}$$

The traditional method of writing the equations of motion for a ship follows from this latter set of transformed equations. As described in Crane et al. (1989), the three forces  $X, Y$ , and  $N$  (referring to the moment  $N$  more generally as a force, for simplicity) can be written as functions of the velocities and accelerations of the ship:

$$\begin{aligned}
 X &= f_x(u, v, r, \dot{u}, \dot{v}, \dot{r}) \\
 Y &= f_y(u, v, r, \dot{u}, \dot{v}, \dot{r}) \\
 N &= f_\nu(u, v, r, \dot{u}, \dot{v}, \dot{r})
 \end{aligned}
 \tag{7}$$

Based on these equations, the forces on a ship's hull are assumed to be composed only of velocity and acceleration terms. Although many more factors are involved in defining this motion, it is assumed for now that they are implicitly included in the terms of Equation (7). Performing a Taylor series expansion of the multivariable functional Equations (7) results in a large number of nonlinear terms. By doing this, it can be shown which parameters will later be determined experimentally. It is important to include these nonlinear terms in order to provide a set of accurate equations whereby nonlinear motions could be simulated once the manoeuvring coefficients are found. In the final equation, however, it is not practical to include nonlinear terms beyond the third order since the increase in accuracy beyond this is not significant. By using only linear terms, only simple manoeuvres could be simulated (slow speeds and low rates of turn). For a more complete explanation of a manoeuvring modern-day ship, these non-linear terms must be present (Gill, 1980).

The final result of this third order Taylor series expansion is written as (Crane et al., 1989):

$$\begin{aligned}
 (\Delta_z - X_z) \dot{u} = & X^o + X_u \delta u + \frac{1}{2} X_{uu} \delta u^2 + \frac{1}{6} X_{uuu} \delta u^3 + \frac{1}{2} X_{vv} v^2 + \frac{1}{2} X_{rr} r^2 \\
 & + \frac{1}{2} X_{\delta\delta} \delta_R^2 + \frac{1}{2} X_{vvv} v^2 \delta u + \frac{1}{2} X_{rrr} r^2 \delta u + \frac{1}{2} X_{\delta\delta\delta} \delta_R^2 \delta u \\
 & + (X_{vr} + \Delta_z) vr + X_{v\delta} v \delta_R + X_{r\delta} r \delta_R + X_{vrv} vr \delta u + X_{v\delta v} v \delta_R \delta u \\
 & + X_{r\delta r} r \delta_R \delta u
 \end{aligned}$$

$$\begin{aligned}
 (\Delta_y - Y_y) \dot{v} - Y_r \dot{r} = & Y^o + Y_v \delta u + Y_{vv} \delta u^2 + Y_v v + \frac{1}{6} Y_{vvv} v^3 + \frac{1}{2} Y_{vrv} vr^2 + \frac{1}{2} Y_{v\delta\delta} v \delta_R^2 \\
 & + Y_{vv} v \delta u + \frac{1}{2} Y_{vvv} v \delta u^2 + (Y_r - \Delta_y \mu_1) r + \frac{1}{6} Y_{rrr} r^3 + \frac{1}{2} Y_{rvr} rv^2 \\
 & + \frac{1}{2} Y_{r\delta\delta} r \delta_R^2 + Y_{rv} r \delta u + \frac{1}{2} Y_{rvv} r \delta u^2 + Y_{r\delta} \delta_R + \frac{1}{6} Y_{\delta\delta\delta} \delta_R^3 + \frac{1}{2} Y_{\delta\delta v} \delta_R v^2 \quad (8) \\
 & + \frac{1}{2} Y_{\delta r} \delta_R r^2 + Y_{\delta v} \delta_R \delta u + \frac{1}{2} Y_{\delta vv} \delta_R \delta u^2 + Y_{vr\delta} vr \delta_R
 \end{aligned}$$

$$\begin{aligned}
 (I_z - N_z) \dot{r} - N_v \dot{v} = & N^o + N_u \delta u + N_{uu} \delta u^2 + N_v v + \frac{1}{6} N_{vvv} v^3 + \frac{1}{2} N_{vrv} vr^2 \\
 & + \frac{1}{2} N_{v\delta\delta} v \delta_R^2 + N_{vv} v \delta u + \frac{1}{2} N_{vvv} v \delta u^2 + N_r r + \frac{1}{6} N_{rrr} r^3 \\
 & + \frac{1}{2} N_{rvr} rv^2 + \frac{1}{2} N_{r\delta\delta} r \delta_R^2 + N_{rv} r \delta u + \frac{1}{2} N_{rvv} r \delta u^2 + N_{r\delta} \delta_R \\
 & + \frac{1}{6} N_{\delta\delta\delta} \delta_R^3 + \frac{1}{2} N_{\delta\delta v} \delta_R v^2 + \frac{1}{2} N_{\delta r} \delta_R r^2 + N_{\delta v} \delta_R \delta u + \frac{1}{2} N_{\delta vv} \delta_R \delta u^2 \\
 & + N_{vr\delta} vr \delta_R
 \end{aligned}$$

These equations have been simplified somewhat by eliminating numerous terms that appear due to the mathematics of expanding the functional equation as a Taylor series. Upon closer

examination of the physical meaning of these terms, it becomes clear that not all are necessary, for physical reasons. A detailed explanation of the dismissal of these terms is given in Crane et al. (1989).

The common practice is to nondimensionalise these coefficients by using parameters related to the ship's principal dimensions and the environment in which it operates. The next section develops the nondimensionalising terms through dimensional analysis techniques and will be used in conjunction with the equations of motion to write the final version of these equations. Based on the results, then, the method of experimentation derivatives can be determined, considering equipment limitations.

### 3.3 DIMENSIONAL ANALYSIS AND SIMILARITY

In order to design an experimental process for the problem described, it is necessary to first determine the parameters that affect the manoeuvrability of a ship. Only after a clear understanding of the problem is it possible for such parameters to be written and for this reason, various works by authors in the field of ship-ice interaction were consulted. As described above, the aim of this work is to determine the effect of a broken ice field on the manoeuvrability of a ship transiting it. It is necessary to determine the variables involved in order to decide on important aspects of the experimental design such as similitude requirements, and to ensure that the equations developed are the most convenient for analytic application. The functional relationship

$$\begin{Bmatrix} X \\ Y \\ N \end{Bmatrix} = \Phi(g, \rho_w, \rho_i, \mu, V, \dot{\psi}, \ddot{\psi}, \dot{\psi}, L, B, T, \Delta_s, \Delta_i, C, f, t, I_z, \sigma_c, \sigma_f, E, \delta_x) \quad (9)$$

completely defines the variables involved in determining hull forces for a ship manoeuvring in a broken ice field. These variables will be used for the derivation of functional relationships in the development of the ship manoeuvrability equations, and give an indication of the parameters that should be considered in design of the experiments. The

variable dimensions are given, assuming the Mass, Length, Time system of units, or  $M, L, T$  and assumes the SI system of units (Table 3.1). For more detail on the methods and theory of dimensional analysis, the reader is referred to the works of Sharp & Moore (1983), Barr (1985), Sharp & Moore (1988) and Sharp et al. (1992).

It is possible to reduce the number of variables by considering some simplifications and assumptions. However, variables are not removed from the analysis unless it is certain that the problem definition will not suffer. The following variables can be removed from the similarity analysis:

- $\psi, \dot{\psi}$  the towing tank is not equipped with apparatus to vary heading angle accurately while a model is being towed down the tank.
- $\alpha_c, \alpha_f, E$  the ice is assumed to interact with the ship purely in a rigid-body manner (i.e. no bending failure or compression of ice pieces will occur).

Table 3.1 Variable dimensions, assuming the  $[M][L][T]$  system.

Variable		Units
$X, Y$	$\text{kg} \cdot \text{m} \cdot \text{s}^{-2}$	$[M][L][T]^{-2}$
$N$	$\text{kg} \cdot \text{m}^2 \cdot \text{s}^{-2}$	$[M][L]^2[T]^{-2}$
$g$	$\text{m} \cdot \text{s}^{-2}$	$[L][T]^{-2}$
$\rho_w, \rho_i$	$\text{kg} \cdot \text{m}^{-3}$	$[M][L]^{-3}$
$\mu$	$\text{kg} \cdot \text{m}^{-1} \cdot \text{s}^{-1}$	$[M][L]^{-1}[T]^{-1}$
$V$	$\text{m} \cdot \text{s}^{-1}$	$[L][T]^{-1}$
$\psi$	radians	---
$\dot{\psi}$	radians $\cdot \text{s}^{-1}$	$[T]^{-1}$
$\dot{V}$	$\text{m} \cdot \text{s}^{-2}$	$[L][T]^{-2}$
$\ddot{\psi}$	radians $\cdot \text{s}^{-2}$	$[T]^{-2}$
$L, B, T$	m	$[L]$
$\Delta_o, \Delta_i$	kg	$[M]$
$l$	m	$[L]$
$I_c$	$\text{kg} \cdot \text{m}^2$	$[M][L]^2$
$\sigma_o, \sigma_f$	$\text{kg} \cdot \text{m}^{-1} \cdot \text{s}^{-2}$	$[M][L]^{-1}[T]^{-2}$
$E$	$\text{kg} \cdot \text{m}^{-1} \cdot \text{s}^{-2}$	$[M][L]^{-1}[T]^{-2}$
$\delta_f$	radians	---

Keeping the above simplifications and assumptions in mind, the functional equation can be rewritten as:

$$\begin{Bmatrix} X \\ Y \\ N \end{Bmatrix} = \Phi(g, \rho_w, \rho_l, \mu, V, L, B, T, \Delta_x, \Delta_l, h, I_z, C, f, \psi, \delta_x) \quad (10)$$

Since terms  $C$ ,  $f$ ,  $\psi$  and  $\delta_x$  in the functional equation are nondimensional, it would be pointless to include them in the analysis and so they are added on to the nondimensional equations written later. Vessel acceleration  $\dot{V}$  is also not included in this analysis, since the acceleration due to gravity would represent any acceleration terms in the analysis.

Using the method as outlined by Sharp and Moore (1988), matrices can be developed which allow for deduction of nondimensional terms, and provide the analyst with the ability to test different configurations of variables, as long as the matrix deduced meets the requirement of the method.

First, we construct a matrix to define the  $X$  and  $Y$  forces on the hull:

$$\begin{bmatrix} & V & \rho_w & L & | & g & \mu & B & T & \Delta_x & \Delta_l & \rho_l & h & I_z & X, Y \\ \mathbf{M} & 0 & 1 & 0 & | & 0 & 1 & 0 & 0 & 1 & 1 & 1 & 0 & 1 & 1 \\ \mathbf{L} & 1 & -3 & 1 & | & 1 & -1 & 1 & 1 & 0 & 0 & -3 & 1 & 2 & 1 \\ \mathbf{T} & -1 & 0 & 0 & | & -2 & -1 & 0 & 0 & 0 & 0 & 0 & 0 & 0 & -2 \end{bmatrix} \quad (11)$$

The variables  $V$ ,  $L$  and  $\rho_w$  were chosen to be repeated in the analysis, since they will not be measured in the testing process, and thus allow for the formulation of convenient nondimensional terms (the parameters to be measured are related to forces only and thus should appear the fewest number of times possible in the nondimensional equation). Also, by using these three terms for repetition it is anticipated that several of the resulting nondimensional terms will be of a familiar form.

Similarly, a matrix can be constructed for determination of  $N$  - the yaw moment:

$$\begin{bmatrix} & V & \rho_w & L & | & g & \mu & B & T & \Delta_x & \Delta_y & \rho_l & h & I_z & N \\ \mathbf{M} & 0 & 1 & 0 & | & 0 & 1 & 0 & 0 & 1 & 1 & 1 & 0 & 1 & 1 \\ \mathbf{L} & 1 & -3 & 1 & | & 1 & -1 & 1 & 1 & 0 & 0 & -3 & 1 & 2 & 2 \\ \mathbf{T} & -1 & 0 & 0 & | & -2 & -1 & 0 & 0 & 0 & 0 & 0 & 0 & 0 & -2 \end{bmatrix} \quad (12)$$

By inverting the  $3 \times 3$  matrix in the left portion of Equations (11) and (12) and multiplying by the remainder of each matrix, the following can be obtained:

$$\begin{bmatrix} & g & \mu & B & T & \Delta_x & \Delta_y & \rho_l & h & I_z & X,Y \\ V & 2 & 1 & 0 & 0 & 0 & 0 & 0 & 0 & 0 & 2 \\ \rho_w & 0 & 1 & 0 & 0 & 1 & 1 & 1 & 0 & 1 & 1 \\ L & -1 & 1 & 1 & 1 & 3 & 3 & 0 & 1 & 5 & 2 \end{bmatrix} \quad (13)$$

$$\begin{bmatrix} & g & \mu & B & T & \Delta_x & \Delta_y & \rho_l & h & I_z & N \\ V & 2 & 1 & 0 & 0 & 0 & 0 & 0 & 0 & 0 & 2 \\ \rho_w & 0 & 1 & 0 & 0 & 1 & 1 & 1 & 0 & 1 & 1 \\ L & -1 & 1 & 1 & 1 & 3 & 3 & 0 & 1 & 5 & 3 \end{bmatrix} \quad (14)$$

Here, Equations (13) and (14) refer to Equations (11) and (12) respectively and are used to form the dimensionless functional equations for surge, sway, and yaw forces as:

$$\begin{bmatrix} X \\ V^2 L^2 \rho_w \\ Y \\ V^2 L^2 \rho_w \\ N \\ V^2 L^3 \rho_w \end{bmatrix} = \Phi \left( \frac{gL}{V^2}, \frac{\mu}{V \rho_w L}, \frac{B}{L}, \frac{T}{L}, \frac{\Delta_x}{\rho_w L^3}, \frac{\Delta_y}{\rho_w L^3}, \frac{\rho_l}{\rho_w}, \frac{h}{L}, \frac{I_z}{\rho_w L^3}, C, f, \psi, \delta_R \right) \quad (15)$$

Examination of Equation (15) shows that a more recognisable result can be produced through compounding of terms:

- for the first term, invert and take the square root,
- for the second term, set  $\mu/\rho_w = \nu$  (kinematic viscosity) and invert, and
- for the left-hand-side of the equation, divide the denominator by one half to obtain a nondimensionalising factor of the form  $1/2mV^2$ .

The resulting equation would be:

$$\left( \frac{\frac{X}{\frac{1}{2}V^2L^2\rho_w}}{\frac{Y}{\frac{1}{2}V^2L^2\rho_w}} \right) = \Phi \left( \frac{V}{\sqrt{gL}}, \frac{VL}{\nu}, \frac{B}{L}, \frac{T}{L}, \frac{\Delta_s}{\frac{1}{2}\rho_wL^3}, \frac{\Delta_i}{\frac{1}{2}\rho_wL^3}, \frac{\rho_i}{\rho_w}, \frac{h}{L}, \frac{I_z}{\rho_wL^2}, C, f, \psi \right) \quad (16)$$

Several terms in Equation (16) appear familiar, and several important points related to similarity can be raised about the experiments. In general, when conducting scaled model experiments, the best situation (most accurate) would be to satisfy dynamic, kinematic, and geometric similarity. With this in mind, we consider the following terms from Equation (16):

- $\frac{V}{\sqrt{gL}}$  This is the Froude number, which should be equal for both the model and prototype.
- $\frac{VL}{\nu}$  This is the Reynolds number, which should also be the same for both model and prototype.
- $\frac{B}{L}, \frac{T}{L}, \frac{\Delta_s}{\frac{1}{2}\rho_wL^3}$  These are geometric ratios relating to the ship, and must be the same for model and prototype in order for the ship to be considered geometrically similar.

- $\frac{\rho_i}{\rho_w}, \frac{\Delta_i}{\frac{1}{2}\rho_w L^3}, \frac{h}{L}$ 

Similarly, these are the geometric ratios relating to the model ice, and must be the same for model and prototype in order for the ice environment to be considered geometrically similar to the full scale situation. Based on this condition for similarity, a material must be chosen to model the ice pieces that has the same density as the full scale and is cut to similar geometry.
- $\frac{I_z}{\rho_w L^5}$ 

This ratio is related to vessel's mass moment of inertia, and must be the same in both model and prototype in order for the ship's motions to be considered similar.
- $C$ 

The concentration of ice cover, as specified by this parameter, must be equal in both model and prototype.
- $f$ 

Care must be taken to ensure that the friction factor between hull and ice is the same for model and full scale, otherwise the accuracy of the model measurements will be in error.
- $\psi$ 

Finally, the heading angle of the ship should be the same in model and prototype.

One problem encountered above is related to the necessity to have both Reynolds and Froude similarity. It is obvious from the form of these equations that both cannot be satisfied at the same time. Based on past work and review of material from researchers in ship model testing, it was decided that since the movement of a ship on the surface of water is dominated by gravitational forces, Froude similitude should be obeyed. Since the effects related to Reynolds number are considered to be small in this type of test, their effect on error in the measurements should be quite small.

If the necessary conditions are met in the above points, the experiments should provide useful results, and using the nondimensional terms (Equation 16), the equations of motion (Equations 8) are rewritten in standard nondimensional form as:

$$\begin{aligned}
(\Delta'_s - X'_u)u' &= X''^o + X''_u \delta u' + \frac{1}{2} X''_{uu} \delta u'^2 + \frac{1}{6} X''_{uuu} \delta u'^3 + \frac{1}{2} X''_{vv} v'^2 + \frac{1}{2} X''_{\delta\delta} \delta_R^2 \\
&\quad + \frac{1}{2} X''_{vvv} v'^2 \delta u' + \frac{1}{2} X''_{\delta\delta\delta} \delta_R^2 \delta u' + X''_{v\delta} v' \delta_R + X''_{v\delta v} v' \delta_R \delta u' \\
(\Delta'_s - Y'_v)v' &= Y''^o + Y''_u \delta u' + Y''_{uu} \delta u'^2 + Y''_v v' + \frac{1}{6} Y''_{vvv} v'^3 + \frac{1}{2} Y''_{v\delta\delta} v' \delta_R^2 + Y''_{vv} v' \delta u' \\
&\quad + \frac{1}{2} Y''_{vvv} v' \delta u'^2 + Y''_{\delta\delta} \delta_R + \frac{1}{6} Y''_{\delta\delta\delta} \delta_R^3 + \frac{1}{2} Y''_{\delta\delta v} \delta_R v'^2 + Y''_{\delta\delta} \delta_R \delta u' + \frac{1}{2} Y''_{\delta\delta\delta} \delta_R \delta u'^2 \quad (17) \\
-N'_v v' &= N''^o + N''_u \delta u' + N''_{uu} \delta u'^2 + N'_v v' + \frac{1}{6} N''_{vvv} v'^3 + \frac{1}{2} N''_{v\delta\delta} v' \delta_R^2 \\
&\quad + N''_{vv} v' \delta u' + \frac{1}{2} N''_{vvv} v' \delta u'^2 + N''_{\delta\delta} \delta_R + \frac{1}{6} N''_{\delta\delta\delta} \delta_R^3 + \frac{1}{2} N''_{\delta\delta v} \delta_R v'^2 + N''_{\delta\delta} \delta_R \delta u' \\
&\quad + \frac{1}{2} N''_{\delta\delta\delta} \delta_R \delta u'^2
\end{aligned}$$

Since the tests to be conducted involve straight line towing with no dynamic change in ship heading angle, the reader will notice that the rotational terms related to  $r$  and  $\dot{r}$  have been removed from these equations. Removing the surge equation and various unnecessary terms from equation (17) we get:

$$\begin{aligned}
(\Delta'_s - Y'_v)v' &= Y''^o + Y'_v v' + \frac{1}{6} Y''_{vvv} v'^3 + \frac{1}{2} Y''_{v\delta\delta} v' \delta_R^2 + Y''_{\delta\delta} \delta_R + \frac{1}{6} Y''_{\delta\delta\delta} \delta_R^3 + \frac{1}{2} Y''_{\delta\delta v} \delta_R v'^2 \\
-N'_v v' &= N''^o + N'_v v' + \frac{1}{6} N''_{vvv} v'^3 + \frac{1}{2} N''_{v\delta\delta} v' \delta_R^2 + N''_{\delta\delta} \delta_R + \frac{1}{6} N''_{\delta\delta\delta} \delta_R^3 + \frac{1}{2} N''_{\delta\delta v} \delta_R v'^2 \quad (18)
\end{aligned}$$

where each term in the first equation represents sway force and each term in the second equation represents yaw moment. The prime (') notation is used here to designate a nondimensionalised variable. The following factors were used:

$$\begin{aligned}
\Delta'_s &= \frac{\Delta_s}{\frac{1}{2} \rho_w L^3} \quad ; \quad v' = \frac{v}{V} \quad ; \quad \dot{v}' = \frac{\dot{v}L}{V^2} \\
Y'_v &= \frac{Y_v}{\frac{1}{2} \rho_w L^2 V} \quad ; \quad N'_v = \frac{N_v}{\frac{1}{2} \rho_w L^2 V} \\
Y'_v &= \frac{Y_v}{\frac{1}{2} \rho_w L^3} \quad ; \quad N'_v = \frac{N_v}{\frac{1}{2} \rho_w L^4}
\end{aligned} \quad (19)$$

### 3.4 METHODS FOR DETERMINING COEFFICIENTS

Based on the above analysis, a brief discussion of the experimental method for determining hydrodynamic coefficients for a ship must be given. Hydrodynamic coefficients can be determined through a number of different ways of experimentation, however, very few research organisations can experimentally determine all coefficients in-house, since the apparatus needed are quite specialised for testing to find certain types of coefficients. A summary of these types of experiments, coefficients determinable, and types of motion are given in Table 3.2.

Table 3.2 Experimental methods available for determining hydrodynamic coefficients (Gill, 1980 & Crane et al., 1989).

Coefficient	Type	Motion	Test Method	
$Y_v$	Linear	Sway	SLT, PMM	
$N_v$	Hull	Sway	SLT, PMM	
$Y_{ar}$	Nonlinear Hull Damping	Yaw	ROT, PMM, FM	
$N_{ar}$		Yaw	ROT, PMM, FM	
$Y_{vv}$		Sway	SLT	
$N_{vv}$		Sway	SLT	
$Y_{rr}$		Yaw	ROT	
$N_{rr}$		Yaw	ROT	
$Y_f$		Acceleration	Sway	PMM
$N_f$			Sway	PMM
$Y_r$	Yaw		PMM	
$N_r$	Yaw		PMM	
Note:	SLT Straight Line Towing ROT Rotating Arm Test PMM Planar Motion Mechanism FM Free Running Model			

As can be seen in the table, only a small number of coefficients can be found in the towing tank of the Faculty of Engineering and Applied Science (MUN) due to the fact that the only test method available is the straight-line towing technique.

The rotating arm test involves a very specialised piece of equipment and is expensive since only the rotational hydrodynamic coefficients can be determined in such a facility. Also, the testing tank must be quite large to obtain good accuracy. The other methods - planar motion mechanism and free running model testing are also quite specialised and the latter is useful mainly for validating the predictions from a set of experiments (Crane et al., 1989 and Gill, 1980). A planar motion mechanism was developed for use in conventional long and narrow towing tanks for the measurement of velocity-dependant, rotary and acceleration derivatives (Crane et al., 1989).

The technique for determining coefficients in the straight-line tow test is reasonably simple - a ship model is towed down the tank a number of times while varying speed and heading angle between tests. Forces in the  $x$  and  $y$  directions are measured, along with tow carriage speed. The data is plotted as mean measured force on the  $y$ -axis ( $X$ ,  $Y$ , or  $N$ , depending on which coefficient is to be computed) and corresponding velocities on the  $x$ -axis. The slope of the line resulting from regression fit to the data gives the value of the linear hydrodynamic derivative in question. A new technique for determining the sway acceleration derivatives is also proposed in this thesis using straight-line towing with tow carriage acceleration. This technique is described in Chapter 5 along with the standard methods used to experimentally determine other straight-line derivatives.

If a full complement of a ship's coefficients is required, those which cannot be measured would have to be predicted using empirical or semi-empirical methods laid out by various experts in the field (Chapter 2). A comparison of the coefficients determined in this thesis is made with semi-empirical methods in Chapter 6.

Development of the surge ( $X$ ) equation of motion is a vital part of nonlinear analysis for simulation of tight manoeuvres (high rates of turn), since such manoeuvres involve large

speed losses (Crane et al., 1989). Since we are considering only linear manoeuvres in this thesis, the equation for surge can be legitimately removed from the analysis.

### 3.5 TEST MATRIX AND FULL-SCALE IMPLICATIONS

The test matrix given in Table 3.3 was decided upon in order to produce a comprehensive set of results. The total number of towing tank tests required to complete this test matrix was 480 (resulting from 2 ship models, 2 surface conditions, 2 constant velocities, 2 constant accelerations, 5 rudder angles and 6 heading angles).

Table 3.3 Experiment test matrix.

Variables	Values
Ship Models	M.V. Arctic & R-Class hullform
Heading Angles	0°, 2°, 4°, 6°, 8° & 10° (all to port side)
Rudder Angles	10° & 5° to port, 10° & 5° to stbd & 0°
Constant Carriage Velocities	0.5 & 1.0 m/s
Constant Carriage Accelerations	0.02 & 0.04 m/s <sup>2</sup>
Water Surface Conditions	Open & Pack Ice

These parameters were chosen to satisfy reasonable ranges of the parameters and in order to provide realistic inputs when considering the full-scale situation. Scaling the tow velocities and pack ice sizes to prototype resulted in the values given in Table 3.4. While the higher velocities may be a little high for operations in ice environments, they are still not beyond the realm of realistic values. Pack ice sizes were based on wax pancakes available in storage. The full-scale sizes show that the individual pieces can be classed as thin to medium first year ice ranging from ice cakes to small floes. Details of the models, equipment and tests conducted are given in the following chapters.

Consideration was also given to potential towing tank blockage effects. Using the blockage correction calculation given by Conn et al. (1953) it was estimated that the

blockage correction factor would be approximately 1% for the M.V. Arctic at 10° heading angle with a carriage speed of 1m/s. This represents the worst case for blockage effects over the entire test matrix and is considered to be negligible.

Table 3.4 Full scale values for velocities tested and wax sizes.

Scale & Ship	Velocity (m/s)		Wax Diameter (m)				Wax Thickness (m)
Model	0.5	1.0	0.10	0.15	0.20	0.25	0.013
1:80 (M.V. Arctic)	4.5	9.0	8.08	12.00	16.08	19.68	1.040
1:40 (R-Class)	3.2	6.4	4.04	6.000	8.04	9.84	0.520

# Chapter 4: Description and Preparation of Apparatus

## 4.1 SHIP MODELS

Two icebreaking hullform models were tested in the towing tank facility at the Faculty of Engineering and Applied Science, Memorial University of Newfoundland – a 1:80 scale model of the M.V. Arctic and a 1:40 scale model of the R-Class icebreaker hullform (see Table 4.1 for model particulars).

In the full scale, the M.V. Arctic is an existing bulk carrier that was modified for use in ice environments to ASPPR Class 4. The R-Class hullform is an ASSPR Class 3 (Edwards et al., 1981) icebreaking hullform. Several Canadian Coast Guard vessels utilise this design, most notably the CCGS Pierre Radisson and the CCGS Louis St. Laurent.

The models were both equipped with workable rudders that could be set to pre-marked static rudder angles (in 5° increments). Thus, rudder angle could be accurately set to a known, repeatable rudder angle for each test. For the open water test series, both models were fitted with bow turbulence stimulators. These were removed for pack ice tests. These small brass studs were positioned at the bow, spaced approximately every 2cm from the keel to just above the waterline. The studs were installed in order to prevent laminar flow over the models and thus reduce the effect of Reynolds number scaling problems (see Chapter 3).

In general, when testing a ship model for manoeuvrability, propulsion gear is added to the model (scaled propeller, shafting, and motor) to better represent the full-scale. The shaft RPM would be set so that the model operated just at the self-propulsion point, thus improving modeled flow characteristics around the stern of the vessel and the across the

rudder (Crane et al., 1989). Although outfitting models in this way would be preferable, it was not possible for this experimental program due to financial considerations. The M.V. Arctic model, however, was already fitted with a propeller nozzle.

Table 4.1 Ship model particulars.

Variable	R-Class	M.V. Arctic
$\lambda$ (scale)	1:40	1:80
L (m)	2.192	2.456
B (m)	0.484	0.2857
D (m)	0.310	0.204
T (m)	0.1785	0.1371
$\Delta_s$ (kg)	117.6	70.20

Both models were spray painted with yellow polyurethane two part enamel; the M.V. Arctic at the National Research Council's Institute for Marine Dynamics, and the R-Class at Memorial University's Division of Technical Services.

Model characteristics for the M.V. Arctic can be seen in Figure 4.1 and Figure 4.2. Characteristics for the R-Class hullform can be seen in Figure 4.3 and Figure 4.4. Further details of both models are given in Appendix A.

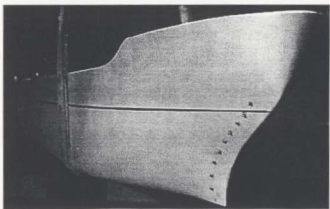


Figure 4.1 Bow view of M.V. Arctic model, showing turbulence stimulators.



Figure 4.2 Stern view of M.V. Arctic model showing the nozzle, rudder, and rudder angle set device.



Figure 4.3 Bow view of the R-Class model, with turbulence stimulators removed for pack ice testing.



Figure 4.4 Stern view of R-Class model showing the rudder, and rudder angle set device.

## 4.2 FORCE MEASUREMENT

### 4.2.1 *Dynamometer Description*

In order to accurately measure the forces expected in the experimental portion of work (surge force, sway force, and yaw moment), it was necessary to use a rigid dynamometer with at least three load cells. An in-house dynamometer was used for this purpose since it was capable of directly measuring forces in the horizontal (x-y) plane. Since two load cells, located equidistant forward and aft of the dynamometer centreline, were used to measure total sway force, it was possible to calculate yaw moment using the distance between the load cells (equal to 0.3685m). It is important to note that each ship model was mounted with its centreline aligned to the centreline of the dynamometer. By doing this, yaw moment was calculated about midships.

The dynamometer was constructed of two rigid plates - a top plate and a bottom plate. The top plate was mounted to the rigid towing device (towing tank carriage) and the bottom plate was mounted to the model through a towing bracket (see Figure 4.5). These two plates were connected to each other by load cells and specially designed flexible linkages (flex-links). Four vertically oriented flex-links connected the top plate directly to the bottom plate, and partially held the weight of the bottom plate. One flex-link connected the top plate mounted surge force load cell to the bottom plate, and a flex-link connected each top plate mounted sway force load cell to the bottom plate. In all, there were a total of three load cells and seven flex-links. Refer to Figure 4.6 and Figure 4.7 for a drawing and photograph of the dynamometer and its components, respectively.

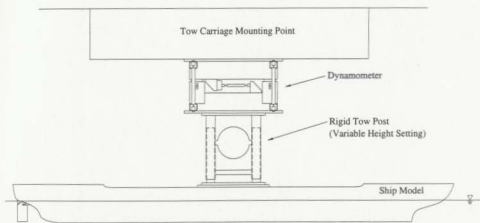


Figure 4.5 Schematic showing dynamometer connection to ship model.

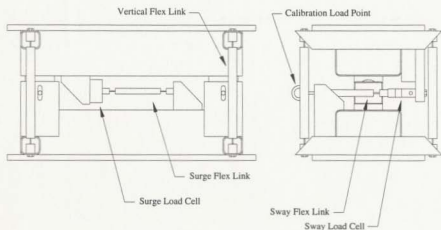


Figure 4.6 Dynamometer schematic and internal components.

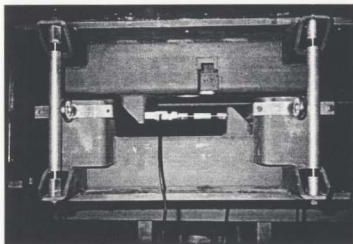


Figure 4.7 Photograph of dynamometer and internal components.

#### 4.2.2 *Sizing the Load Cells*

In order to determine the capacity of load cells to be used in the dynamometer, it was necessary to estimate the forces expected in the experiments. The sizing was done early in the experiment preparation stage, since the expected load would also determine the dimensions of the flex-links.

Since hydrodynamic coefficients for the M.V. Arctic and the R-Class hullform were not readily available, it was deemed reasonable to use coefficients for the Mariner Class hullform as given by Crane et al. (1989). Though these hullforms are not geometrically similar (Table 4.2), it was expected that making an estimate in this way would give forces on the same order of magnitude. To make the estimate a little more conservative, 10% was added to the final values.

Three load cases were considered for the force estimate:

1. Steady State: forces experienced when the model is towed at constant velocity.

2. Transient: forces experienced while the model accelerates to the test velocity.
3. Constant Acceleration: forces experienced as the model is towed at constant acceleration.

Table 4.2 Coefficients, geometric ratios, and appendages for the models tested and the mariner hullform

Variable	Mariner	M.V. Arctic	R-Class
$C_B$	0.61	0.73	0.644
$C_P$	0.62	0.737	0.721
L/B	6.84	8.596	4.529
L/T	21.19	17.91	12.28
B/T	3.10	2.084	2.711
Propeller	NO	NO	NO
Rudder	YES	YES	YES

Clearly, case (2) would result in the greatest dynamometer forces for the open water tests, however, such transient loads are difficult to predict. The usual practice is to estimate the steady state load and double the result to cover transient forces experienced as the model accelerates to the constant velocity (verbal discussions with John Bell, IMD, Spring, 1996).

To estimate the maximum dynamometer force then, it was necessary to determine the maximum force for case (1) and double the result to get a design load. The equations of motion from Chapter 3 were employed in a short computer program to compute the nondimensional force over the range of heading angles  $0^\circ$ ,  $2^\circ$ ,  $4^\circ$ ,  $6^\circ$ ,  $8^\circ$ ,  $10^\circ$ , and rudder angles  $-10^\circ$ ,  $-5^\circ$ ,  $0^\circ$ ,  $5^\circ$ ,  $10^\circ$ . The program output the largest force value along with the heading and rudder angles at which these would occur. The resulting nondimensional maximum open water loads were:

$$X'_{\max} = -0.00630828$$

$$Y'_{\max} = +0.06197770$$

As anticipated, these values occurred at  $\beta = 10^\circ$ , and  $\delta_R = 10^\circ$ . Knowing the nondimensionalising terms from Chapter 3

$$\begin{aligned} X' &= \frac{X}{\frac{1}{2} \rho V^2 L^2} \\ Y' &= \frac{Y}{\frac{1}{2} \rho V^2 L^2} \end{aligned} \quad (20)$$

with  $\rho = 1000 \text{ kg/m}^3$ ,  $V_1 = 1.0 \text{ m/s}$ ,  $V_2 = 0.5 \text{ m/s}$ ,  $L_{mv \text{ arctic}} = 2.456 \text{ m}$ ,  $L_{r\text{-class}} = 2.192 \text{ m}$ , the maximum forces expected on the dynamometer were computed for the M.V. Arctic at  $V_2 = 1.0 \text{ m/s}$  to be:

$$X_{\max} = 19.02 \text{ N}$$

$$Y_{\max} = 186.92 \text{ N}$$

Adding 10% for hull geometrical differences (since we assumed a Mariner hullform):

$$X_{\max} = 21 \text{ N}$$

$$Y_{\max} = 206 \text{ N}$$

Based on this calculation, the decision was made to choose two 223 N maximum load cells for sway force measurement (twice the computed value to cover transient loads) and one 112 lb maximum load cell for surge force measurement (no smaller load cells were available). Details of the load cells used in the dynamometer are given in Appendix B. Using the load information, the size of flex-links was then determined.

### **4.2.3 Flex-Link Design**

Flex-links (Figure 4.8) were used to hold the dynamometer together and transmit forces to the load cells in such a way that only surge force was measured by the surge load cell and only sway force was measured by the sway load cells. The ability of the flex-links to permit this is based on the design, since they are stiff in the axial direction but flexible in the transverse direction (Figure 4.9). Since the load cells were connected to both the top plate (rigidly mounted to the towing carriage) and bottom plate (rigidly attached to the model), any horizontal force on the model would cause movement of the bottom plate relative to the top plate, and thus a deflection in the load cells. When calibrated, this load cell deflection was output as a force (for detailed description of the calibration procedure, see Section 5.2). It was important when designing the flex-links that both transverse flexibility and axial strength be maximized. By doing this, it was possible to minimize the effect of cross-talk between the three load cells. Some amount of cross-talk was unavoidable in this situation due to the nature of the dynamometer's design (i.e. all load cells were indirectly connected to each other). By making the links very flexible in the transverse direction, energy lost in bending links perpendicular to the applied load was kept low. The design of these components was based on a spreadsheet developed by engineers and technicians at the National Research Council's Institute for Marine Dynamics (Figure 4.10). This spreadsheet is used to perform bending calculations from simple beam theory and a stiffness buckling calculation based on the axial strength of cylindrical members.

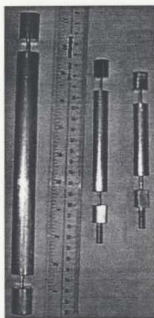


Figure 4.8 Photograph of three different flex-link sizes used.

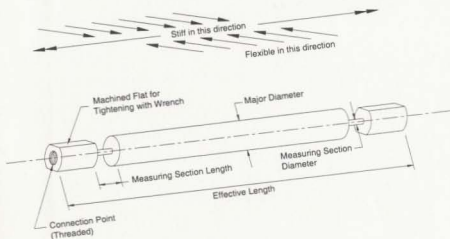


Figure 4.9 Schematic of flex-link indicating directions of desirable flexibility and stiffness.

**Diameter Calculation for Measuring Section of Flex-Links for Single Axis Load Cell**  
(Aluminum 7075-T651)

Design Criteria	Sway Links		Surge Links		Vertical Links		Notes
	Min.	+ Tol.	Min.	+ Tol.	Min.	+ Tol.	
Design Load Capacity (lb)	50	50	25	25	105	105	
Material Yield Point	72000	72000	72000	72000	72000	72000	
Material Young's Modulus (lb)	10400000	10400000	10400000	10400000	10400000	10400000	
Effective Length for Flexible Link	3.9	3.9	2.4	2.4	9.0	9.0	
Length of the Measuring Section	0.39	0.39	0.50	0.50	0.50	0.50	
Major Diameter	0.75	0.75	0.51	0.51	0.75	0.75	
Trial Diameter from P/A Ratio	0.0297	0.0297	0.0210	0.0210	0.0431	0.0431	
Actual Diameter for Measuring Section	0.1024	0.1028	0.0709	0.0713	0.1500	0.1550	Enter a value for testing
Axial Stiffness	101912	102547	38977	40410	139230	146263	Uses A/E/L for the large and small diameters
Flexural Stiffness	11	11	12	12	4	4	Uses fixed guided cantilever equation
Axial to Flexural Ratio	9254	9179	3417	3376	32796	30208	
Buckling Slenderness Ratio	12	12	23	22	11	10	Uses effective length = 0.8 for fixed guide
Critical Buckling Stress	677613	882836	201359	203602	902144	963289	Uses Euler's equation. Valid for slenderness ratio > 53
Actual Compressive Stress	6076	6029	6306	6266	5942	5960	This is P/A for diameter chosen
Load at which Buckling Occurs	593	597	264	267	1272	1359	Based on Fig. 14.3 1-7 Design of Welded Structures

Figure 4.10 Sample of the flex-link design spreadsheet.

Trial particulars (design load capacity, effective length for flex-link, length of measuring section, and major diameter) were entered in the spreadsheet. Using these values, a minimum trial diameter for the measuring section of the flex link was calculated. See Table 4.3 and Figure 4.9 for an explanation of the meaning of these terms. Two values computed in the spreadsheet were used to ensure the design criteria were met. These were the axial to flexural stiffness ratio (A/F ratio) and load at which buckling occurs. The A/F ratio was judged according to the criteria in Table 4.4 and provided a check on the amount of transverse flexibility in the flex-link design. Checking the load at which buckling occurs ensured the flex-link would not buckle under normal expected loads; this parameter was deemed acceptable as long as it was above the design load capacity specified. If the spreadsheet output design did not meet these two criteria, new input values were entered and the criteria checked again. When the design criteria were met, a diameter was chosen slightly above the minimum trial diameter that was convenient for manufacturing purposes.

Table 4.3 Input and output parameters for flex-link design.

Parameter	Description	Type
Design Load Capacity	Capacity of load cell to which the flex-link is connected.	Input
Effective Length	Overall length of the flex link, dictated by the dynamometer geometry and physical size of the load cell chosen.	Input
Measuring Section Length	Length of narrow diameter section where bending occurs (Figure 4.9).	Variable
Major Diameter	Diameter of flex-link body (Figure 4.9)	Variable
Measuring Section Diameter	Diameter of the narrow section where bending occurs (Figure 4.9)	Output

The design spreadsheet also computed all the values for a specified tolerance above the minimum dimension. Thus, desired tolerances could be placed on the engineering drawings to a maximum value above the dimension given, while still having confidence that the flex-link would meet the necessary design requirements in the range specified. Details of the flex-links that were designed and utilised in the tests are given in Appendix B.

All flex-links were designed using this spreadsheet method, where load cell capacities were used as design loads for the associated surge and sway flex-links. The design load on the vertical flex links, however, was slightly more involved, since the loads experienced by these flex-links were predominantly caused by vertical forces as a result of the moment from horizontal loads on the model. The forces on the model were assumed to act at the end of the tow post connecting the model to the dynamometer.

Table 4.4 A/F Ratio rating criteria.

A/F Ratio	Comment
A/F > 8000	Optimal
8000 > A/F > 5000	Good
5000 > A/F > 3000	Acceptable
3000 > A/F	Unacceptable

Figure 4.11a depicts the force acting on the tow post, Figure 4.11b shows the force transferred to the bottom plate as a moment, and Figure 4.11c shows it as a couple - two vertical forces acting in opposite directions through the axis of each vertical flex-link. The mathematical formulation is given here:

$$\begin{aligned} \text{Moment, } M &= F_h \cdot h = 2(F_v \cdot s/2) = F_v \cdot s \\ \therefore F_h \cdot h &= F_v \cdot s \rightarrow F_v = F_h \cdot h / s \end{aligned}$$

Since  $F_h = 245 \text{ N}$ ,  $h = 57.8 \text{ cm}$ ,  $s = 30.5 \text{ cm}$ , then  $F_v = 465 \text{ N}$  (per two flex-links)

For each flex-link, then, it was expected that the maximum load would be 232.5 N. In order to estimate possible transient loads, this estimate was doubled to make the design load 465N for each vertical flex-link. Using this load, the vertical flex-links were designed using the spreadsheet method outlined above.

The material used for flex-links was chosen to be 7075 T651-aluminum (commonly referred to as aircraft aluminum). The main reason for this choice of materials is based on strength and flexibility characteristics - since the forces expected in the tank tests were reasonably low, the flex links required would have to be slight; manufacturing slight flex links from weaker 6061 T6-aluminum would be difficult.

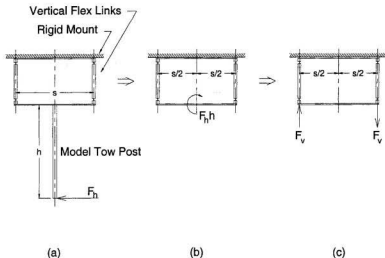


Figure 4.11 Conversion of tow post horizontal force to vertical flex-link force through moment equation.

Although these designs met the necessary requirements, some cross-talk between the channels would still be expected. However, when conducting a carefully controlled calibration of the dynamometer (Section 5.2), it was possible to measure this cross-talk and later remove it mathematically from the measured test data.

### 4.3 TOWING TANK

The fluids laboratory facilities at Memorial University of Newfoundland's Faculty of Engineering and Applied Science include a towing/wave tank primarily used for testing models of ships and offshore structures. The facility is equipped with a carriage that spans the tank and can be operated up to speeds of 5 m/s. The tank is 54.7m long, 4.57m wide, and 3m deep. A wave generator is located at one end and a wave-damping beach at the other (see Figure 4.12 for tank details).

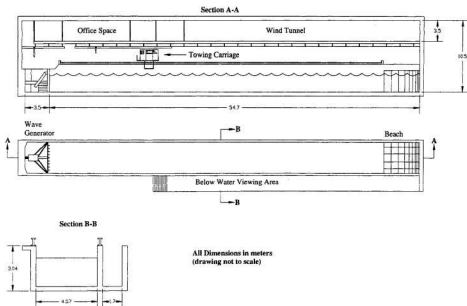


Figure 4.12 Towing tank schematic.

Before testing began, it was necessary to calibrate the velocity measurement transducers. This was done by driving the carriage down the tank at known pre-calibrated constant velocities, while using a computer to measure the output from transducers on the carriage. Thus, the constant velocity measurements were plotted against known velocities and the calibration stored in a calibration file for when testing began.

As previously described, half of the tests conducted were constant acceleration tests. Since normal operation of the towing carriage involved either towing models at constant speed, or measuring motion response to waves, it was necessary for special apparatus to be setup. In order to produce a constant acceleration of the carriage, a function generator and oscilloscope were wired to the control panel of the towing carriage. The function generator was set to produce a triangular waveform where the peak voltage, on the Y-axis, represented the maximum velocity desired and time was shown on the X-axis (Figure 4.13). The resulting acceleration could be found as the slope of the triangular

waveform. This setup was tested for a number of cases and found to be smooth, accurate, and repeatable (Figure 4.14).

The temperature and specific gravity of water in the tank were measured at the start of the test series and found to be 17.8°C and 1.0 respectively.

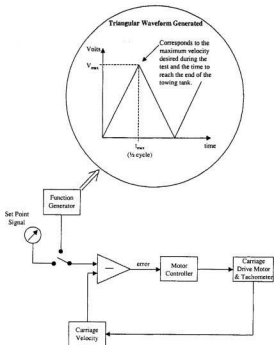


Figure 4.13 Carriage acceleration wiring schematic

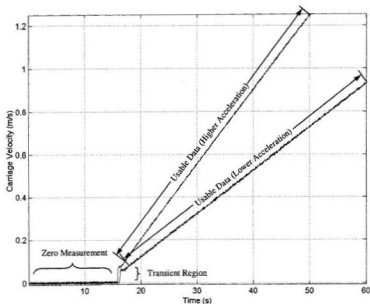


Figure 4.14 Carriage acceleration test plot showing velocity as a function of time

## 4.4 MODEL ICE

The paraffin wax used to model broken ice floes was stored in the fluids laboratory from previous test series simulating broken ice floes. Predominantly, the plan shape of the wax was hexagonal and consisted of four different sizes 88.1mm, 131.5mm, 175.1mm and 211.2mm average inscribed diameter (Figure 4.15), although an amount of smaller, broken wax pieces was also present. Average thickness of the wax was found to be 13.1mm. The wax used for these experiments was the same as that employed by Aboulazm (1989) who indicated it had a specific density of 0.88, and a coefficient of kinetic friction of 0.2. Aboulazm (1989) did not specify the way in which this friction coefficient was measured (ice-ice or hull-ice). According to Williams (2002), normal full-scale friction coefficients are in the range of 0.1 to 0.15, indicating that the coefficient of 0.2 may be high.



Figure 4.15 Three different wax sizes used during the tests

Through verbal discussion with an experienced research engineer at the National Research Council's Institute for Marine Dynamics (Williams, 1996), it was recommended that the pack ice portion of the experiments be conducted in concentrations greater than 80%; forces on a ship's hull in pack ice tend to be close to those in open water below about 80% (refer to Table 4.5 for the observed ranges). Based on this recommendation, it was decided that a surface coverage of 90% (or as close as possible to this) would be maintained throughout the pack ice portion of testing.

Table 4.5 Typical hull forces associated with ice coverage (Personal Conversation, Mary Williams, 1996).

Ice Concentration	Typical Hull Force
0% to 60%	Close to open water
60% to 80%	Marginally above open water
80% to 100%	Rapid increase in loads

Available containers of wax were weighed in order to obtain an estimate of the maximum attainable surface coverage (Table 4.6). A variety of samples were taken to estimate the average wax geometric properties (see Table 4.7). Of the four different sizes, 50 samples of both sizes 1 and 2 were taken, since these were the predominant wax pieces available. Also, because they were more difficult to locate, only 10 samples were taken of size 3, and 5 samples of size 4. Although it is not known what the actual proportion of each size was, these two larger sizes did not represent a significant portion of the population.

Table 4.6 Weights of individual containers of paraffin wax.

Container #	Total Weight (kg)	Container Weight (kg)	Wax Weight (kg)
1	326.6	58.1	268.5
2	337.0	58.1	278.9
3	353.8	58.1	295.7
4	521.6	72.6	449.0
<b>Total</b>			<b>1292.1</b>

Table 4.7 Mean and standard deviation of sampled wax geometry.

Size	Sample Size	Mass (g)		Thickness (mm)		Circumscribed Diameter (mm)	
		Mean	St. Dev.	Mean	St. Dev.	Mean	St. Dev.
1	50	79	8	12.9	1.4	101	5
2	25	169	12	13.2	1.5	150	4
3	10	323	15	13.3	1.1	201	3
4	5	468	18	12.8	1.0	246	3

The thickness, circumscribed diameter and mass of each sample was measured and recorded. Using the average measured thickness, total wax weight, and density of paraffin, the total attainable surface coverage was then determined as

$$M_{wax} = \rho_{wax} V_{wax} \Rightarrow M_{wax} = \rho_{wax} A_{wax} l \Rightarrow A_{wax} = \frac{M_{wax}}{\rho_{wax} l}$$

$$\therefore A_{wax} = \frac{1292.1kg}{(880 \frac{kg}{m^3}) \cdot (0.0131m)}$$

$$\Rightarrow A_{wax} \approx 112m^2$$

Knowing that the total surface area of the towing tank is 250m<sup>2</sup>, it was necessary to reduce the available tank length significantly to 27.2m to provide a total tank area of 124.3m<sup>2</sup> and an overall pack ice coverage of 90%. This was done by attaching two pieces of 2" x 6" lumber to a moveable catwalk spanning the tank so that the lumber sat in the water preventing the wax pieces from moving past it (Figure 4.16).

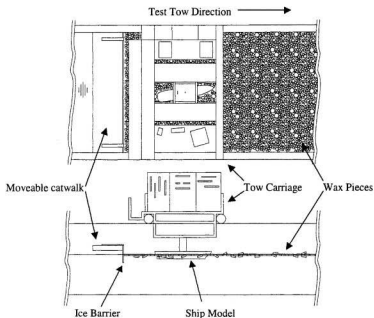


Figure 4.16 Elevation and plan view schematics of ice barrier, ship model and wax pieces

Image analysis of a photograph taken from above a typical wax-covered area of water (Figure 4.17) shows that the surface coverage was actually 83% or 103.2m<sup>2</sup> (refer to Appendix C for details of this calculation). Tests were then conducted in the reduced portion of the tank. Although test lengths were less than that for open water, useful data were still collected for all cases.



Figure 4.17 Photograph of typical wax-covered area of tank.

# Chapter 5: Experimental Method

## 5.1 GENERAL

Experimental methods will be detailed in this chapter. The process of model testing has been broken into three components:

- dynamometer calibration;
- pre-test procedure for the models; and
- testing procedure for open water and pack ice for both constant velocity and acceleration tests.

## 5.2 DYNAMOMETER CALIBRATION

The following method of dynamometer calibration is based on a six degree of freedom dynamometer calibration method developed at the National Research Council (personal conversations with Dr. Bruce Parsons, Institute for Marine Dynamics, NRC, 1996). The dynamometer used in the experiments (as described in Section 4.2.1) contained three load cells - one parallel with the ship's x-axis and two orthogonal, to measure surge and forward and aft sway forces respectively as the model was towed. If only a simple calibration of the individual load cells was conducted, direct test readings from each load cell would be slightly in error, due to crosstalk. The dynamometer was calibrated in such a way that the crosstalk could be removed from the test results mathematically during analysis.

Crosstalk calibration coefficients were determined through careful calibration of each load cell after the dynamometer had been assembled. By conducting the calibration after assembly of the dynamometer, it was possible to measure forces in all load cells during

the calibration of each specific load cell. Thus, a value of crosstalk could be obtained for all load cells as a function of the load in a single load cell.

Considering the equation for the applied load in the x-direction:

$$X^{App} = a_1 \cdot X^{Meas} + b_1 \cdot Y_F^{Meas} + c_1 \cdot Y_A^{Meas} \quad (21)$$

Similarly, for the other two load cells:

$$\begin{aligned} Y_F^{App} &= a_2 \cdot X^{Meas} + b_2 \cdot Y_F^{Meas} + c_2 \cdot Y_A^{Meas} \\ Y_A^{App} &= a_3 \cdot X^{Meas} + b_3 \cdot Y_F^{Meas} + c_3 \cdot Y_A^{Meas} \end{aligned} \quad (22)$$

Writing these equations in matrix form, we obtain:

$$\begin{Bmatrix} X^{App} \\ Y_F^{App} \\ Y_A^{App} \end{Bmatrix} = \begin{bmatrix} a_1 & b_1 & c_1 \\ a_2 & b_2 & c_2 \\ a_3 & b_3 & c_3 \end{bmatrix} \begin{Bmatrix} X^{Meas} \\ Y_F^{Meas} \\ Y_A^{Meas} \end{Bmatrix} \quad (23)$$

Here we notice that the 3x3 matrix is the calibration matrix, where the off-diagonal terms are the cross-talk calibration coefficients.

By conducting a calibration experiment, the applied load is known and the load in each load cell is measured; hence the only unknown is the calibration matrix. Inverting the matrix Equation (23), we get the following:

$$\begin{Bmatrix} X^{Meas} \\ Y_F^{Meas} \\ Y_A^{Meas} \end{Bmatrix} = \begin{bmatrix} I_1 & J_1 & K_1 \\ I_2 & J_2 & K_2 \\ I_3 & J_3 & K_3 \end{bmatrix} \begin{Bmatrix} X^{App} \\ Y_F^{App} \\ Y_A^{App} \end{Bmatrix} \quad (24)$$

When only the surge (X) load cell is calibrated, we get the following:

$$\begin{aligned}
 X^{Meas} &= I_1 \cdot X^{App} & I_1 &= \frac{X^{Meas}}{X^{App}} \\
 Y_F^{Meas} &= I_2 \cdot X^{App} & \rightarrow I_2 &= \frac{Y_F^{Meas}}{X^{App}} \\
 Y_A^{Meas} &= I_3 \cdot X^{App} & I_3 &= \frac{Y_A^{Meas}}{X^{App}}
 \end{aligned}
 \tag{25}$$

The  $J$  and  $K$  coefficients could be computed in the same manner. These inverted coefficients are simply the slopes determined from plotting the applied calibration load against the measured load. When all  $I$ ,  $J$ , and  $K$  coefficients have been computed, the matrix is inverted back to find the  $a$ ,  $b$ , and  $c$  coefficients. These coefficients are then used with the original matrix formulation to give the calibrated forces in each of the load cells, with the cross-talk errors removed.

When the dynamometer was assembled, every connection was carefully tightened to ensure no torsional bending of flex-links occurred. The dynamometer was mounted securely to the calibration structure and a calibration bracket attached to the structure that consisted of an aluminum frame and a pulley (Figure 5.1). This system allowed for the application of a known load to each load cell within the dynamometer. A set of known weights was used to calibrate the dynamometer. First, a separate load cell was calibrated directly using the known weights (Figure 5.2). Termed the *in-line load cell*, this load cell was used for accurately recording load measurements directly applied to the dynamometer (Figure 5.3). Doing this reduced the potential for errors due to wire stretching and pulley friction if the applied load were simply assumed to be the mass on the weight pan multiplied by gravitational acceleration.

It was important that the load was applied directly in-line with the axis of the load cell being calibrated. This ensured the load measured by the in-line load cell was exactly that registered by the load cell being calibrated.

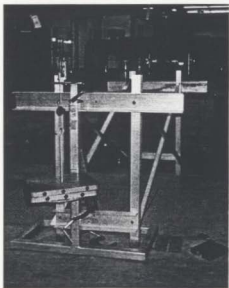


Figure 5.1 Calibration bracket showing weights on weight pan during a step in the calibration process.

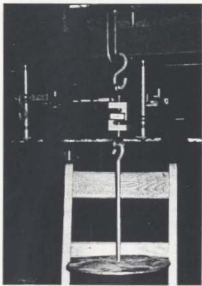


Figure 5.2 In-line load cell calibration setup.

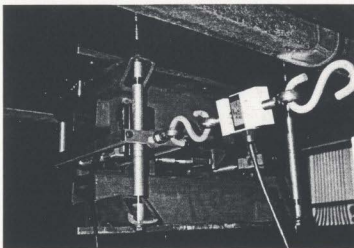


Figure 5.3 Close-up of in-line load cell during calibration of the aft sway load cell.

Electrical signals from each load cell were recorded on a computer after passing through an analog to digital converter and a signal conditioner (Figure 5.4). Results of each step in the calibration process were plotted, manually recorded and examined before proceeding. Results of the calibration experiment are given in Section 6.2.



Figure 5.4 Computer setup used for calibration experiment, along with A/D converter and signal conditioner.

### **5.3 PRE-TEST PROCEDURE FOR SHIP MODELS**

Before tank testing began, the sliding portion of the adjustable height tow post was mounted securely to the first model at midships. By mounting the tow post at this location, the yaw moment could be calculated easily since the dynamometer centre would be coincident with the model centre of gravity and no moment transfer would be required in the analysis stage.

The model was then placed in a small ballasting tank where weights were added to bring the model to the proper draft. Weights were added in such a way as to ensure the model was on an even keel (not trimmed) and not heeled. These angles were checked using an electronic inclinometer (Figure 5.5 & Figure 5.6). Ballasting the model also ensured that little or no vertical load was imparted to the dynamometer from the model when testing began. The model was then weighed and transferred to the towing tank. Here it was attached to the upper portion of the tow post which was, in turn, connected securely to the bottom of the calibrated dynamometer. The ship-side of the tow post was inserted into the dynamometer side of the tow post and fastened securely together, holding the ship model rigidly at the design waterline.

The model's inertial properties were not determined, since the tests were captive model tests where the model was constrained in all degrees of freedom.

### **5.4 TOWING TANK TESTS**

With the model in place and the tow post sliders inserted into the dynamometer-mounted portion of the tow post, the overall tank water level was increased until the model was in the proper position for testing. The tow post was then securely fastened together and data acquisition equipment connected to the tow carriage computer.

Since removal of wax from the tank would require draining the tank and some amount of cleaning, it was logically decided to begin the testing process with open water tests.



Figure 5.5 M.V. Arctic being ballasted to its design waterline in the ballasting tank. Here, an inclinometer is used to check that the model is not heeled to a significant amount.

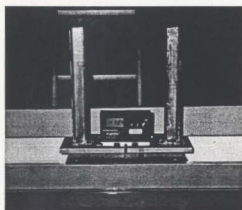


Figure 5.6 M.V. Arctic being ballasted to its design waterline in the ballasting tank. Here, an inclinometer is used to check that the model is on an even keel.

### 5.4.1 *Open Water*

Both models were tested in open water initially for the constant velocity (Figure 5.7) and acceleration test types. The procedure outlined below in point form was followed for both constant velocity and acceleration tests in the series:

- Towing carriage was positioned at the start point for each test.
- Model's heading angle was set.
- Model's rudder angle was set.
- To avoid erroneous dynamometer readings, time was spent waiting for the water surface to become calm.
- When water surface was calm, the data acquisition system was started recording the zero load value in the dynamometer load cells.
- For constant velocity tests, the calibrated voltage was dialled into the towing carriage control panel and the carriage was accelerated to the set velocity. For constant acceleration tests, the triangular waveform generated by the function generator was used to gradually increase the voltage input to the carriage control panel and thus cause the carriage to accelerate down the tank at a constant rate.
- When either the data acquisition system finished recording for the set time or the length of the towing tank had been reached, the towing carriage was decelerated to a stop and reversed back to the starting position.
- The new rudder angle was then set for the next test and time was spent again, waiting for the tank water surface waves to dissipate.
- While waiting for the water surface to become calm, data plots from the test just conducted were reviewed and where possible, results were manually recorded in a test log book. Any reworking of the test matrix was done if required by what was observed in the data plots.
- When all rudder angles were tested for a given heading angle, the new heading angle was set and the process repeated again until all tests were completed.

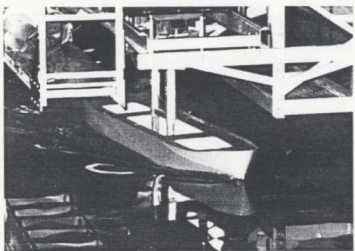


Figure 5.7 R-Class model being towed at  $6^\circ$  heading angle down the towing tank in open water.

#### 5.4.2 Pack Ice

Upon completion of the open water tests, the procedure outlined below was followed to conduct constant velocity and acceleration tests in pack ice for each model:

- A moveable catwalk was installed with a barrier to effectively reduce the test length of the tank by keeping wax pieces in one area only.
- Wax was added to the tank and spread-out to get an even coverage over the water surface (Figure 5.8).
- The approximate surface concentration was determined using image analysis (as outlined in Appendix C).
- The same procedure as outlined in the previous section (Section 5.4.1) was followed, with the following exceptions: time between tests was shorter due to the damping effect of the wax on surface waves, An attempt was made to spread out the wax with rake while reversing back to start position, since the test process resulted in much rafting and uneven distribution of wax in the tank (Figure 5.9).

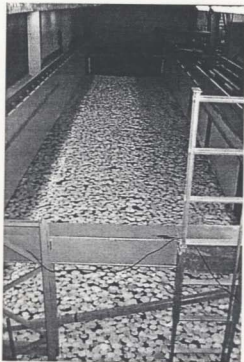


Figure 5.8 Towing tank before a test in pack ice. Note the high surface concentration.

### **5.4.3 Concluding the Testing Process**

At end of the pack ice tests, wax was manually removed by draining water from the tank and scooping it by dip net into storage containers. The dynamometer was removed from the towing carriage and disassembled. Flex-links were then examined to determine if any bent, twisted or fractured components could be found. No problems were found with these instruments.



Figure 5.9 Stern view of the M.V. Arctic ship model showing the channel in pack ice as it passes through.

# Chapter 6: Results and Discussion

## 6.1 GENERAL

This chapter provides results from the various tests conducted, including calibration results, constant velocity and constant acceleration test results for the M.V. Arctic and R-Class models in both open water and pack ice.

A discussion of these results is also presented here in terms of a comparison between the open water and pack ice conditions, differences and similarities between both models, comparison of manoeuvring coefficients obtained experimentally with those obtained from equations given in the literature, comparison of the constant acceleration to the constant velocity results and the overall meaning of the findings of this experiment.

## 6.2 CALIBRATION EXPERIMENT RESULTS

The procedure of dynamometer calibration is described in detail in Section 5.2. A calibration plot for the in-line load cell is given in Figure 6.1. Since this load cell was always used in tension, the convention assumed was that a negative applied load was a tensile load. Similarly, the forward sway load cell calibration plot is given in Figure 6.2, the aft sway load cell calibration plot is given in Figure 6.3 and the surge load cell calibration plot is given in Figure 6.4. These provide the main source of load cell calibration data, however, for a complete set of calibration plots, including measurement of crosstalk between channels, the reader is referred to Appendix D.

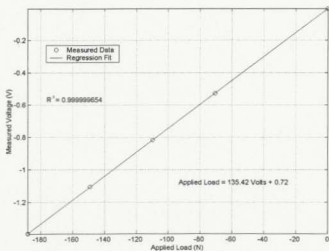


Figure 6.1 Calibration plot of applied load (N) vs. voltage measured in the in-line load cell (negative applied load implies tension).

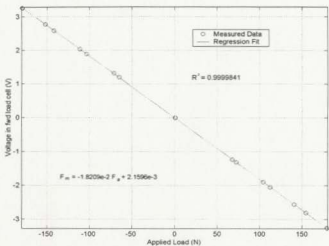


Figure 6.2 Forward load cell calibration plot of applied load (N, as measured by the in-line load cell) vs. voltage measured in the forward load cell (negative applied load implies tension, positive applied load implies compression).

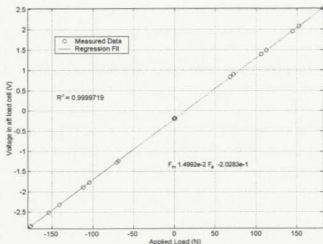


Figure 6.3 Aft load cell calibration plot of applied load (N, as measured by the in-line load cell) vs. voltage measured in the aft load cell (negative applied load implies tension, positive applied load implies compression).

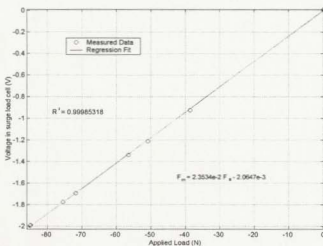


Figure 6.4 Surge load cell calibration plot of applied load (N, as measured by the in-line load cell) vs. voltage measured in the surge load cell (negative applied load implies tension, positive applied load implies compression).

Shown with each calibration plot is the equation for the least squares linear regression fit through the data and the associated correlation coefficient  $r^2$ . Since the  $r^2$  values are quite high, the calibration fits for each individual load cell are considered very good (always 0.999 and better, where 1.0 would imply that all the data are explained by the linear regression fit). Following the method outlined in Section 5.2, these results were used to determine the dynamometer calibration matrix shown as Equation (26). As expected, the diagonal terms in the matrix (associated with the calibration of the individual load cells) are considerably larger than the off-diagonal terms (associated with the crosstalk between load cells), since the crosstalk values are of second order importance.

$$\begin{Bmatrix} X^{App} \\ Y^{App}_{Fuel} \\ Y^{App}_{Aft} \end{Bmatrix} = \begin{bmatrix} 42.479 & -0.226 & -0.574 \\ -1.025 & -54.909 & 0.445 \\ 1.014 & 0.179 & 66.685 \end{bmatrix} \begin{Bmatrix} X^{Meas} \\ Y^{Meas}_{Fuel} \\ Y^{Meas}_{Aft} \end{Bmatrix} \quad (26)$$

Careful inspection of the plots for aft sway load cell crosstalk from forward sway load cell calibration and forward sway load cell crosstalk from aft load cell calibration reveals that least squares linear regression fits do not predict the data as well as would be preferred. These differences were detected during the calibration experiment process and the dynamometer surveyed for loose or bent components. No obvious problems were detected and so the calibration process was repeated, giving the same results. It was recommended in the interest of time and based on the second order nature of the crosstalk values that the experiment should precede.

## 6.3 CONSTANT VELOCITY TEST RESULTS

### 6.3.1 Method of Analysis

Data for each constant velocity test were processed by first calibrating each time series for each channel, taking a mean value for the zero portion of each channel in each test, computing the mean value for the steady state portion of each channel in each test and subtracting the zero value from the mean of the steady state to get the mean absolute

value for each channel. Sample plots of all channels measured during a single constant velocity test are given in Figure 6.5.

An attempt was made at filtering the data to remove any noise present in the measurements. A Butterworth filter was designed and applied to the data, however, the resulting filtered mean values were almost exactly the same as the unfiltered means. It was decided that a simple mean value would be used for the analysis of each constant velocity test.

To determine the manoeuvring coefficients given in Equation (18) ( $Y'_v, Y'_{vv}, Y'_\delta, Y'_{\delta\delta}, N'_v, N'_{vv}, N'_\delta$  &  $N'_{\delta\delta}$ ), the mean value for each test was nondimensionalised (according to the method laid-out in Chapter 3) and plotted against nondimensional sway speed. Sway force was computed as the sum of the aft and forward loads, while yaw moment (about the model centre of gravity) was computed knowing the distance between the aft and forward sway load cells. A family of nonlinear regression curves was fitted through the multivariate data as a function of nondimensional sway velocity and rudder angle. The model used to fit the data was based on a simplified version of Equation (18):

$$\begin{aligned} Y' &= Y'_v v' + \frac{1}{6} Y'_{vv} v'^3 + Y'_\delta \delta'_R + \frac{1}{6} Y'_{\delta\delta\delta} \delta'^3_R \\ N' &= N'_v v' + \frac{1}{6} N'_{vv} v'^3 + N'_\delta \delta'_R + \frac{1}{6} N'_{\delta\delta\delta} \delta'^3_R \end{aligned} \quad (27)$$

Cross-coupled terms (not shown in Equation 27) between sway velocity and rudder angle were computed but found to be very small in magnitude. These values have not been presented. The coefficients determined from the multiple nonlinear regression analysis were analogous to the manoeuvring coefficients.

As would be expected, different values of the manoeuvring coefficients were determined for open water tests and pack ice cover tests. These are presented and discussed in the following sections.

R-Class Model, 10° Heading, 5° Rudder to STBD, Constant Velocity

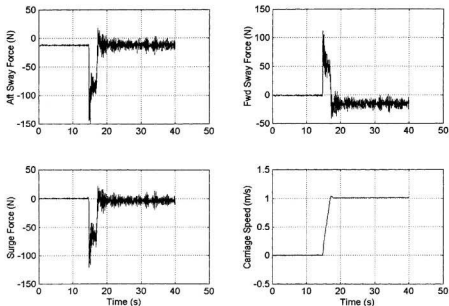


Figure 6.5 Sample plot of all four calibrated channels measured during a constant velocity open water test of the R-Class model set at 10° heading angle, 5° rudder angle to starboard. Note that zeros have not been removed from these plots.

### 6.3.2 Open Water Tests

Results of the open water analysis are presented in Figure 6.6, Figure 6.7, Figure 6.8 and Figure 6.9. These figures present the upper and lower bounds of the data (from 10° starboard rudder to 10° port rudder). To avoid clutter, data points and curves for rudder amidships and 5° rudder to port and starboard have not been shown in these figures. Plots showing results for all rudder angles are given in Appendix E

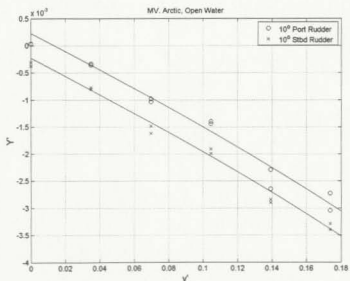


Figure 6.6 Nondimensional sway force vs. nondimensional sway velocity for the M.V. Arctic ship model constant velocity test series in open water.

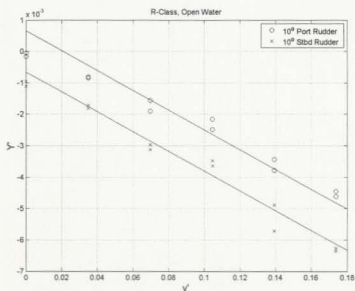


Figure 6.7 Nondimensional sway force vs. nondimensional sway velocity for the R-Class hullform model constant velocity test series in open water.

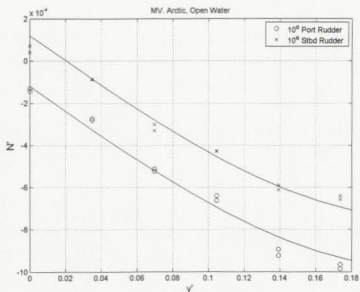


Figure 6.8 Nondimensional yaw moment vs. nondimensional sway velocity for the M.V. Arctic ship model constant velocity test series in open water.

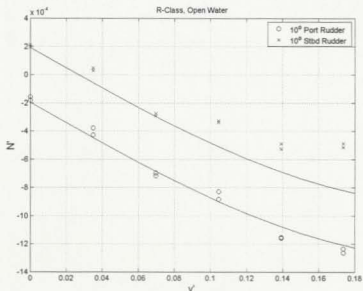


Figure 6.9 Nondimensional yaw moment vs. nondimensional sway velocity for the R-Class hullform model constant velocity test series in open water.

Results from this analysis show good agreement between the data points and the fits to the data. Table 6.1 and Table 6.2 summarise the manoeuvring coefficients for the M.V. Arctic and R-Class hullform respectively as determined from the experimental results, along with those found using Equations (1), (2), (3) & (4) in Section 2.3.2. The semi-empirically determined values agree well with those found experimentally, except for the  $N'_v$  coefficient for the R-Class model which is a little low from the experimental methods.

Table 6.1 Open water sway and yaw manoeuvring coefficients computed for the M.V. Arctic model (-- means the coefficient could not be predicted using this method).

Coefficient	Wagner-Smitt (1971)	Norrbin (1971)	Innoe (1981)	Clarke (1982)	This Thesis
$Y'_v$	$-1.560 \times 10^{-2}$	$-1.690 \times 10^{-2}$	$-1.640 \times 10^{-2}$	$-1.570 \times 10^{-2}$	$-1.655 \times 10^{-2}$
$Y'_{vv}$	--	--	--	--	$-2.796 \times 10^{-1}$
$Y'_\delta$	--	--	--	--	$2.760 \times 10^{-5}$
$Y'_{\delta\delta}$	--	--	--	--	$-4.007 \times 10^{-7}$
$N'_v$	$-6.000 \times 10^{-3}$	$-6.500 \times 10^{-3}$	$-6.200 \times 10^{-3}$	$-6.200 \times 10^{-3}$	$-5.917 \times 10^{-3}$
$N'_{vv}$	--	--	--	--	$2.492 \times 10^{-1}$
$N'_\delta$	--	--	--	--	$-8.285 \times 10^{-6}$
$N'_{\delta\delta}$	--	--	--	--	$-6.756 \times 10^{-8}$

Noticing that certain coefficients have positive and negative values is significant. Due to the sign convention assumed and the physical meaning of these coefficients,  $Y'_v$  and  $N'_\delta$  should always be negative (Crane et al., 1989). This is true for the experimentally determined coefficients presented here.

Similarly, the coefficient  $Y'_\delta$  should always be positive (Crane et al., 1989) which is also the case for the experimentally determined coefficients presented here. The coefficient  $N'_v$  may be either negative or positive, but for usual ship forms it is negative (Crane et al., 1989). This is also the case for the experimental results presented here. If the latter coefficient were positive, it would imply that the stern is dominant for that ship.

Table 6.2 Open water sway and yaw manoeuvring coefficients computed for the R-Class hullform model (-- means the coefficient could not be predicted using this method).

Coefficient	Wagner-Smitt (1971)	Norrbin (1971)	Innoe (1981)	Clarke (1982)	This Thesis
$Y'_v$	$-3.320 \times 10^{-2}$	$-3.610 \times 10^{-2}$	$-3.700 \times 10^{-2}$	$-3.540 \times 10^{-2}$	$-3.167 \times 10^{-2}$
$Y'_{vv}$	--	--	--	--	$-7.914 \times 10^{-3}$
$Y'_\delta$	--	--	--	--	$4.822 \times 10^{-5}$
$Y'_{\delta\delta}$	--	--	--	--	$1.868 \times 10^{-7}$
$N'_v$	$-1.290 \times 10^{-2}$	$-1.380 \times 10^{-2}$	$-1.330 \times 10^{-2}$	$-1.450 \times 10^{-2}$	$-0.725 \times 10^{-2}$
$N'_{vv}$	--	--	--	--	$2.795 \times 10^{-1}$
$N'_\delta$	--	--	--	--	$-1.758 \times 10^{-5}$
$N'_{\delta\delta}$	--	--	--	--	$-1.102 \times 10^{-7}$

### 6.3.3 Pack Ice Tests

Results of the pack ice analysis are presented in Figure 6.10, Figure 6.11, Figure 6.12 and Figure 6.13. These figures present the upper and lower bounds of the data (from 10° starboard rudder to 10° port rudder). To avoid clutter, data points and curves for rudder

amidships and 5° rudder to port and starboard have not been shown in these figures. Plots showing results for all rudder angles are given in Appendix E

The time history data for each test in pack ice appeared to be a slightly more noisy signal, as would be expected. This greater noise can be attributed to the random impact of pack ice pieces against the hull. The signal became more noisy during tests at higher sway speeds due to the increased number of impacts from a combination of higher heading angle and higher tow speed. This noise frequently showed increases in the load trace, followed by drops in load. These increases could be attributed to floes piling up against the side of the model with the decreases coming when the floes were cleared. Since the interaction process was assumed to be random, a simple mean value was fit through the data as was previously described for the open water analysis.

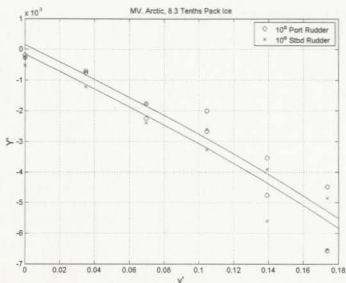


Figure 6.10 Nondimensional sway force vs. nondimensional sway velocity for the M.V. Arctic ship model constant velocity test series in 8.3 tenths ice cover.

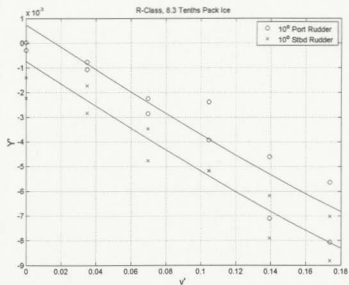


Figure 6.11 Nondimensional sway force vs. nondimensional sway velocity for the R-Class hullform model constant velocity test series in 8.3 tenths ice cover.

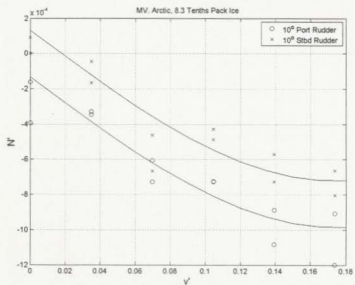


Figure 6.12 Nondimensional yaw moment vs. nondimensional sway velocity for the M.V. Arctic ship model constant velocity test series in 8.3 tenths pack ice.

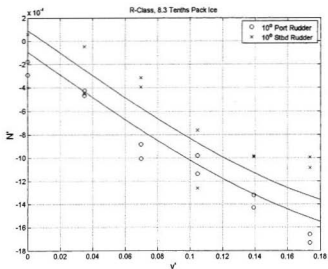


Figure 6.13 Nondimensional yaw moment vs. nondimensional sway velocity for the R-Class hullform model constant velocity test series in 8.3 tenths pack ice.

Inspection of the constant velocity pack ice results reveals several trends in relation to the open water test series:

- in all cases, as would be expected, the loads are higher than what was measured in open water,
- nonlinearity of the regression fit was always slightly increased, except for the M.V. Arctic yaw moment which was considerably increased,
- the spread in the data points ( $Y'$  &  $N'$ ) increased with nondimensional sway speed ( $v'$ ),
- the bow remained dominant in all cases and
- rudder angle differences were less distinct in pack ice than in open water.

It is difficult to effectively compare the manoeuvring ability of the two models tested based on the results, due to the fact that the same model ice was used in both test series

but the ship models were both different scales. Nondimensionalising the forces helps bring the results to a common ground, however, the environment is essentially different for each ship model.

Assuming that the manoeuvring coefficients in ice are the sum of open water and ice components (Kendrick, 1984), the effect of ice on the manoeuvring coefficients can be shown (refer to Table 6.3 and Table 6.4).

Table 6.3 Sway and yaw manoeuvring coefficients computed for the M.V. Arctic model in 8.3 tenths pack ice (showing the open water and ice components of the overall coefficient).

Coeff.	M.V. Arctic		
	Total in Pack Ice	Open Water Component	Ice Component
$Y'_v$	$-2.794 \times 10^{-2}$	$-1.655 \times 10^{-2}$	$-1.139 \times 10^{-2}$
$Y'_{vv}$	$-6.378 \times 10^{-1}$	$-2.796 \times 10^{-1}$	$-3.582 \times 10^{-1}$
$Y'_\delta$	$1.822 \times 10^{-5}$	$2.760 \times 10^{-5}$	$-9.380 \times 10^{-6}$
$Y'_{\delta\delta}$	$-5.096 \times 10^{-8}$	$-4.007 \times 10^{-7}$	$3.497 \times 10^{-7}$
$N'_v$	$-7.284 \times 10^{-3}$	$-5.917 \times 10^{-3}$	$-1.367 \times 10^{-3}$
$N'_{vv}$	$4.871 \times 10^{-1}$	$2.492 \times 10^{-1}$	$2.379 \times 10^{-1}$
$N'_\delta$	$-6.441 \times 10^{-6}$	$-8.285 \times 10^{-6}$	$1.844 \times 10^{-6}$
$N'_{\delta\delta}$	$-3.265 \times 10^{-7}$	$-6.756 \times 10^{-8}$	$-2.589 \times 10^{-7}$

Table 6.4 Sway and yaw manoeuvring coefficients computed for the R-Class hullform model in 8.3 tenths pack ice (showing the open water and ice components of the overall coefficient).

Coeff.	R-Class		
	Total in Pack Ice	Open Water Component	Ice Component
$Y'_v$	$-4.511 \times 10^{-2}$	$-3.167 \times 10^{-2}$	$-1.344 \times 10^{-2}$
$Y'_{vv}$	$6.246 \times 10^{-1}$	$-7.914 \times 10^{-3}$	$6.325 \times 10^{-1}$
$Y'_\delta$	$3.941 \times 10^{-5}$	$4.822 \times 10^{-5}$	$-8.810 \times 10^{-6}$
$Y'_{\delta\delta}$	$2.578 \times 10^{-6}$	$1.868 \times 10^{-7}$	$2.391 \times 10^{-6}$
$N'_v$	$-9.782 \times 10^{-3}$	$-0.725 \times 10^{-2}$	$-2.532 \times 10^{-3}$
$N'_{vv}$	$3.136 \times 10^{-1}$	$2.795 \times 10^{-1}$	$3.410 \times 10^{-2}$
$N'_\delta$	$-2.124 \times 10^{-5}$	$-1.758 \times 10^{-5}$	$-3.660 \times 10^{-6}$
$N'_{\delta\delta}$	$7.146 \times 10^{-7}$	$-1.102 \times 10^{-7}$	$8.248 \times 10^{-7}$

## 6.4 CONSTANT ACCELERATION TEST RESULTS

### 6.4.1 Method of Analysis

In the past it was assumed that the sway acceleration manoeuvring coefficients  $Y'_v$  and  $N'_\delta$  could not be calculated from straight-line test data gathered in a conventional towing tank. This section outlines the method by which these coefficients were, indeed, calculated in a conventional towing tank. Tests were performed using both ship models in open water and pack ice. The resulting acceleration coefficients are given in the following sections along with a comparison to empirical methods for finding the same coefficients.

The method of data analysis to compute these coefficients involved a two-stage processing procedure. In the first stage, the raw data were processed (sample in Figure 6.14). First, each time series was calibrated for each channel and a mean value for the zero portion of each channel in each test was computed. The zero value was then subtracted from each data point for the remainder of the test. The useable portion of each test (starting after the transient portion of the acceleration had finished and ending before the peak velocity) was then stored for processing. A linear regression line was fit to the velocity time history for each test, where the slope of the regression fit equalled the acceleration rate. Since sway and yaw coefficients are the focus of this work, the surge data were not processed. The total sway force was computed as the sum of the forward and aft sway load cell traces and the yaw moment was computed as described in earlier sections.

A regression line was then fit through the data based on the model (Figure 6.15):

$$Y_{fit} = Y_o + Y_v v + Y_{vv} v^3 \quad (28)$$

An attempt was made at filtering the raw data to remove any high frequency noise present in the measurements. A Butterworth filter was designed and applied to the data, however, the resulting filtered traces were almost exactly the same as the regression fit.

The  $Y_o$  values from Equation (28) were tabulated along with sway acceleration,  $\dot{v}$ , and rudder angle for the second stage of processing. A variety of  $\dot{v}$  values could be obtained since the models were towed at different heading angles for 2 constant accelerations.

The second stage of processing involved plotting the values of  $Y_o$  as a function of sway acceleration and rudder angle and performing a multi-linear regression analysis. Since each test was conducted with varying velocity but constant acceleration, heading and rudder angle, the constant  $Y_o$  was assumed to take the form:

$$Y_o = Y_v \dot{v} + Y_{\delta} \delta \quad (29)$$

Results of this analysis are presented in the following sections for open water and pack ice results.

M.V. Arctic Model, 10° Heading, 10° Rudder to PORT, Constant Acceleration

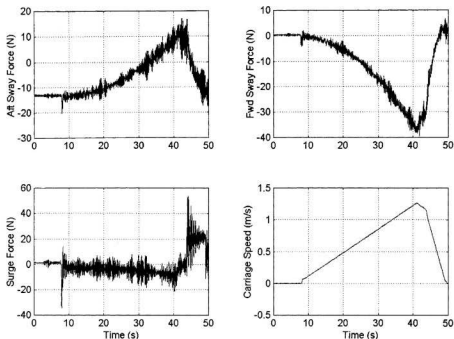


Figure 6.14 Sample plot of all four calibrated channels measured during a constant acceleration open water test of the M.V. Arctic model set at 10° heading angle, 10° rudder angle to port. Note that zeros have not been removed from these plots.

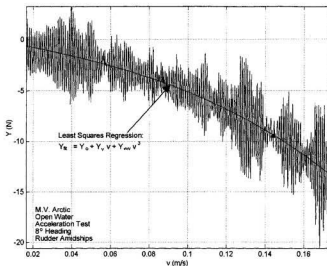


Figure 6.15 Sample plot of total sway force as a function of sway velocity, along with the least squares regression fit to the data.

#### 6.4.2 Open Water Tests

Results of the open water analysis are presented in Figure 6.16, Figure 6.17, Figure 6.18 and Figure 6.19 in dimensional form. These figures present the upper and lower bounds of the data (from  $10^\circ$  starboard rudder to  $10^\circ$  port rudder). To avoid clutter, data points and curves for rudder amidships and  $5^\circ$  rudder to port and starboard have not been shown in these figures. Plots showing results for all rudder angles are given in Appendix F. Dimensional form is used for all plots since it was unclear which velocity to use for nondimensionalising the measured force.

Results from this analysis show good agreement between the data points and the fits to the data. Table 6.5 and Table 6.6 summarise the manoeuvring coefficients for the M.V. Arctic and R-Class hullform respectively as determined from the experimental results, along with those found using Equation (4) in Section 2.3.2. The semi-empirically determined values agree well with those found experimentally, except for the  $N'_v$

coefficient for both models, which is a little low from experimental methods for the R-Class model and an order of magnitude higher from experimental methods for the M.V. Arctic model.

Similar to the check performed in Section 6.3.2, the sign of the experimentally determined acceleration derivative  $Y'_v$  is negative. Crane et al. (1989) reports that this should always be the case, but that the sign for  $N'_v$  is uncertain, depending on whether the bow or stern dominates.

Based on these analyses of constant acceleration test data, it is reasonable to conclude that the sway acceleration coefficients  $Y'_v$  and  $N'_v$  can be found from straight-line towing tests in a conventional towing tank.

Table 6.5 Open water sway and yaw acceleration manoeuvring coefficients computed for the M.V. Arctic model.

Coefficient	Clarke (1982)	This Thesis
$Y'_v$	$-1.150 \times 10^{-2}$	$-1.005 \times 10^{-2}$
$N'_v$	$-4.000 \times 10^{-4}$	$-4.956 \times 10^{-3}$

Table 6.6 Open water sway and yaw acceleration manoeuvring coefficients computed for the R-Class hullform model.

Coefficient	Clarke (1982)	This Thesis
$Y'_v$	$-2.150 \times 10^{-2}$	$-2.293 \times 10^{-2}$
$N'_v$	$-2.700 \times 10^{-3}$	$-6.973 \times 10^{-3}$

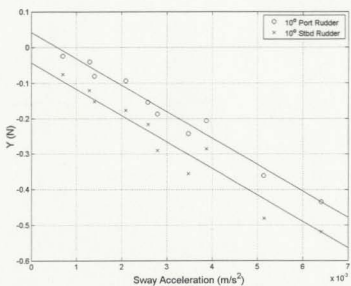


Figure 6.16 Sway force as a function of sway acceleration for the M.V. Arctic model in open water for a family of rudder angles.

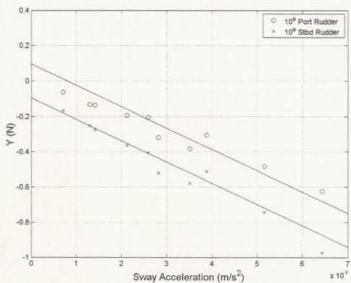


Figure 6.17 Sway force as a function of sway acceleration for the R-Class hullform model in open water for a family of rudder angles.

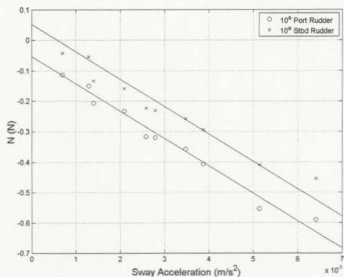


Figure 6.18 Yaw moment as a function of sway acceleration for the M.V. Arctic model in open water for a family of rudder angles.

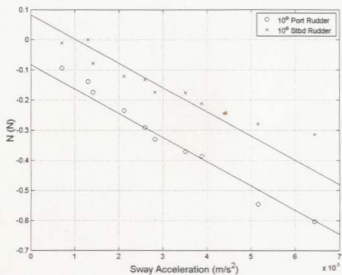


Figure 6.19 Yaw moment as a function of sway acceleration for the R-Class hullform model in open water for a family of rudder angles.

### 6.4.3 *Pack Ice Cover*

Results of the pack ice analysis are presented in Figure 6.20, Figure 6.21, Figure 6.22 and Figure 6.23. These figures present the upper and lower bounds of the data (from 10° starboard rudder to 10° port rudder). To avoid clutter, data points and curves for rudder amidships and 5° rudder to port and starboard have not been shown in these figures.

Similar to constant velocity tests in pack ice, the time history data for each acceleration test in pack ice appeared to be slightly more noisy than in open water. This greater noise can be attributed to the random impact of pack ice pieces against the hull. The signal became more noisy during tests at higher sway speeds due to the increased number of impacts from the combination of higher heading angle and higher tow speed. This noise frequently showed increases in the load trace, followed by drops in load. The increases could be attributed to floes piling up against the side of the model with the decreases coming when the floes were cleared.

Examining the plots for constant acceleration testing in pack ice to determine sway acceleration coefficients revealed the following trends:

- in general, more scatter is present in these plots than for those carried-out in open water,
- differences in loads for varied rudder angle were usually about the same in pack ice as in open water,
- maximum loads were usually about the same or slightly higher, and
- the linear fits through the data were not always very good, often due to high amounts of scatter. This is especially true for the M.V. Arctic test series.

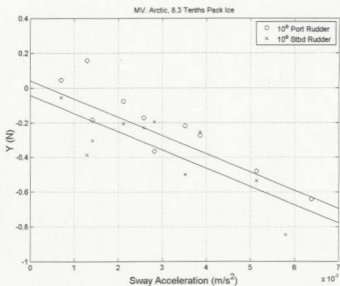


Figure 6.20 Sway force as a function of sway acceleration for the M.V. Arctic model in 8.3 tenths pack ice for a family of rudder angles.

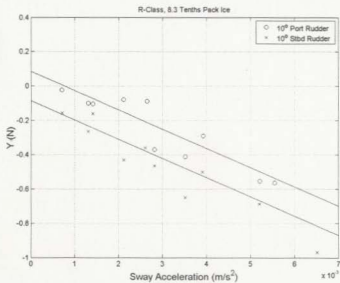


Figure 6.21 Sway force as a function of sway acceleration for the R-Class hullform model in 8.3 tenths pack ice for a family of rudder angles.

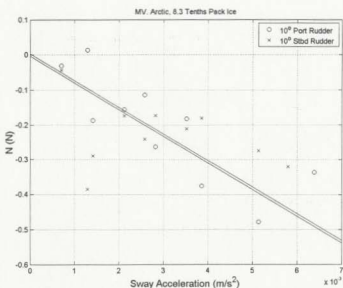


Figure 6.22 Yaw moment as a function of sway acceleration for the M.V. Arctic model in 8.3 tenths pack ice for a family of rudder angles.

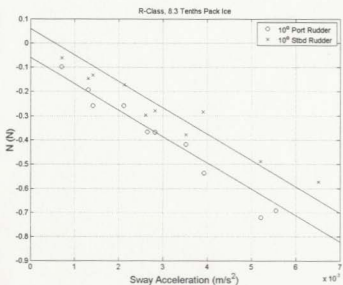


Figure 6.23 Yaw moment as a function of sway acceleration for the R-Class hullform model in 8.3 tenths pack ice for a family of rudder angles.

Table 6.7 Pack ice sway and yaw acceleration manoeuvring coefficients computed for the M.V. Arctic model.

Coefficient	This Thesis
$Y'_\psi$	$-1.421 \times 10^{-2}$
$N'_\psi$	$-4.198 \times 10^{-3}$

Table 6.8 Pack ice sway and yaw acceleration manoeuvring coefficients computed for the R-Class hullform model.

Coefficient	This Thesis
$Y'_\psi$	$-2.272 \times 10^{-2}$
$N'_\psi$	$-9.068 \times 10^{-3}$

## 6.5 DAMPING COEFFICIENT TEST EFFICIENCY

To produce the data plots shown in Section 6.3 for determining the straight-line damping coefficients using constant velocity tests, approximately 60 tests were completed for each model in open water and 60 in pack ice. The time required to conduct these tests and analyse the data is significant and could be costly if testing were done in a refrigerated ice basin. The method used in this section shows that the straight-line damping coefficients can be found by conducting a single constant acceleration test, resulting in savings in time and cost.

The plots shown in Figure 6.24, Figure 6.25, Figure 6.26 and Figure 6.27 give samples of the quality of fit for the constant velocity data to the constant acceleration data under the

same set of conditions. A fit to the data is also provided in these figures which is based on that given in Figure 6.15.

Performing checks of the validity for this new procedure revealed that the new method works best when the range of sway velocities a reasonably high (i.e. low acceleration rates and low heading angles produce a low range of sway velocity, which in turn results in poor fit to the constant velocity data).

It is concluded from this analyses that calculating sway velocity damping coefficients can effectively be completed with many fewer tests if the constant acceleration testing technique is used.

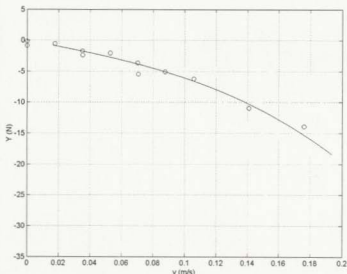


Figure 6.24 Comparison of constant acceleration test results (light lines with dark line regression fit) for the M.V. Arctic model in pack ice, rudder amidships with constant velocity data analysis results for same conditions (circles).

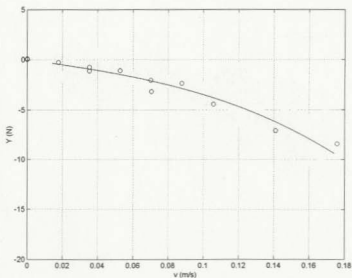


Figure 6.25 Comparison of constant acceleration test results (light lines with dark line regression fit) for the M.V. Arctic model in open water, rudder amidships with constant velocity data analysis results for same conditions (circles).

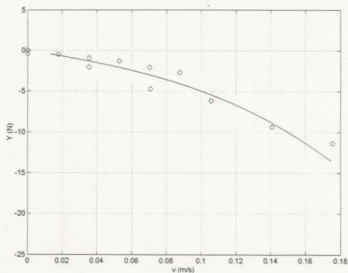


Figure 6.26 Comparison of constant acceleration test results (light lines with dark line regression fit) for the R-Class model in open water, rudder amidships with constant velocity data analysis results for same conditions (circles).

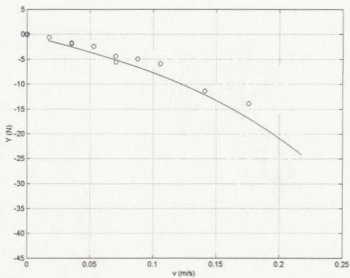


Figure 6.27 Comparison of constant acceleration test results (light lines with dark line regression fit) for the R-Class model in pack ice, rudder amidships with constant velocity data analysis results for same conditions (circles).

## Chapter 7: Conclusions

Two ship models – a 1:40 scale R-Class hullform and a 1:80 scale MV. Arctic – were tested in the Faculty of Engineering and Applied Science towing tank at Memorial University of Newfoundland. The models were tested first in open water and then in modelled pack ice covered water at approximately 8.3 tenths concentration. The pack ice model consisted of various sizes of predominantly hexagonally shaped paraffin wax. Two main types of tests were conducted for both models in each water surface condition – constant velocity and constant acceleration, the latter of which was a new technique proposed for use in determining acceleration manoeuvring coefficients and for reducing the overall number of tests required to determine the sway velocity damping coefficients. The test series consisted of simple straight-line towing for each model with various constant heading and rudder angles. A total of 480 tests were conducted in this study.

An extensive literature survey was conducted that revealed little detailed information about ship manoeuvrability studies in pack ice. The literature indicated that in the past, tests had been successfully carried-out using paraffin wax as a modelling material for pack ice, as long as the strength parameters of the ice were not important. Using paraffin wax as a modelling material allowed for a much less expensive test series to be conducted. Through discussions with experienced researchers, and referring to the limited works in the literature, the experimental procedure was designed and followed carefully.

It was shown that crosstalk in a three-component dynamometer could be mathematically removed by developing a 3x3 calibration matrix whose off-diagonal terms represented the crosstalk coefficients. Removing crosstalk measurements provided a more accurate measurement of the actual load applied to the individual load cells.

For both models, the manoeuvring coefficients for sway velocity damping and rudder angle were calculated using results from the constant velocity segment of the test series.

Only coefficients for the sway and yaw equations were calculated for this study (Table 7.1). The coefficient values found during the open water portion of the test series were compared with those found from semi-empirical methods given in the literature. The coefficients compared closely. As well, the sign of the coefficients for sway force were correct according to the literature and the sign of yaw moment implied that both models were bow-dominant.

Comparison of the pack ice test results with open water for the constant velocity test series showed in general that the loads were higher in magnitude, regression fits were more nonlinear, the spread in the data points increased with increasing sway velocity, the bow remained dominant for both models and differences in force for various rudder angles were less distinct. For both models, rudder effectiveness was found to be reduced in pack ice compared with open water.

Table 7.1 Summary of all manoeuvring coefficients determined from this study for the M.V. Arctic and R-Class models in open water and pack ice.

Coefficient	M.V. Arctic		R-Class	
	Open Water	Pack Ice	Open Water	Pack Ice
$Y'_v$	$-1.655 \times 10^{-2}$	$-2.794 \times 10^{-2}$	$-3.167 \times 10^{-2}$	$-4.511 \times 10^{-2}$
$Y'_{vv}$	$-2.796 \times 10^{-1}$	$-6.378 \times 10^{-1}$	$-7.914 \times 10^{-3}$	$6.246 \times 10^{-1}$
$Y'_\delta$	$2.760 \times 10^{-5}$	$1.822 \times 10^{-5}$	$4.822 \times 10^{-5}$	$3.941 \times 10^{-5}$
$Y'_{\delta\delta}$	$-4.007 \times 10^{-7}$	$-5.096 \times 10^{-8}$	$1.868 \times 10^{-7}$	$2.578 \times 10^{-6}$
$N'_v$	$-5.917 \times 10^{-3}$	$-7.284 \times 10^{-3}$	$-7.250 \times 10^{-3}$	$-9.782 \times 10^{-3}$
$N'_{vv}$	$2.492 \times 10^{-1}$	$4.871 \times 10^{-1}$	$2.795 \times 10^{-1}$	$3.136 \times 10^{-1}$
$N'_\delta$	$-8.285 \times 10^{-6}$	$-6.441 \times 10^{-6}$	$-1.758 \times 10^{-5}$	$-2.124 \times 10^{-5}$
$N'_{\delta\delta}$	$-6.756 \times 10^{-8}$	$-3.265 \times 10^{-7}$	$-1.102 \times 10^{-7}$	$7.146 \times 10^{-7}$
$Y'_r$	$-1.005 \times 10^{-2}$	$-1.421 \times 10^{-2}$	$-2.293 \times 10^{-2}$	$-2.272 \times 10^{-2}$
$N'_r$	$-4.956 \times 10^{-3}$	$-4.198 \times 10^{-3}$	$-6.973 \times 10^{-3}$	$-9.068 \times 10^{-3}$

Comparing the results of the R-Class hullform model to those of the M.V. Arctic model, it can be seen that the magnitude of the nondimensional first order R-Class coefficients is always greater than that for the M.V. Arctic coefficients in both open water and pack ice. Since both models were tested in the same set of conditions, these differences can be attributed directly to the hullform differences. The coefficients of form and geometric ratios given in Table 7.2 show that the R-Class model is far less slender and blocky than the M.V. Arctic model.

Table 7.2 Hullform ratios and coefficients for the M.V. Arctic and R-Class models.

Variable	M.V. Arctic	R-Class
$C_B$	0.73	0.644
$C_P$	0.737	0.721
L/B	8.596	4.529
L/T	17.91	12.28

It was shown that by employing constant tow carriage acceleration, manoeuvring coefficients for sway acceleration could be determined for open water (Table 7.1). For this technique, however, results of the analysis in pack ice were poor, particularly for the M.V. Arctic model. Therefore, confidence in the acceleration coefficients determined in ice using this test technique is not as high as it is for those found in the open water test series.

Finally, it has been shown that through the use of constant tow carriage acceleration, the sway velocity damping coefficients can be calculated in a fraction of the time required by using constant velocity testing methods.

## Chapter 8: Recommendations

Numerous recommendations have come to light through the study described in this thesis. These recommendations include aspects of the study that could be improved upon in future work as well as directions for further study. These are summarised in point form below.

### *Improvements to test procedure:*

- Testing of ship manoeuvrability would be better done where the model is free to heave, pitch and roll as it would do in heavy ice conditions (Kostilainen, 1986). This was not the case with the work presented here, due to physical testing constraints. By allowing such motions, the researcher does not simplify the problem by overlooking the cross-coupling of manoeuvring motions with various motions in other degrees of freedom, as would be done in free-running model tests for manoeuvring coefficients. Consideration of cross-coupling terms when manoeuvring in ice is especially important if the model is permitted to heave, pitch and roll freely.
- Though the use of paraffin as an ice modelling material is justified, since no ice breaking took place in the tests described in this thesis, it would be best to use a refrigerated ice model. In this way, the crushing behaviour of the ice is modelled along with frictional, geometric and buoyancy characteristics. Also, if wishing to compare the results for several models in ice, this would allow for scaling of the ice model so that the two models are tested in the same environment.
- For the constant velocity test series, transient loads from high carriage acceleration governed the design of flex-links and load cell capacity. A device should be employed which holds the model during the transient portion of the tests and releases it during the steady state portion so that load cells can be sized smaller and hence better resolution gained on the data measured.

- Care should be taken when selecting tow speeds to ensure that the full-scale values are realistic, especially when operating in an ice environment.
- It would be useful to verify the coefficients determined in this thesis with other model test data, especially the acceleration coefficients.
- Scale effects should be examined before the results from this study can be utilised for performing manoeuvring simulations (in conjunction with the remaining coefficients required).
- If using the acceleration technique to find the straight-line sway velocity damping coefficients, it is recommended the researcher tow at a reasonably high sway acceleration, otherwise the results may over-predict the coefficients.
- It is preferable that model scale be as large as possible for the tank in which testing is taking place.
- Precaution should be taken, when using paraffin as an ice modelling material, to ensure that the material does not become entrapped in other tow tank equipment such as the wave damping beach and the wave maker.
- Numerous tests were video taped using a hand-held video recorder during the course of the experiments. While this information is useful qualitatively, it is recommended that video be directly linked to the data collection system in order to identify any specific interesting points in the data being collected.
- Ship models tested for manoeuvrability should have scaled propellers installed and operated at the self propulsion point so that flow across the rudder and stern of the model are reproduced correctly.
- Where a dynamometer is used consistently for measuring loads on ship hulls, it is recommended that the test facility have installed a dedicated calibration jig to ensure applied loads can be measured accurately and the dynamometer can be properly surveyed.

***Future Work:***

- The new techniques employed for determining acceleration coefficients and damping coefficients from straight line towing with carriage acceleration should be investigated further.
- Continued development of the manoeuvring equations of motion for ships in pack ice is recommended to ensure that the manoeuvring coefficients in pack ice are well represented as the sum of open water derivatives plus an ice component.

## Chapter 9: References

- Aboulazm, A.F. (1989). *Ship Resistance in Ice Floe Covered Waters*. Ph.D. thesis to Memorial University of Newfoundland.
- Aboulazm, A.F. (1993). Ice Forces Involved in Steady Ship Turning in Pack Ice. International Conference on Marine Simulation and Ship Manoeuvrability - MARSIM '93, St. John's, Newfoundland.
- Barnes, P., D. Tabor & J. Walker (1971). The Friction and Creep of Polycrystalline Ice. Proceedings of the Royal Society of London, A324, pp. 127-155.
- Barr, D.I.H. (1985). Matrix Procedures for Dimensional Analysis. International Journal of Mathematics in Education, Science, and Technology, Vol. 16, No. 5.
- Barr, R.A. (1993). A Review and Comparison of Ship Maneuvering Simulation Methods. SNAME Transactions, Vol. 101.
- Belyakov, V.B. (1984). A New Modelled Ice. Gorky Polytechnic Institute. Translated by ECTC, New York, # T-844-09.
- Biancardi, C.G. (1997). An Alternative Methodology for Calculating Ship Manoeuvring Coefficients at the Design Stage. International Shipbuilding Progress, 44, No. 440, pp. 273-297.
- Brown, R.P. (1990). Design Criteria for Rudders, Steering Gears, Nozzles and Rudder Ice Knives for Arctic Vessels. Ictech Conference, SNAME.
- Cammaert, A.B. & D.B. Muggeridge (1988). *Ice Interaction with Offshore Structures*. Van Nostrand Reinhold, New York.

- Cammaert, A.B., R.G. Tanner & G.P. Tsinker (1983). Design of Ice Management System for Arctic LNG Dock, POAC '83, Vol 3, pp. 242-252.
- Clarke, D. (1982). The Application of Manoeuvring Criteria in Hull Design Using Linear Theory. The Royal Institute of Naval Architects (RINA), London.
- Conn, J.F.C., H. Lackenby & Walker (1953). BSRA Resistance Experiments on the Lucy Ashton, Transaction of the Royal Institute of Naval Architects (RINA), Vol. 95, p. 350.
- Crane, C.L., H. Eda & A. Landsburg (1989). *Principles of Naval Architecture Volume III: Motions in Waves and Controllability – Chapter 9: Controllability*, The Society of Naval Architects and Marine Engineers, New Jersey.
- Daley, C.G. (1984). BAFFIN – a Dynamic Ship/Ice Interaction Model. Paper No. F, Ice Tech-84 Symposium, Calgary, Alberta, pp. F1-F8.
- Edwards, Jr., R.Y., M.A. Dunne, G. Comfort, V. Bulat & B Johnson (1981). Results of Full Scale Trials in Ice of CCGS Pierre Radison. Spring Meeting/STAR Symposium, SNAME, Ottawa, Ontario.
- Edwards, Jr., R.Y., R.A. Major, J.K. Kim, J.G. German, J.W. Lewis & D.R. Miller (1976). Influence of Major Characteristics of Icebreaker Hulls on their Powering Requirements and Maneuverability in Ice, SNAME Annual Meeting.
- Edwards, Jr., R.Y., J.W. Lewis, J.W. Wheaton & J. Coburn, Jr. (1972). Full-Scale and Model Tests of a Great Lakes Icebreaker. The Society of Naval Architects and Marine Engineers (SNAME) Transactions, Vol. 80, pp. 170-207.

- Enkvist, E. (1972). On the Ice Resistance Encountered by Ships Operating in the Continuous Mode of Icebreaking. Swedish Academy of Engineering and Science in Finland, Report No. 24, Helsinki, Finland.
- Enkvist, E. (1983). The New Fine-Grained Model Ice of Wartsila Artic Research Centre. Wartsila Report D 33, Helsinki, Finland.
- Enkvist, E. & S. Makinen (1984). A Fine-Grain Model-Ice. Proceedings of the IAHR Ice Symposium, 1984, Volume II, pp. 217-227, Hamburg, Germany.
- Enkvist, E. (1990). Ice Model Tests as a Ship Design Tool. Proceedings of the IAHR Ice Symposium, Volume I, pp. 15-42, Espoo, Finland.
- Freitas, A. (1979). *Experimental Investigation of a Novel Icebreaker Concept*. Thyssen Nordseewerke, Emden, Germany.
- Gill, A.D. (1980). The Analysis and Synthesis of Ship Manoeuvring. A Report of the National Maritime Institute (Great Britain), Report Number NMIR20 SMTR8003, pp. 209-225.
- Grande, O., V.M. Arunachalam & D.B. Muggerridge (1983). Model Tests of Wave Attenuation in Ice. Proceedings of the 7<sup>th</sup> International POAC, Helsinki, Finland, Vol. 3, pp 143-152.
- Harzo, E., R. Falls, D.A. Walden (1979). Ship Manoeuvrability Safety Studies. The Society of Naval Architects and Marine Engineers, New York.
- Herfjord, K. (1982). Model Tests in Ice on Canadian Coast Guard R-Class Icebreaker. Marine Structures and Ships in Ice, Report No. 81-08, Norway.

- IAHR (1992). Second Report of the IAHR Working Group on Ice Modelling Materials. Proceedings of the 11<sup>th</sup> International Symposium on Ice, Volume 3. Banff, Alberta, pp. 1527-1536.
- Innoe, S., M. Hirano, & K. Kijima. (1981). Hydrodynamic Derivatives on Ship Manoeuvring. International Shipbuilding Progress, Vol. 28, No. 321, May, 1981.
- Jalonen, R. & L. Ilves (1990). Experience with a Chemically-Doped Fine-Grained Model Ice. Proceedings of the IAHR Ice Symposium. Volume 2, pp. 639-651, Espoo, Finland.
- Jebaraj, C., A.S.J. Swamidas & L.Y. Shih (1989). Numerical Modelling of Ship/Ice Interaction, National Research Council Canada Institute for Marine Dynamics Report IR-1989-02.
- Joba, J.C. (1985). *Ships Navigating in Ice - A Selected Bibliography - Vol III, 1980-84*, Transport Canada, Canadian Government Publishing Centre, Report No. TP 3855E.
- Jones, S.J. (1989). A Review of Ship Performance in Level Ice. Proceedings of the 8<sup>th</sup> OMAE Conference, The Hague, March 1989.
- Keinonen, A.J. (1983). Major Scaling Problems with Ice Model Testing of Ships. Proceedings of the 20<sup>th</sup> General Meeting of the American Towing Tank Conference, Vol. II, pp. 595-611.
- Kendrick, A.M., N. Dadachanji & B. Quart (1984). M.V. Arctic Manoeuvring Performance in Ice: Final Report. Project Report Prepared for Transportation Development Centre, Montreal, Quebec, Report Number TP 5684E.
- Kijima, K., S. Inoue & M. Hirano (1981). Hydrodynamic Derivatives on Ship Manoeuvring. International Shipbuilding Progress, Vol. 28, No. 321.

- Kijima, K., S. Inoue, M. Hirano & J. Takashima (1988). A Practical Calculation Method of Ship Manoeuvring Motion, International Shipbuilding Progress.
- Kostilainen, V. (1986). Problems in Physical Modelling of the Propulsion and Manoeuvring of Ice Transiting Ships. Proceedings of the 1<sup>st</sup> Ice Technology Conference, Cambridge, Massachusetts, pp. 323-331.
- Kotras, T., J. Lewis & R. Etzel (1977). Hydraulic Modelling of Ice-Covered Waters. Fourth International Conference on Port and Ocean Engineering Under Arctic Conditions - POAC '77, St. John's, Newfoundland, Volume I.
- Koyama, K., M. Yoshida, K. Izumiyama, S. Uto, N. Kanada, H. Shimoda, H. Tabuchi & H. Kitagawa (1988). Mechanical Properties of Ethylene Glycol Ice. Annual Meeting of the Ship Research Institute, No. 52, Tokyo, Japan.
- Lavrov, V.V. (1969). Deformation and Strength of Ice. NSF-Translation TT 70 50120.
- Lewis, J.W., F.W. DeBord & V.A. Bulat (1982). Resistance and Propulsion of Ice-Worthy Ships. SNAME Transactions, Vol. 90, pp. 249-76.
- Menon, B.C., I.F. Glen & I.M. Bayly (1986). Analysis and Design of Steering Components for Arctic Class Ships. SNAME Transactions, Vol. 94, pp. 75-91.
- Michel, B. (1978). Ice Mechanics. Les Presses de l'University de Laval, Quebec.
- Narita, S., M. Innoue, S. Kishi & Y. Yamauchi (1988). The Model Ice of the NKK Ice Model Basin. Proceedings of the IAHR Ice Symposium, 1988, Volume I, pp. 782-792, Sapporo, Japan.

- Nikolaev, E. & M. Lebedeva (1980). On the Nature of Scale Effects in Manoeuvring Tests with Full-Bodied Ship Modelling. Proceedings of the 13<sup>th</sup> Symposium on Naval Hydrodynamics, Tokyo.
- Nogid, L.M. (1959). Model Representation of a Ship Going Through a Continuous Ice Field or Pack Ice. Transactions of the Leningrad Shipbuilding Institute, No. 28, 45 pages.
- Norrbin, N.H. (1971). Theory and Observations on the Use of a Mathematical Model for Ship Manoeuvring in Deep and Confined Waters. Elanders Boktryckeri Aktiebolag, Publications of the Swedish State Shipbuilding Experimental Tank, Goteborg, Sweden.
- Nortala-Hoikkanen, A. (1990). FGX Model Ice at the MASA-Yards Arctic Research Centre. Proceedings of the IAHR Ice Symposium. Volume 3, pp. 247-259, Espoo, Finland.
- Oltmann, P., S.D. Sharma & K. Wolff (1980). An Investigation of Certain Scale Effects in Manoeuvring Tests with Ship Models. Proceedings of the 13<sup>th</sup> Symposium on Naval Hydrodynamics, Tokyo.
- Peyton, H. (1966). *Sea Ice Strength*. University of Alaska.
- Peirce, T.H. & A.L. Hart (1990). Icebreaker Manoeuvrability. Proceedings of the 2<sup>nd</sup> International Conference on Ice Technology for Polar Operations. Cambridge University, U.K.
- Riska, K. & P. Varsta (1977). State-of-Art Review of Basic Ice Problems for a Naval Architect. Ship Laboratory report of the Technical Research Centre of Finland, Espoo, Finland.

- Sanderson, T.J.O. (1988). *Ice Mechanics*. Graham and Trotman Ltd., London, UK.
- Schwarz, J. (1977). *New Developments in Modelling Ice Problems, POAC '77, St. John's, Newfoundland, Volume I*.
- Schwarz, J., K. Hirayama & H. Wu (1974). *Effect of Thickness on Ice Forces, Offshore Technology Conference, Texas*.
- Schwarz, J., P. Jochmann & L. Hoffman (1978). *Prediction on the Icebreaking Performance of the German Polar Vessel, Hamburgische Schiffbau-Versuchsanstalt*.
- Sharp, J.J. & E. Moore (1983). *Partial Analysis and Matrix Methods, International Journal of Mathematics in Education, Science, and Technology, Vol. 14, No. 4*.
- Sharp, J.J. & E. Moore (1988). *A Systematic Approach to the Development of Echelon Matrices for Dimensional Analysis, International Journal of Mathematics in Education, Science, and Technology, Vol. 19, No. 3*.
- Sharp, J.J., A. Deb & M.K. Deb (1992). *Applications of Matrix Manipulation in Dimensional Analysis Involving Large Numbers of Variables. Marine Structures, Vol. 5*.
- Spencer, D.S. & G.W. Timco (1990). *CD Model Ice: A Process to Produce Correct Density Model Ice. Proceedings of the IAHR Ice Symposium, Volume 2, pp. 745-755, Espoo, Finland*.
- Tang, C.L. (1990). *Sea Ice on the Northern Grand Banks. Report of a Workshop on the Canadian Perspective on Sea Ice, Sydney, B.C.*

- Tatinclaux, J.C. & K. Hirayama (1982). Determination of the Flexural Strength and Elastic Modulus of Ice from In Situ Flexural Beam Tests. *Cold Regions Science and Technology*, Vol. 6, pp. 37-47.
- Thomas III, W.L. & L.A. Schultz (1990). Model Tests of a Naval Combatant in Broken Ice Fields. *Proceedings of the 2<sup>nd</sup> International Conference on Ice Technology for Polar Operations*. Downing College, Cambridge University, UK, pp. 155-165.
- Timco, G.W. (1979). The Mechanical and Morphological Properties of Doped Ice, *Proceedings of POAC '79*, Trondheim, Norway, pp. 719-739.
- Timco, G.W. (1980). The Mechanical Properties of Saline-Doped and Carbamide (Urea)-Doped Model Ice. *Cold Regions Science and Technology*, Vol. 3, pp. 45-56.
- Timco, G.W. (1981a). A Comparison of Several Chemically-Doped Types of Model Ice. *Proceedings of the IAHR Symposium on Ice*, pp. 489-502, Quebec City.
- Timco, G.W. (1981b). Invited Commentary: On the Test Methods for Model Ice. *Cold Regions Science and Technology* 4, pp. 269-274.
- Timco, G.W. (1983a). Model Testing of Structures in Ice: Consideration of Scale Effects. *Proceedings of the 20<sup>th</sup> General Meeting of the ATTC*, Vol. II, pp. 613-625.
- Timco, G.W. (1983b). Uniaxial and Plane-Strain Compressive Strength of Model Ice. *Annals of Glaciology*, Vol. 4, pp. 289-293.
- Timco, G.W. (1984). Ice Forces on Structures: Physical Modelling Techniques. *Proceedings of the 2<sup>nd</sup> IAHR State-of-the-Art Report on Ice Forces on Structures*;

Published in Proceedings of the IAHR Ice Symposium, Vol. 4, pp. 117-150, Hamburg, Germany.

- Timco, G.W. (1985). Flexural Strength and Fracture Toughness of Urea Model Ice. *Journal of Energy Resources Technology*, Vol. 107, pp. 498-505.
- Timco, G.W. (1986). EG/AD/S: A New Type of Model Ice for Refrigerated Towing Tanks. *Cold Regions Science and Technology*, Vol. 12, pp. 175-195.
- Tryde, P. (1975). Intermittent Ice Forces Acting on Inclined Wedges. *Proceedings of the IAHR International Symposium on Ice, Hannover, NH*, pp. 339-344.
- Tue-Fee, K. & A. Keinonen (1986). Full-Scale Maneuvering Tests in Level Ice of Canmar Kigoriak and Robert LeMeur. *Marine Technology*, Vol. 23, No. 2, pp. 131-138.
- Vance, G.P. (1980). State of the Art of Ship Model Testing in Ice, *Proceedings of the 19<sup>th</sup> Annual American Towing Tank Conference*.
- Varsta, P. (1983). Modelling of Impact Between Ship Hull and Ice. *POAC '83*, pp. 760-777.
- Wagner Smitt, L. (1970). Steering and Manoeuvring Full Scale and Model Tests (Parts 1 and 2). *European Shipbuilding 1970* (19) No.6 and 1971 (2) No. 1.
- Weeks, W. & A. Assur (1969). *The Mechanical Properties of Sea Ice*. CRREL, USA.
- Williams, F.M. (1996). *Personal Discussions at the Institute for Marine Dynamics, National Research Council of Canada*.
- Williams, F.M. (2002). *Formal thesis review comment*.

Williams, F.M. & P. Waclawek (1998). Physical Model Tests for Ship Manoeuvring in Ice. Proceedings of the 25<sup>th</sup> American Towing Tank Conference, Iowa.

Williams, F.M. et al. (1992). Full Scale Trials in Level Ice with Canadian R-Class Icebreaker. SNAME Annual Meeting, New York.

Wilkman, G. & T. Mattsson (1991). Ice Model Tests as a Tool to Study and Improve the Performance of Ships in Ice. Eleventh International Conference on Port and Ocean Engineering Under Arctic Conditions - POAC '91, St. John's, Newfoundland, Volume II.

## **Appendix A : Ship Model Details**

Table A.1 M.V. Arctic model (1:80 scale) particulars.

Particular	Value
Length Between Perpendiculars (m)	2.456
Length on Waterline (m)	2.510
Waterline Beam Amidships	0.286
Waterline Beam at Maximum Section (m)	0.286
Draft Amidships (m)	0.137
Draft at Maximum Section (m)	0.137
Maximum Draft (m)	0.137
Parallel Middle Body from Aft of Midships (m)	0.049
Parallel Middle Body to Forward of Midships (m)	0.565
Area of Midships Station (m <sup>2</sup> )	0.039
Area of Maximum Station (m <sup>2</sup> )	0.039
Centre of Buoyancy Forward of Midships (m)	0.044
Centre of Aft Body Buoyancy Forward of Midships (m)	-0.471
Centre of Fore Body Buoyancy Forward of Midships (m)	0.503
Centre of Buoyancy Above Datum (m)	0.073
Wetted Surface Area (m <sup>2</sup> )	1.109
Volume of Displacement (m <sup>3</sup> )	0.073
Displacement (tonnes of Salt Water)	0.075
Centre of Flotation Forward of Midships (m)	0.002
Centre of Flotation (Aft Body), Forward of Midships (m)	-0.549
Centre of Flotation (Fore Body) Forward of Midships (m)	0.547
Area of Waterline Plane (m <sup>2</sup> )	0.616
Vertical Centre of Gravity (Above Datum) (m)	0.096
Longitudinal Centre of Gravity (from Aft Perpendicular) (m)	1.270
Metacentric Height (m)	0.029
Transverse Metacentric Radius (m)	0.051
Longitudinal Metacentric Radius (m)	3.430

Table A.2 R-Class hullform model (1:40 scale) particulars.

Particular	Value
Length Between Perpendiculars (m)	2.192
Length on Waterline (m)	2.325
Waterline Beam Amidships	0.484
Waterline Beam at Maximum Section (m)	0.484
Draft Amidships (m)	0.174
Draft at Maximum Section (m)	0.175
Equivalent Level Keel Draft (m)	0.179
Parallel Middle Body from Aft of Midships (m)	0.185
Parallel Middle Body to Forward of Midships (m)	-0.185
Area of Maximum Station (m <sup>2</sup> )	0.077
Centre of Buoyancy Forward of Midships (m)	0.008
Centre of Buoyancy Above Datum (m)	0.097
Wetted Surface Area (m <sup>2</sup> )	1.335
Volume of Displacement (m <sup>3</sup> )	0.159
Displacement (tonnes of Fresh Water)	0.159
Centre of Flotation Forward of Midships (m)	-0.018
Centre of Flotation Above Keel (m)	0.174
Area of Waterline Plane (m <sup>2</sup> )	0.900
Transverse Metacentric Radius (m)	0.122
Longitudinal Metacentric Radius (m)	2.400

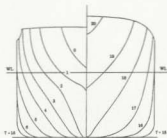


Figure A. 1 M.V. Arctic lines plan body view.

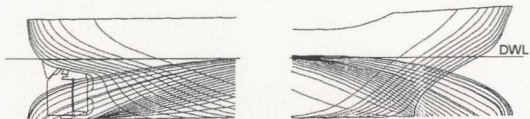


Figure A. 2 M.V. Arctic lines plan profile and plan views with parallel midbody section removed.

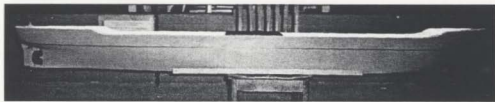


Figure A. 3 Elevation view of M.V. Arctic ship model.



Figure A. 4 Stern view of M.V. Arctic, clearly showing the stern shape and propeller nozzle.

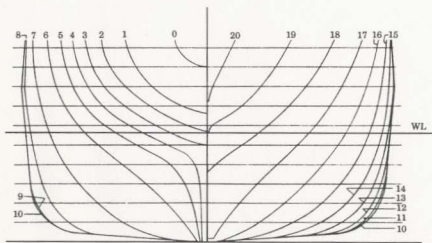


Figure A. 5 R-Class lines plan body view.

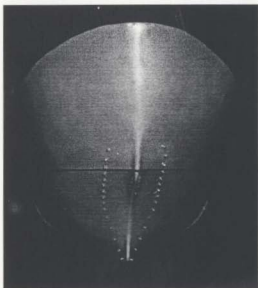


Figure A. 6 View of R-Class hullform bow, showing turbulence stimulator studs at and below the waterline.

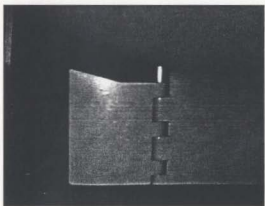


Figure A. 7 Close-up view of R-Class rudder specifically designed and installed for these tests.

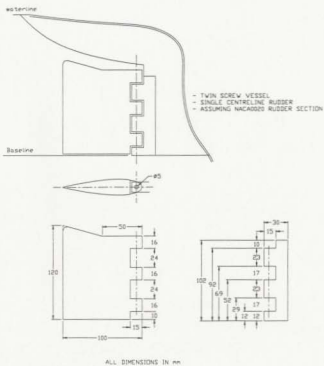


Figure A. 8 R-Class rudder design details.

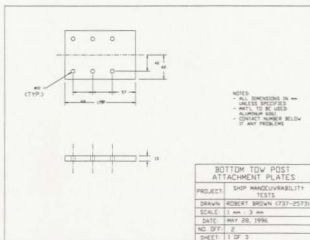


Figure A. 9 Tow post model attachment plate show drawing.

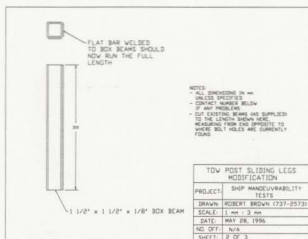


Figure A. 10 Tow post sliding leg modification shop drawing.

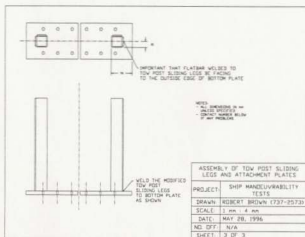


Figure A. 11 Tow post model attachment plate and sliding leg assembly.

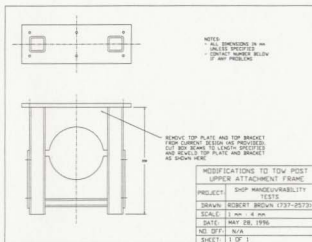


Figure A. 12 Tow post dynamometer attachment plate modification shop drawing.

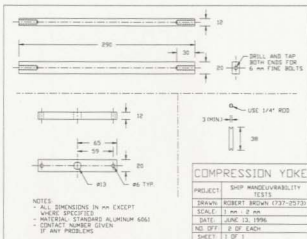


Figure A. 13 Calibration compression yoke shop drawing.

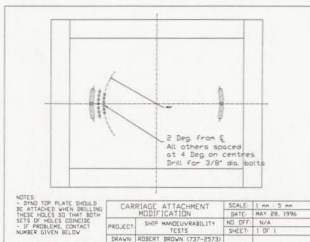


Figure A. 14 Carriage-dynamometer mounting plate modification shop drawing.

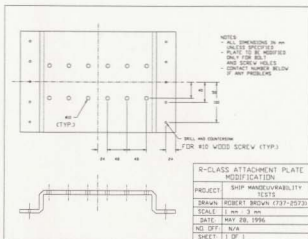


Figure A. 15 R-Class model attachment plate modification shop drawing.

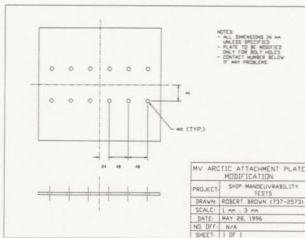


Figure A. 16 M.V. Arctic model attachment plate modification shop drawing.

## **Appendix B : Load Cell and Flex-Link Details**

## B.1 Load Cells

Two types of load cells were installed in the dynamometer – “S” and “Puck” - type. These instruments were borrowed from the Institute for Marine Dynamics – National Research Council (IMD-NRC).

### “S” - Type

Two “S” - Type load cells were installed to measure forward and aft sway loads on the ship model. The maximum capacity of this load cell type was 223 N. A schematic of the load cell is given in Figure B. 1, along with the manufacturer’s certificate of conformance and calibration in Figure B. 2.

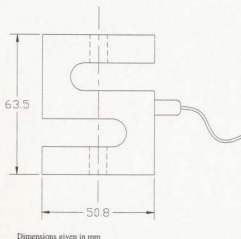


Figure B. 1 Schematic for “S” – Type load cell used for measurement of sway forces on the ship model.

# TRANSDUCERS TRANSDUCERS TRANSDUCERS II

14030 Balsa Lane  
 Cerritos, California 90701  
 Telephone (714) 739-1991  
 TWX 910-596-1433



## CERTIFICATE OF CONFORMANCE

WE CERTIFY THAT THE MATERIAL AND/OR PARTS DESCRIBED BELOW HAVE BEEN MANUFACTURED IN ACCORDANCE WITH ALL APPLICABLE INSTRUCTIONS AND SPECIFICATIONS. PHYSICAL AND CHEMICAL DATA PERTAINING TO THIS ORDER ARE AVAILABLE AT OUR PLANT FOR YOUR INSPECTION. ALL CALIBRATIONS PERFORMED WITH STANDARDS DIRECTLY TRACEABLE TO NATIONAL BUREAU OF STANDARDS.

LOAD CELL OUTPUT IS IN MILLIVOLTS PER VOLT, CORRECTED TO STANDARD GRAVITY (980.665CM/SEC/SEC). THEREFORE, THE OUTPUT IS IN POUNDS FORCE.

## CALIBRATION CERTIFICATE

Model No.	T363-50-20F1
Serial No.	88899
CAPACITY	50 LBS.
EXCITATION	10 VDC
Abs FS OUTPUT	+3.2775 MV/V
NON-LINEARITY	-0.017% FS
HYSTERESIS	+0.008% FS
ZERO BAL.	+0.0117 MV/V
INPUT RES	353.2 Ohms
OUTPUT RES	351.3 Ohms
THERMAL ZERO COEFFICIENT	< 0.15% F.S./100 F
THERMAL SENS. COEFFICIENT	< 0.00% F.S./100 F
INSULATION RESISTANCE	> 5000 MEGOHMS @ 50 VDC
COMPENSATION TEMP. RANGE	0 F TO 130 F

### ELECTRICAL CONNECTIONS TENSION Positive

RED	+	INPUT
GRN	-	OUTPUT
WHT	-	OUTPUT
BLK	-	INPUT
ORG		SHIELD

T.I. Standard

CERTIFY BY: JOE PETTY  
 MGR. QUALITY ASSURANCE

Figure B. 2 Manufacturer's certificate of conformance and calibration for "S" - Type load cell.

### "Puck" - Type

One "Puck" - Type load cell was installed to measure surge loads on the ship model. The maximum capacity of this load cell was 111 N. A schematic of this load cell is given in Figure B. 3, along with the manufacturer's Certificate of conformance and calibration in Figure B. 4.

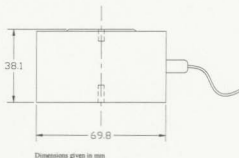


Figure B. 3 Schematic for "Puck" – Type load cell used for measurement of surge forces on the ship model.

**INSTALLATION**

The Model D187 load cell may be operated either horizontally or vertically or any angle in between provided the load is applied straight through the loading axis, i.e., on the center line of the threaded holes. The cell is sealed and compensated for normal barometric changes. It will withstand operation in areas of high humidity, but it will expand to be corrected.

For use in which both tension and compression forces may be applied (such as in a strain mounted dynamometer), use of spherical rod end bearings is recommended. For compression only a load button should be mounted at the top of the cell.

**NOTE:** Load button thread length must be 1/4" x 1/4". Torque the load button to 30 in. lbs. Rod ends should be threaded into the center holes until the bottom nut, then backed out one turn. Torque the nut and use nuts to 30 in. lbs.

**WIRING (Each bridge)**

When connected as shown, output pins are active (pin 1 to sensor load, IEEE753B Signal Code)

Use only shielded cable to connect the cell to the indicator. The use of Belden Cable (or equivalent quality) is recommended. Use Belden 8723 for cables 20 feet or less. Use Belden 8725 for cables over 20 feet.

Use 60/40 rosin core solder for connections and clean with rosin solvent after soldering. Check all connections for continuity. Connections at the readout instrument are to be according to the instrument manufacturer's instructions.

**CALIBRATION DATA**

**BRIDGE RESISTANCE (OHMS)**

Bridge A: Exc.  $(350.0) \pm 0.2$  ;  $R_2 = 350.0$

Bridge B: Exc.  $(50) \pm 0.2$

**OUTPUT (mV/V)**

Bridge A: Comp.  $(2) \pm 1.31 \pm 1$  ;  $T_{0.1} = 2 \pm 1.27$

Bridge B: Comp.  $(2) \pm 1$  ;  $T_{0.1} = 1$

**NONLINEARITY (% of F.S.)**

Bridge A:  $(0.01)$  ; Bridge B:  $(0.01)$

**HYSTERESIS (% of F.S.)**

Bridge A:  $(0.02)$  ; Bridge B:  $(0.02)$

**SHUNT CALIBRATION: Resistor  $60 \pm 0.1$  ohms**

Bridge	Pins	Wires	Equivalent Load
A	B/D	Green/Black	17.10 lbs. Comp.
	B/A	Green/Red	17.08 lbs. Tens.
B	B/D	Green/Black	lbs. Comp.
	B/A	Green/Red	lbs. Tens.

**SPECIFICATIONS**

SENSOR: 4 arm strain gage bridge  
 EXCITATION VOLTAGE: 20 VDC or VAC RMS Max. ✓  
 ZERO BALANCE: Within 5% of rated output  
 REPEATABILITY: 0.02% of full scale  
 OVERLOAD: 150% of rated capacity  
 EFFECT OF TEMP. ON ZERO: 0.002% of F.S./°F  
 EFFECT OF TEMP. ON OUTPUT: 0.002% of F.S./°F  
 COMPENSATED TEMP. RANGE: 70°F to 170°F

USEABLE TEMP. RANGE: -65°F to 200°F  
 SHUNT CALIBRATION: An electronic signal equivalent to that produced by a known load can be obtained by shunting one arm of the load cell's strain gage bridge with a precision wire-wound resistor. Shunt resistor and equivalent load values for this load cell are shown above. They are determined during factory calibration of the load cell.

**NOTE:** To make shunts, one lead wire of the shunt is connected to one lead of the load cell and the indicator used has an input impedance of at least 50k ohms.

Figure B. 4 Manufacturer's certificate of conformance and calibration for "Puck" – Type load cell.

## B.2 Flex-Links

Flex-Links (described in Section 4.2.3) were designed to be stiff in the axial direction and flexible in the transverse direction. These instruments were designed to meet the criteria laid-out during the design of the experiments. Dimensions of the flex-links used are given in Table B. 1.

Table B. 1 Flex link dimensions.

<b>Flex-Link</b>	<b>Minor Diameter (mm)</b>	<b>Major Diameter (mm)</b>	<b>Measuring Section Length (mm)</b>	<b>Effective Length (mm)</b>	<b>Endcap Length (mm)</b>
Vertical	2.03	19.05	12.70	228.60	23.50
Surge	2.03	12.7	12.70	92.08	15.88
Sway	1.52	12.7	12.70	117.48	15.88

## **Appendix C : Image Analysis of Wax Concentration**

Mocha™ image analysis software was used to compute the total wax coverage in a representative area of the tank. The photo (Figure C. 1) was scanned as a .bmp file type and read by the software. The image was then calibrated to determine the units of measurement. Calibration was based on the known size of the ship's bow shown in the right-hand side of the image. The overall area of the image (Figure C. 2) was then determined and, using brightness thresholds, the ship's bow area (Figure C. 3) and water area (Figure C. 4). Table C. 1 summarises these areas.

Table C. 1 Summary of areas measured.

Object	Area (mm <sup>2</sup> )
Entire Image	19227.9
Water	3200.0
Ship Model Bow	437.3

Wax concentration is calculated as:

$$\begin{aligned}C &= 1.00 - A_{\text{water}} / (A_{\text{image}} - A_{\text{ship}}) \\ &= 1.00 - 3200.0 / (19227.9 - 437.3) \\ &= 0.83\end{aligned}$$



Figure C. 1 Photograph taken of a representative portion of the wax-covered towing tank.

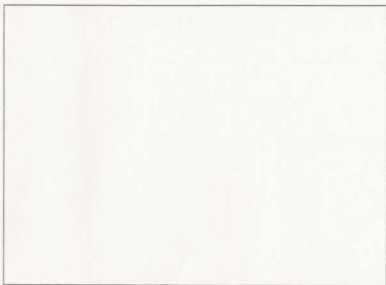


Figure C. 2 Image area overlay (white portion measured i.e. entire image area).



Figure C. 3 Ship model bow area threshold overlay (white portion measured).



Figure C. 4 Water area threshold overlay (white portion measured).

## **Appendix D : Calibration Plots**

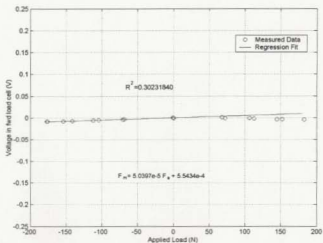


Figure D. 1 Calibration plot of forward sway load cell crosstalk measurement during aft sway load cell calibration (negative applied load implies tension, positive applied load implies compression).

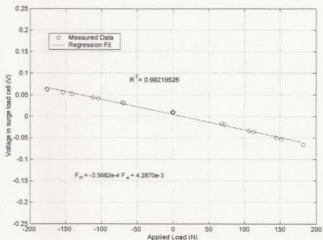


Figure D. 2 Calibration plot of surge load cell crosstalk measurement during aft sway load cell calibration (negative applied load implies tension, positive applied load implies compression).

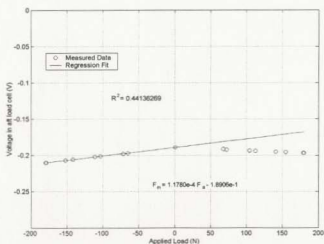


Figure D.3 Calibration plot of aft sway load cell crosstalk measurement during forward sway load cell calibration (negative applied load implies tension, positive applied load implies compression).

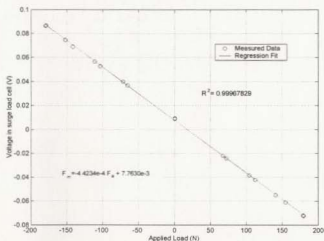


Figure D.4 Calibration plot of surge load cell crosstalk measurement during forward sway load cell calibration (negative applied load implies tension, positive applied load implies compression).

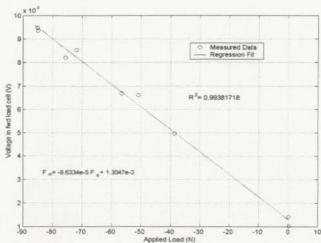


Figure D.5 Calibration plot of forward sway load cell crosstalk measurement during surge load cell calibration (negative applied load implies tension, positive applied load implies compression).

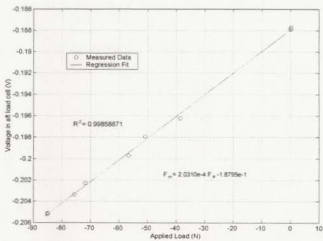


Figure D.6 Calibration plot of aft sway load cell crosstalk measurement during surge load cell calibration (negative applied load implies tension, positive applied load implies compression).

## **Appendix E : Constant Velocity Test Results**

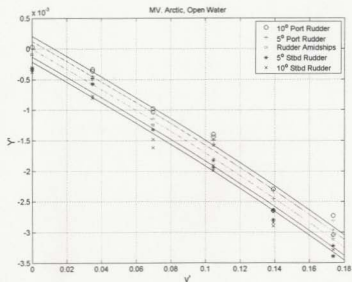


Figure E. 1 Nondimensional sway force as a function of nondimensional sway velocity for all rudder angles for the M.V. Arctic model in open water.

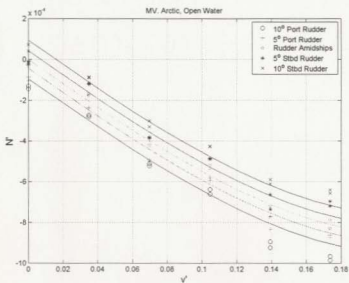


Figure E. 2 Nondimensional yaw moment as a function of nondimensional sway velocity for all rudder angles for the M.V. Arctic model in open water.

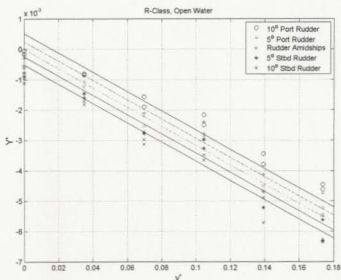


Figure E. 3 Nondimensional sway force as a function of nondimensional sway velocity for all rudder angles for the R-Class model in open water.

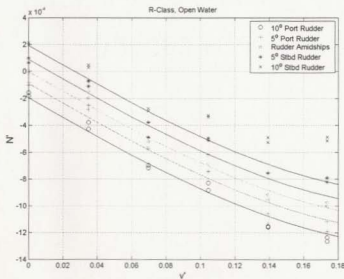


Figure E. 4 Nondimensional yaw moment as a function of nondimensional sway velocity for all rudder angles for the R-Class model in open water.

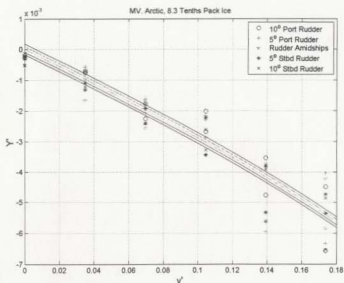


Figure E. 5 Nondimensional sway force as a function of nondimensional sway velocity for all rudder angles for the M.V. Arctic model in pack ice.

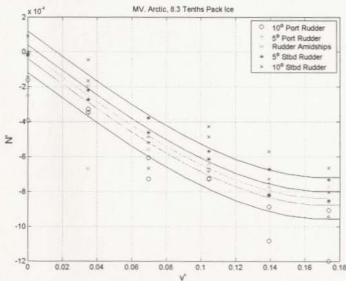


Figure E. 6 Nondimensional yaw moment as a function of nondimensional sway velocity for all rudder angles for the M.V. Arctic model in pack ice.



Figure E. 7 Nondimensional sway force as a function of nondimensional sway velocity for all rudder angles for the R-Class model in pack ice.

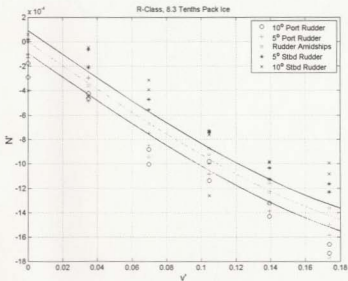


Figure E. 8 Nondimensional yaw moment as a function of nondimensional sway velocity for all rudder angles for the R-Class model in pack ice.

## **Appendix F: Constant Acceleration Test Results**

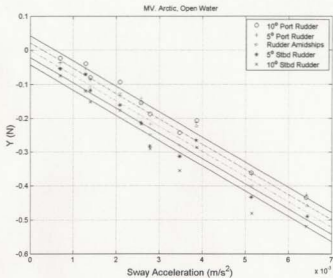


Figure F. 1 Sway force as a function of sway acceleration for all rudder angles for the M.V. Arctic model in open water.

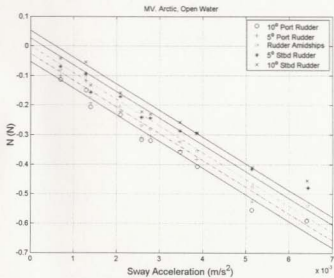


Figure F. 2 Yaw moment as a function of sway acceleration for all rudder angles for the M.V. Arctic model in open water.

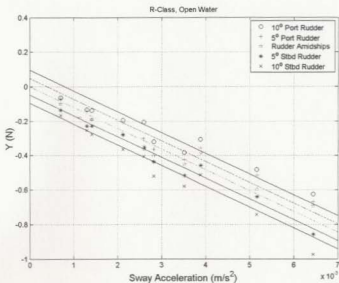


Figure F. 3 Sway force as a function of sway acceleration for all rudder angles for the R-Class model in open water.

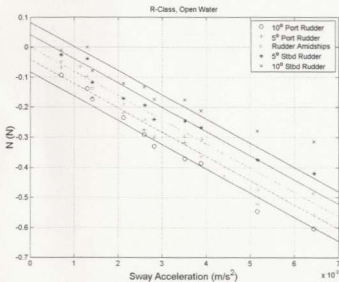


Figure F. 4 Yaw moment as a function of sway acceleration for all rudder angles for the R-Class model in open water.

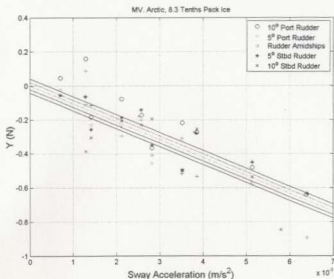


Figure F. 5 Sway force as a function of sway acceleration for all rudder angles for the M.V. Arctic model in pack ice.

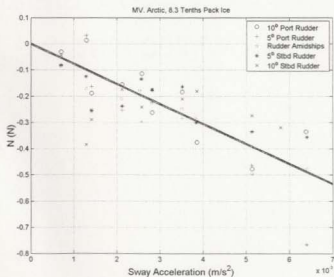


Figure F. 6 Yaw moment as a function of sway acceleration for all rudder angles for the M.V. Arctic model in pack ice.

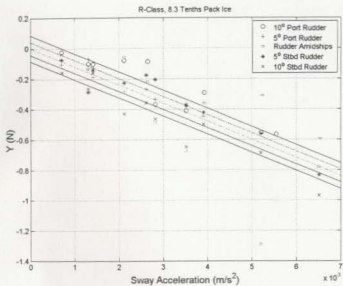


Figure F. 7 Sway force as a function of sway acceleration for all rudder angles for the R-Class model in pack ice.

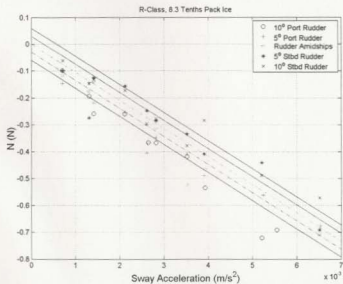


Figure F. 8 Yaw moment as a function of sway acceleration for all rudder angles for the R-Class model in pack ice.







